Brown Boveri Review

4

April 1970, Volume 57 Baden/Switzerland

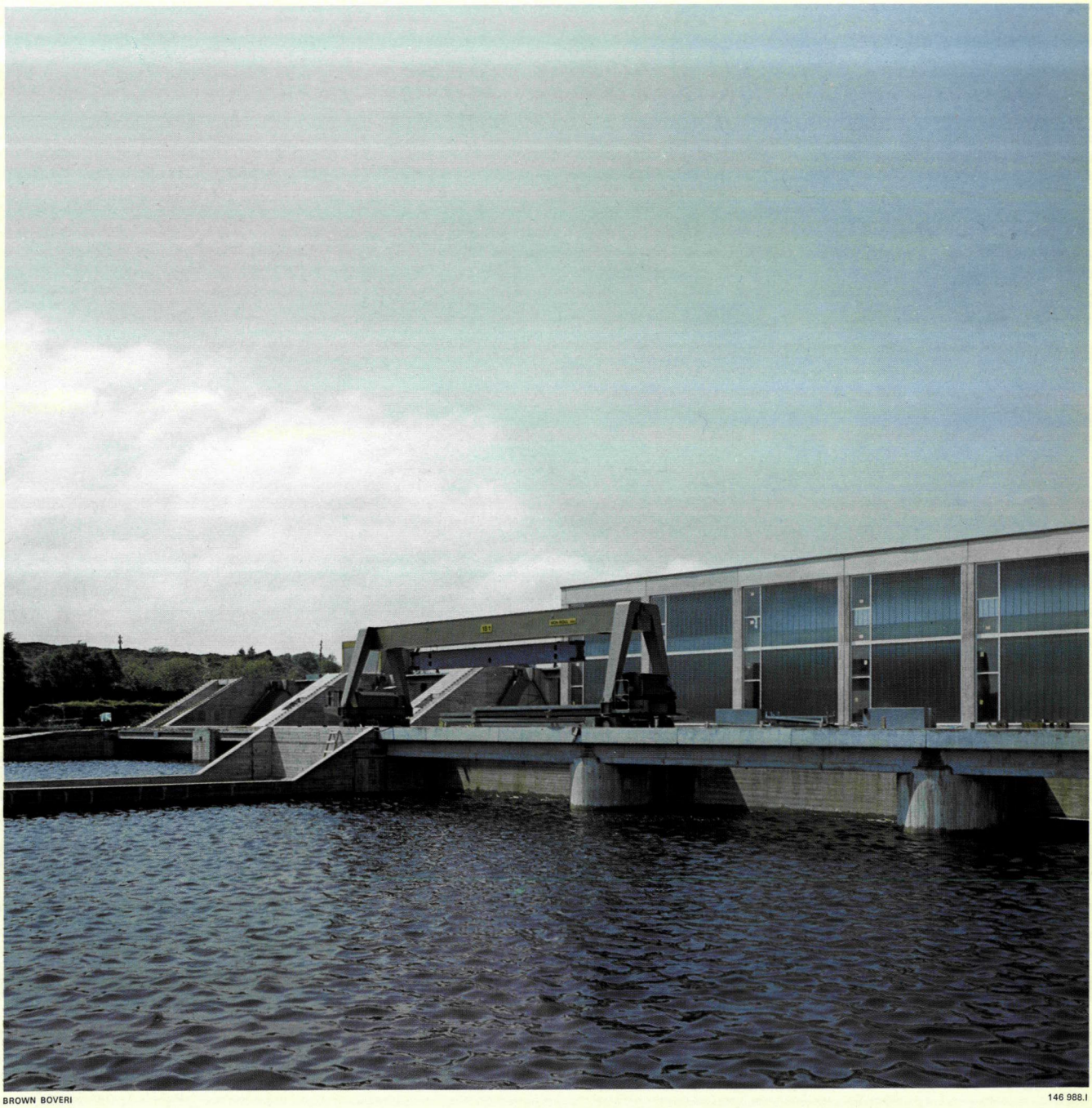

BROWN BOVERI

146 988.I

Brown Boveri Review

4

April 1970, Volume 57 Baden/Switzerland p. 149–204

Published by Brown, Boveri & Company, Limited, CH-5401 Baden/Switzerland
Printed by Buchdruckerei Effingerhof AG, Brugg
Obtainable direct from the publisher

Cover:

Flumenthal power station of the Aare-Tessin AG für Elektrizität (Atel), with three generators, each of 9500 kVA, driven direct by bulb turbines
(Photo by courtesy of Motor-Columbus Ltd.)

Contents

Design Aspects of Induction Motors for Traction Applications with Supply through Static Frequency Changers

H. Largiadèr

621.313.333:621.335
621.333

A great deal of progress has been made during the last few years in the field of controlled semiconductor engineering. This has brought us within reach of building electric traction vehicles powered by squirrel-cage motors supplied through static frequency changers. Induction motors are easier to build than commutator motors and require less maintenance. Comparisons are drawn between an existing commutator motor and an induction motor which is intended to supersede it. For the same output the induction motor weighs 15 % less and occupies less space. In the higher speed ranges it develops more power than the commutator motor. Apart from the fundamental oscillation[1] the static frequency changer supplies a number of ripple oscillations of various amplitudes and frequencies. These cause additional losses of about 20 % of the fundamental wave losses and result in greater temperature rises. Hunting torques are also created with an amplitude of about 5 to 10 % of the rated torque. Increasing the leakage reactance in the motor permits the flow of ripple currents to be contained within given limits. The undesirable effects of the frequency changer, however, can be eliminated by suitably designing the frequency changer/motor unit and using modern heat-resistant insulating materials.

[1] A distinction must be made here between oscillations, which are time harmonics, and waves, which are space harmonics and are dealt with later.

Why Induction Motors?

The idea of using induction motors in traction vehicles is not a new one. Rack-and-pinion motorcoaches driven by Brown Boveri squirrel-cage induction motors are described in [1] and are still in service. The supply frequency is constant and two insulated contact wires are required. This system is therefore suitable only for special railways with a simple track configuration and is out of the question for standard gauge applications. Locomotives with squirrel cage motors were built at Oerlikon about 15 years ago [2]. As far as the motors are concerned the design is very close to modern concepts. Power conversion was, however, carried out electromechanically by rotating frequency changers and therefore the system did not find widespread application.

It became obvious that the only chance of success would be to use a static frequency changer having no moving parts or contacts. It has now become possible to build such frequency changers which supply a three-phase voltage with infinitely variable amplitude and frequency.

The induction motor is expected to have the following advantages over the commutator motor:

- Less maintenance. There are no brushes to change, no commutator to inspect and no brush holders and mechanism to check.
- More output for the same volume or less weight for the same output because the induction motor can be driven at higher speeds. Restrictions relating to peripheral speed of the commutator and also the reactance voltages in the rotating windings do not apply.
- More power in the higher speed ranges. Commutator motors which are already highly utilized at rated speed can often not supply rated power up to maximum speed because the reactance voltages become too great. There is no such restriction with the induction motor.
- Lower initial cost. The induction motor is lighter and its design considerably less complicated than the commutator motor.

The series-wound commutator motor has been developed over a long period to a high degree of sophistication. Every respect is due to the present state of development and there is no pressing need to replace them by induction motors. There is, however, a desire to further reduce maintenance costs and, in certain cases, to install more power. The induction motor would be very suitable in this respect.

Frequency, Voltage and Speed

If the induction motor is operating on variable frequency, the induced voltage E must be set proportional to the frequency f if the motor is to operate with constant flux Φ and therefore

$$E = c \,.\, f \,.\, \Phi \quad [2]$$

[2] Unless otherwise stated

Current I (A), Voltage U, E (V) } r.m.s. values
Magnetic flux Φ (10^{-2} Vs = 10^6 Maxwell), Magnetic induction B (10^{-8} Vs/cm^2 = 1 Gauss) } peak values

Table I: Transmission ratios of some standard gauge locomotives operating in Europe

Locomotive class	Operator	No. of teeth	Ratio
Ae 4/4 I	BLS	36:80	2·22
Ae 6/6	SBB	34:87	2·56
Be 4/4	BT	27:75	2·78
Ae 4/4 II	BLS	26:87	3·346
Re 4/4 II	SBB	33:87	2·46
E 320	DB	20:79	3·95
E 344	DB	21:80	3·81
E 310	DB	25:79	3·16
E 410	DB	25:79	3·16
EL 13	NSB	22:87	3·95
EL 14	NSB	37:92	2·486
1042	OeBB	30:75	2·5

BLS = Berne–Lötschberg–Simplon Railway
SBB = Swiss Federal Railways
BT = Bodensee–Toggenburg Railway
DB = German Federal Railway
NSB = Norwegian State Railways
OeBB = Austrian Federal Railways

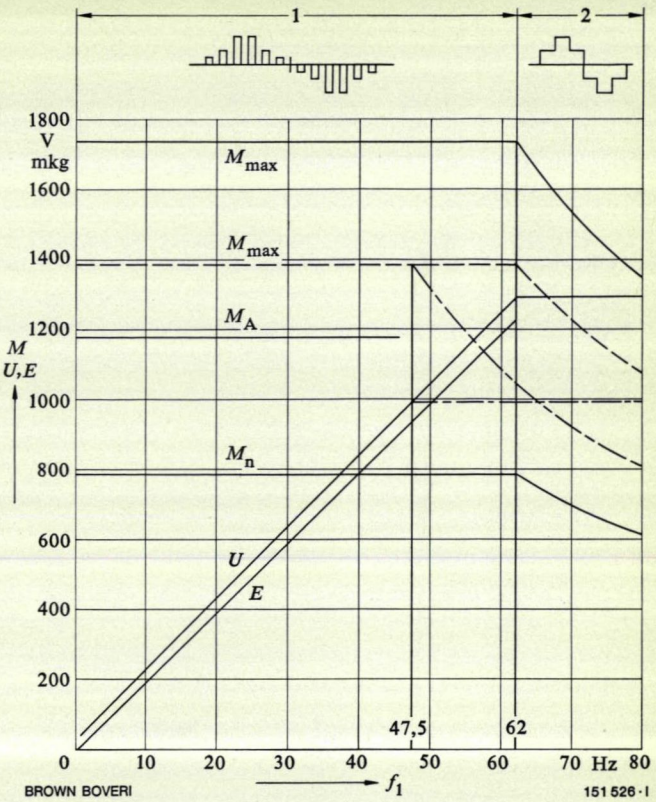

Fig. 1 – Voltage/frequency characteristic of an induction motor

The shape of the voltage supplied to the windings is shown at top.

1 = Linear voltage/frequency characteristic from 0 to 62 Hz. The static frequency changer operates on the undershooting principle
2 = Field weakening range (voltage constant). The static frequency changer supplies a rectangular (six-step) voltage

f_1 = Stator frequency
E = Induced voltage per phase for operating at constant air-gap flux
U = Motor voltage per phase for operating with constant air-gap flux and constant rated current
– · – · – = Motor voltage where field weakening commences at 47·5 Hz
M_n = Rated torque at constant rated current and constant air-gap flux
M_A = Necessary starting torque
——— M_{max} = Breakdown torque
– – – – M_{max} = Breakdown torque at 25 % greater leakage reactance
– · – · – M_{max} = Breakdown torque at 25 % greater leakage reactance but within the field weakening range of 47·5 to 80 Hz

For motor data see Table II.

where c is the machine constant (see footnote). The motor then operates with a linear voltage/frequency characteristic. At constant current the motor develops a constant torque over the whole frequency range.

Because of voltage drops the terminal voltage U must be higher than the induced voltage E. As shown in Fig. 1 the characteristic of U does not pass through the origin.

In order to attain high motor utilization every attempt is made to set the speed, and therefore also the transmission ratio, as high as possible. The maximum ratio for the single-stage spur gear transmission is determined to a large extent by the geometry of the wheelset and also by the number of teeth on the pinion, which experience has shown should not be less than 12 to 15. Low power commutator motors frequently permit the maximum mechanically feasible transmission to be used. Even larger transmission ratios (for induction motors) could involve two-stage spur or even epicyclic gearing. The economics of each individual case would require investigation.

On the other hand the maximum transmission ratio for high-power motors in the 500 to 1000 kW per axle range is determined by the peripheral speed of the commutator and by the reactance voltage. As shown in Table I the usual number of teeth on the pinion is between 22 and 36 and the transmission ratios are between 2·2 and 3·5:1 with a maximum of 4:1. Where induction motors are used the transmission ratio can be even higher while still retaining single-stage spur gearing.

Once the speed has been decided on, the frequency can be found from $f = \frac{pn}{60}$. The number of pole pairs is usually determined by the basic design principles for induction motors. In most cases the best results are obtained with four-pole motors.

The optimum values for voltage and frequency and the number of poles must be decided from case to case and brought into accord with the design of the static frequency changer. The principle here is that the frequency changer and motor, considered as an entity, must be designed to an optimum from both technical and economic aspects.

The general aspects of operating an induction motor with variable frequency and voltage need not be investigated here as they have already been given enough space in the literature [3, 4, 5, 6, 7]. Let us confine ourselves to the aspects of designing induction motors for traction applications and use a sample calculation to illustrate them.

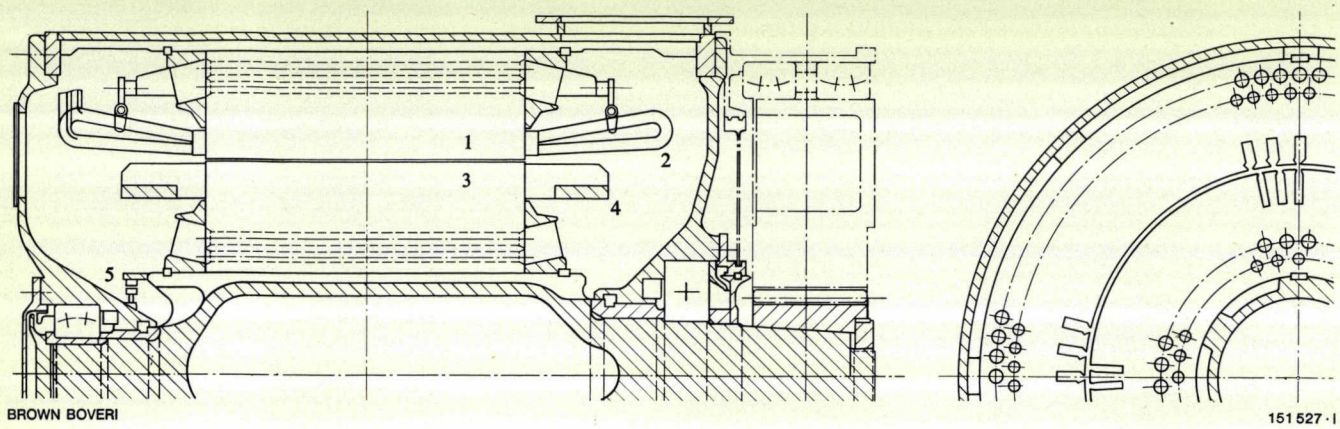

Fig. 2 – Sections through an induction traction motor

1 = Stator
2 = Stator winding
3 = Rotor
4 = Squirrel-cage winding
5 = Tacho-generator

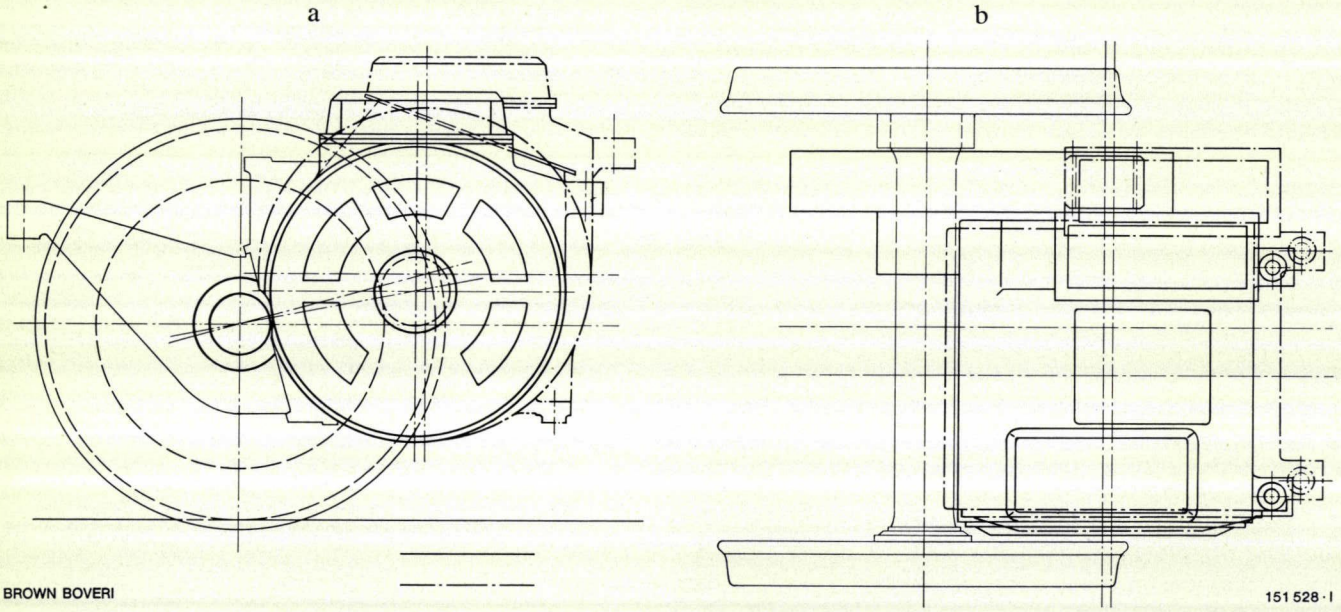

Fig. 3 – Wheelset with commutator motor compared with the induction motor intended to supersede it

a: End view
b: Top view
– · – · – = Commutator motor
——— = Induction motor
Driving wheel diameter = 1250 mm
For motor data see Table II.

Comparing Induction Motors with Commutator Motors

In order to provide strong evidence for a realistic comparison it was assumed that an existing locomotive would have to be fitted with induction motors. The class Ae 4/4 II high-power $B'_0B'_0$ rectifier locomotive with electrical equipment by Brown Boveri and owned by the Berne–Lötschberg–Simplon Railway and described in [8] was chosen as the guinea pig.

The induction motors used to replace the commutator motors were derived from a stationary type. Its design features are shown in Fig. 2. As opposed to its stationary counterpart it has axial cooling (no radial cooling slots) to keep the length down. This compact arrangement has lately found application in the Brown Boveri range of stationary induction motors [9]. The air gap was increased because of the shocks occurring during traction service. The two-layer winding is contained in the semi-enclosed stator slots. Each layer has several series windings. The rotor winding

Table II: Comparison between an existing commutator motor as described in [8] and an induction motor of the same output rating and which is intended to supersede it. The main mechanical and electrical data are given.

		Existing Ae 4/4 II locomotive with commutator motors	Calculated values of induction motors for comparison
Motor			
Type		Pulsating current commutator motor	Squirrel-cage induction motor
Current		Rectified a.c. $16^2/_3$ Hz	Three-phase
Voltage range	V	0 to 1000[1]	0 to 1300[2]
Frequency range	Hz	0	0 to 80
No. of poles		8	4
Rated service data at 75 km/h		1145 kW, 980 V,[1] 1250 A,[1] 1150 rev/min	1145 kW, 1000 V,[2] 430 A,[2] 1414 rev/min, 47·5 Hz
Starting current	A	1700	1150
Max. speed (at 125 km/h)	rev/min	1880	2360
Permissible output at max. speed	kW	900 (approx.)	1500 (approx.)
No. of motors		4	4
Connection		All motors parallel	Separate supply to each motor
Weight	kg	3650	3150
Manufacturing costs	%	100	50 (approx.)
Drive			
Type		Brown Boveri spring drive with hollow shaft stub	
Wheel dia/axle dia	mm	1250/190	1250/190
Vertical travel of bogie suspension	mm	± 25	± 25
Transmission ratio		26:87 = 1:3·35	20:87 = 1:4·35
Locomotive			
Max. speed	km/h	125	125
Weight	10^3 kg	80	80
Tractive effort on starting	10^3 kg	32	32

[1] = Mean d.c. value
[2] = Per phase

is of the normal deep-bar type with copper short-circuit rings and bars. The bell-shaped rotor body is characteristic of Brown Boveri traction motors and combines the advantages of low weight and high flexural rigidity. The second feature is particularly welcome in view of the small air gap.

The more important data of the motor and drive are shown in Table II for comparison with those of the existing commutator motor type GRLM 763 St. It is obvious that the induction motor is lighter. The weight saving is about 15 %, thanks mainly to the 30 % higher transmission ratio. The number of poles is halved. The 4·35:1 transmission ratio is noticeably higher than that of many of the locomotives listed in Table I. It becomes obvious here that there is no restriction with regard to peripheral commutator speed as far as the induction motor is concerned. As shown in Fig. 3 the induction motor occupies less space on the bogie. Its overall dimensions are smaller and the distance between the centre-line of the axle and that of the motor is also smaller. If all possibilities were exploited the transmission ratio could be raised by a further 17 % to 5·1:1. The weight of the motor would then be 2800 kg which would be a saving of 22 %. The transmission ratio was limited to 4·35:1 because of the upper frequency limit of the static frequency changer.

A comparison of the respective weights agrees favourably with the results of a similar investigation carried out previously and described in [10]. In this case the existing motors of a Swiss Federal Railways class Re 4/4 II locomotive were used for comparison. They weighed 3860 kg for a power rating of 1195 kW. The calculated weight of a corresponding induction motor was 3200 kg which means a weight saving of 17 %.

Operating an Induction Motor with a Static Frequency Changer

For the purposes of this comparison a static frequency changer operating on the undershooting or 'subharmonic' principle was decided upon. The principle of this static frequency changer which was developed by Brown Boveri is described in [7]. The fundamental oscillation is in the form of an undershoot of the relatively high chopper frequency, hence the name undershoot principle. Various authors [4, 5, 6, 7] have stated that it is of advantage to operate the motor with constant air gap flux. The linear voltage/frequency characteristic corresponding to this is shown in Fig. 1. It applies to the 0 to 62 Hz frequency range. The duty point of the motor is at 47·5 Hz and the voltage is held constant between 62 and 80 Hz. In accordance with the voltage equation the flux is no longer constant but, instead, reduces in the ratio $\frac{f_1}{f_2}$ where $f_1 = 62$ Hz and f_2 is any arbitrary frequency between 62 and 80 Hz. The breakdown torque reduces in the same ratio but remains adequately large. Drawing an analogy with the series-wound commutator motor this is referred to as the 'field weakening range'. This design arrangement is very suitable for the purpose and has several advantages for both motor and frequency changer. Neither has to be overdimensioned for voltage. In any case the linear voltage rise up to 80 Hz would result in an excess of available power which is no longer necessary at maximum speed and cannot be transmitted to the rails when the motor is operating at rated current. This voltage restriction means a saving in semiconductor devices in the frequency changer.

Control

The motor operates on constant air gap flux. Under all operating conditions the primary voltage U_1 must be set such that this condition is satisfied. Measuring the flux by direct means is a complicated process and fraught with uncertainty, it is determined via the slip which can be derived from the difference between rotor and stator frequencies. A tachometer is fitted to the motor shaft for this purpose. The principle of combined current, slip and speed control is described in [7] and illustrated in Fig. 4. It can be seen that start and finish of each phase are connected to the corresponding frequency changer. Each motor has its own inverter and control system. Parallel supply to all motors from a common frequency changer would by no means ensure even loading on all four axles because of the differences in diameters of the driving wheels. Differences of up to 20 mm on driving wheels of 1250 mm diameter have to be tolerated within any traction bogie. Although this is a relatively small discrepancy (1·6 %) it is twice as large as the rated motor slip and would result in one motor running under no load while the other would be absorbing far too much current. The fixed shunt characteristic of induction motors makes itself felt in a disagreable manner here and incurs higher investment in heavy current and control equipment because each motor requires its own control system.

The control system limits the slip to a maximum permissible breakdown slip. The motor always operates in the range between synchronism and the balance point but in practice a respectful distance from the balance point is always maintained. Because of the continuously diminish-

Fig. 4 – Basic circuit diagram

Heavy current components
A = Transformer
B = Rectifier
C = LC smoothing unit
D = Inverter
E = Induction motor
F = Smoothing choke

Control components
1 = Speed regulator
2 = Current/slip characteristic
3 = Slip regulator
4 = Synchro transmitter
5 = Slip measuring device
6 = Grid control set
7 = Tacho-generator
n = Speed

Δn = Slip speed
i = Stator current
f = Stator frequency
$2U_g$ = Voltage in d.c. intermediate circuit

Indices
w = Set value
x = Actual value

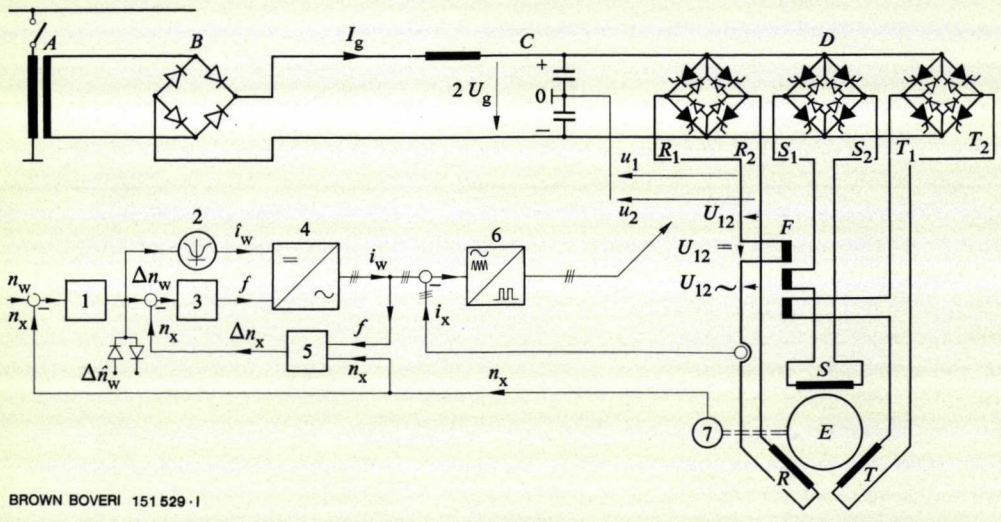

BROWN BOVERI 151 529 · I

ing power factor the torque curve is very flat at this point. Measures are therefore taken to ensure that the starting current does not exceed 60 to 70 % of the breakdown current.

Supply through the static frequency changer, as described above, combined with the control system provide the motor with good operating conditions and, from this, certain important factors apply to the design of the motor, such as:

– In the range between synchronism and the balance point the induction motor develops a torque which is approximately proportional to current. In this respect it behaves similarly to the commutator motor. The rotor resistance R_2' need not be designed as large as for starting with slip $s = 1$. The resistance may be as small as available space will allow (tooth saturation). This means that the temperature rise is kept within acceptable limits, even when starting under heavy load. The motor operates with low slip and high efficiency. As is usual for traction motors the starting current is between 170 and 200 % of the rated current and not several hundred per cent as is the case when starting with slip $s = 1$.

– Certain limitations are incurred, however, by the requirements of the inverter and the control system. In order to measure the slip to be able to control it without involving too much expensive equipment, its absolute value must not be too small.

– The breakdown torque normally has a certain safety factor to cater for voltage fluctuations in the supply system. This can now be dispensed with because the voltage is kept constant in the intermediate direct voltage circuit. Fluctuations of between + 15 % and − 20 % in the contact wire are compensated.

Time Harmonics in the Terminal Voltage

The very nature of static frequency changer engineering ensures that, apart from the fundamental wave, there are a number of time harmonics of various frequencies and amplitudes in the supply voltage. It is shown in [5] which harmonics occur during the undershooting process and how the motor current harmonics can be determined by graphical means. This process is very apt in this case because fractional harmonics can be dealt with without involving a complex mathematical process.

These considerations apply only to the frequency range involving rectangular voltages, i.e. 62 to 80 Hz in Fig. 3. In this range all the harmonics are of full numbers and of odd orders of magnitude. It has been shown in [11] how the sense of rotation of full number harmonics can be determined by applying the Fourier analysis. The amplitude, sense of rotation and slip of the harmonics contained in the rectangular voltages are given in Table III. All harmonics which can be divided by three are of the same phase and cannot therefore create a rotating field. They would create very high currents in the individual phases of the circuit shown in Fig. 4 if the smoothing chokes F were not present. These chokes prevent them from reach-

Table III: Amplitude, sense of rotation and slip of the harmonics contained in the rectangular voltage

Ordinal number ν	Amplitude	Sense of rotation	Angular velocity of the rotating field relative to the rotor at $s_1 = 0$	Slip s_ν at $s_1 = 0$
1	1	+	0	0
3	0·333	0		
5	0·2	−	− 6	1·2
7	0·143	+	+ 6	0·858
9	0·11	0		
11	0·091	−	− 12	1·09
13	0·077	+	+ 12	0·925
15	0·0665	0		
17	0·059	−	− 18	1·06
19	0·0525	+	+ 18	0·948
21	0·0475	0		
23	0·0435	−	− 24	1·042
25	0·04	+	+ 24	0·96

$s_\nu = \frac{\nu - 1 + s_1}{\nu}$ Slip of the harmonics with positive sense of rotation

$s_\nu = \frac{\nu + 1 - s_1}{\nu}$ Slip of the harmonics with negative sense of rotation

$s_1 = \frac{n_1 - n}{n_1}$ Slip of the fundamental oscillation (n_1 = synchronous speed, n = actual speed)

ing the windings. The following equations apply for the phase voltages which have a six-step waveform:

$$u_R = U_1\sqrt{2}\left[\sin \omega t + \frac{1}{5}\sin 5\,\omega t + \frac{1}{7}\sin 7\,\omega t + \frac{1}{11}\sin 11\,\omega t + \frac{1}{13}\sin 13\,\omega t + \ldots\right]$$

$$u_S = U_1\sqrt{2}\left[\sin\left(\omega t - \frac{2\pi}{3}\right) + \frac{1}{5}\sin\left(5\,\omega t - \frac{4\pi}{3}\right) + \frac{1}{7}\sin\left(7\,\omega t - \frac{2\pi}{3}\right) + \frac{1}{11}\sin\left(11\,\omega t - \frac{4\pi}{3}\right) + \ldots\right]$$

$$u_T = U_1\sqrt{2}\left[\sin\left(\omega t - \frac{4\pi}{3}\right) + \frac{1}{5}\sin\left(5\,\omega t - \frac{2\pi}{3}\right) + \frac{1}{7}\sin\left(7\,\omega t - \frac{4\pi}{3}\right) + \frac{1}{11}\sin\left(11\,\omega t - \frac{2\pi}{3}\right) + \ldots\right]$$

where
u_R, u_S and u_T are the instantaneous voltage values in phases R, S, T and $U_1\sqrt{2}$ is the amplitude of the fundamental wave.

How Time Harmonics Affect the Motor

As a matter of pure conjecture and without knowing the exact method of calculation, the following effects can be expected of the harmonics:

– the voltage harmonics cause current harmonics and flux harmonics resulting in additional copper and iron losses,
– depending on sense of rotation they can cause useful or braking torque at the motor and
– interaction between various harmonics can cause hunting.

These various effects caused by time harmonics must be considered separately from the effects of ripple due to the non-sinusoidal distribution of the current sheet (which creates ripple in the induction wave) and the slotting (slot harmonics in the induction wave). These are dependent solely on the geometry of the machine and occur even with purely sinusoidal terminal voltage.
The principle of superposition is assumed to apply for the calculation. Each harmonic has its own equivalent circuit diagram, as presented in [12]. All calculations are carried out in the same manner as for the fundamental oscillation; the only difference being that the processes take place at a higher frequency level.
A condition of applying the principle of superposition is that the current circuits under consideration are linear. This condition applies for calculating the additional copper losses but not for the iron losses because of the non-linearity of the magnetic field. According to [13] the very small amount of additional iron losses to be expected does not justify the time-consuming calculations involved in taking this non-linearity into account.

Fig. 5 – Resistances and leakage reactances of the induction motor referred to the frequency range 0 to 1000 Hz

f_1 = Stator frequency
f_2 = Rotor frequency
Parameters: Winding temperatures, a = 20 °C, b = 75 °C, c = 150 °C

1 = Stator resistance R_1 (a': at 20 °C but without taking skin effect outside the slot into account)
2 = Rotor resistance R_2 (a'': at 20 °C but without taking skin effect outside the slot into account)
3 = Rotor slot leakage permeability λ_{n2}
4 = Total leakage reactance of motor X_σ (d: without taking skin effect at rotor slot into account) for the sample calculation in Table IV at 75 °C
5 = Total motor resistance $R_1 + R_2'$ for the sample calculation in Table IV at 75 °C
For motor data see Table II.

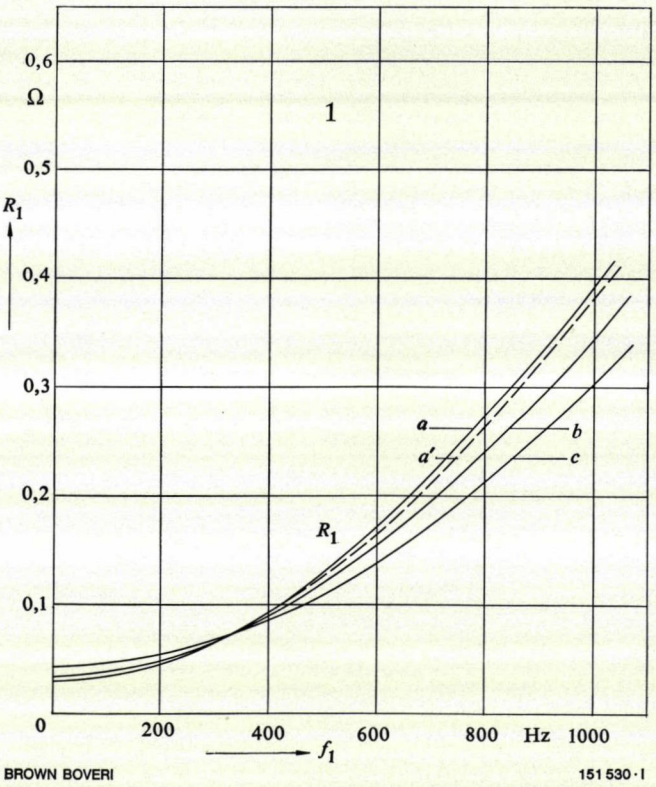

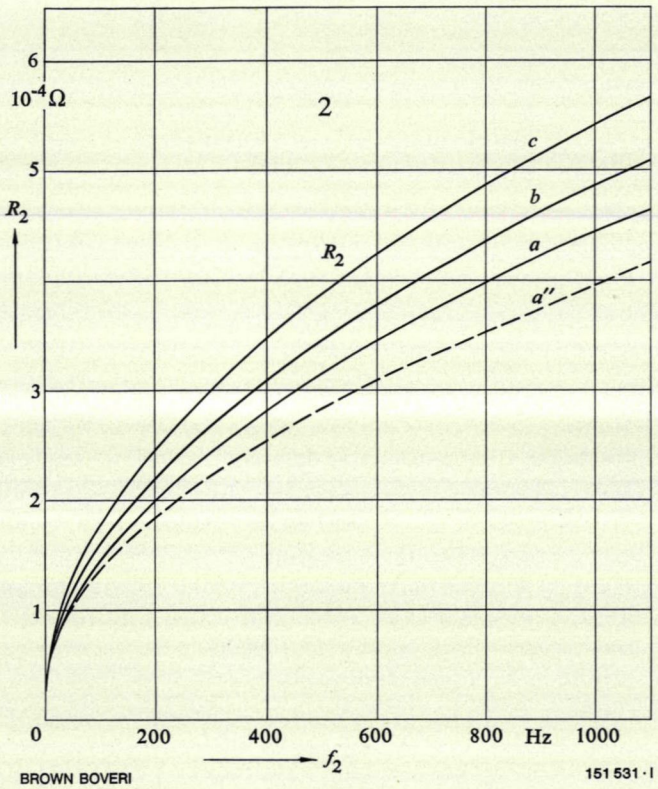
2
$10^{-4}\Omega$
R_2
6
5
3
2
1
0
200
400
600
800
Hz
1000
f_2
c
b
a
a''
R_2
BROWN BOVERI
151 531 · I

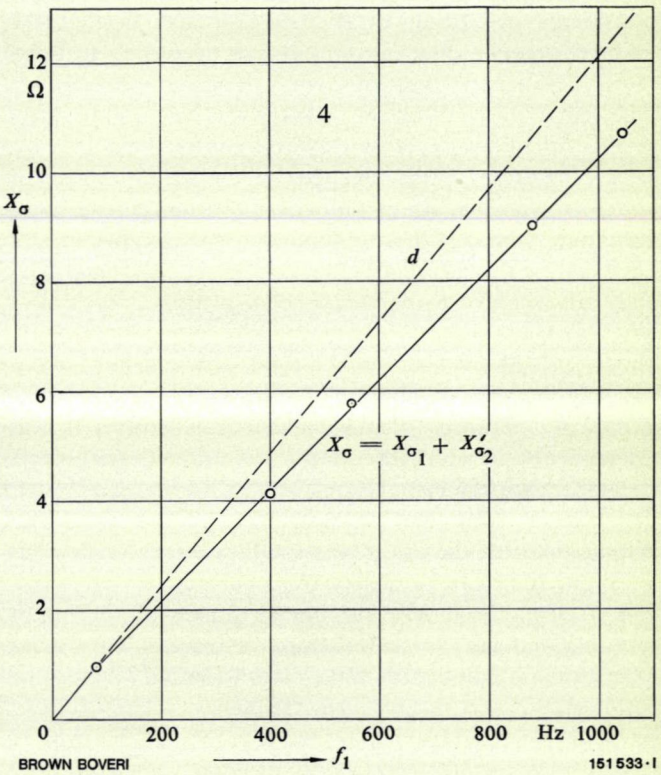
4
Ω
X_σ
12
10
8
6
4
2
0
200
400
600
800
Hz
1000
f_1
d
$X_\sigma = X_{\sigma_1} + X'_{\sigma_2}$
BROWN BOVERI
151 533 · I

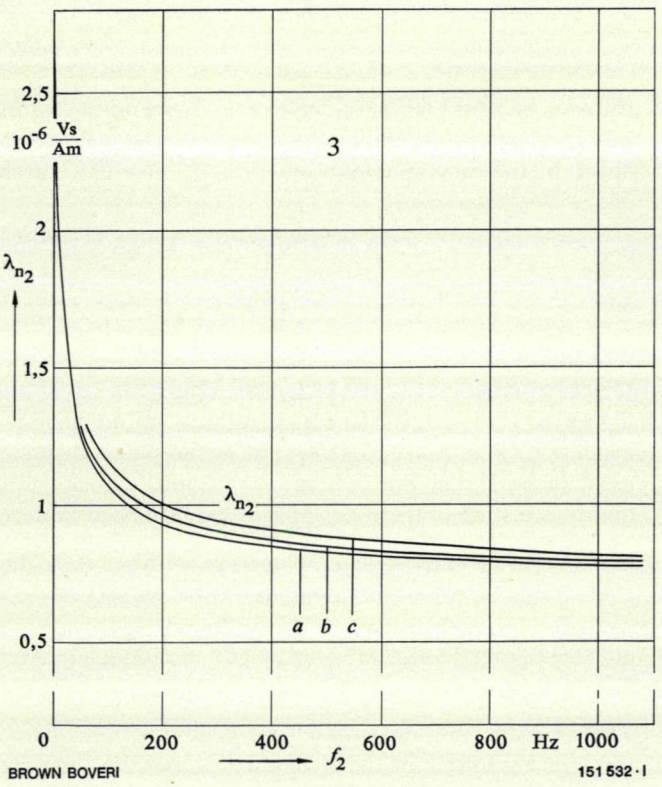
3
$10^{-6}\frac{Vs}{Am}$
λ_{n_2}
2,5
2
1,5
1
0,5
0
200
400
600
800
Hz
1000
f_2
λ_{n_2}
a b c
BROWN BOVERI
151 532 · I

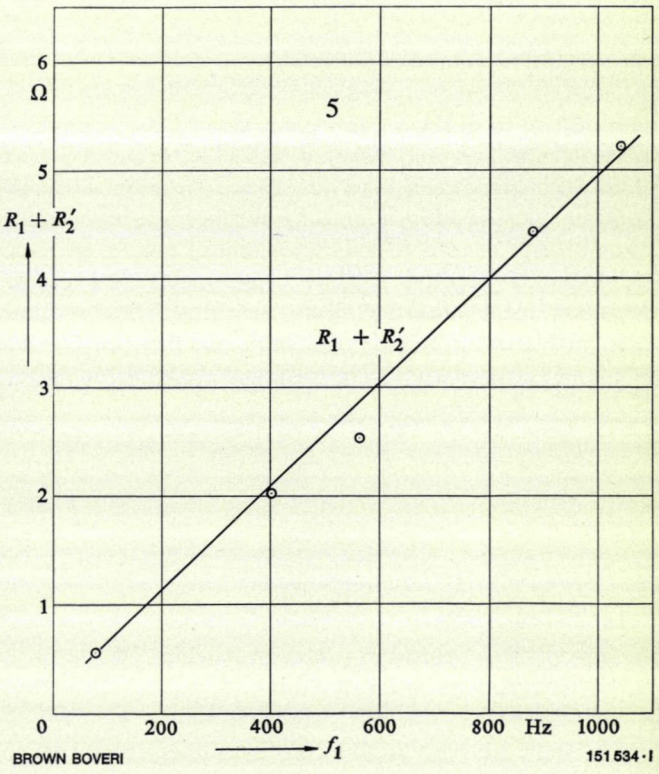
5
Ω
$R_1 + R'_2$
6
5
4
3
2
1
0
200
400
600
800
Hz
1000
f_1
$R_1 + R'_2$
BROWN BOVERI
151 534 · I

Resistances and Reactances of the Time Harmonics

In order to calculate the additional losses and hunting torques it is essential to know the resistance and leakage reactances of each frequency occurring. These values are shown in Fig. 5. The calculation was carried on up to 1000 Hz using 20 °C, 75 °C and 150 °C as parameters in every case.

The ratio of resistances in the stator and rotor windings was calculated according to the classic skin effect formulae. The skin effect of the stator winding outside the slot is considered according to Richter [14] and that of the squirrel-cage winding outside the slot according to Press [15].

The reduction in rotor slot leakage due to the skin effect is also calculated according to well-known formulae.

It is assumed that the leakages of the stator and rotor tooth crowns, the stator and rotor overhangs, the space harmonic (zig-zag) leakage and the leakage due to slot skewing are not affected by the skin effect, in other words they are assumed to be independent of frequency. Stator slot leakage is slightly reduced by skin effect. At 1000 Hz this is only about 1·5 % of the total motor leakage. Considering the very small amount involved (lying within the accuracy tolerances of the leakage calculation) it was decided not to make the stator slot leakage frequency-dependent for the calculation.

It is clearly seen that the skin effect of the stator slot winding outside the slot is very small, whereas a difference of about 10 % can be observed at the squirrel cage winding. Above about 300 Hz the resistance of the stator winding reduces as temperature increases. No similar phenomenon is apparent at the rotor winding. The turning point here is at a much higher frequency.

In spite of the huge reduction in rotor slot leakage to about 30% (at 1000 Hz) of its original value, the total leakage reactances with and without skin effect are only about 15 % apart. The rotor slot leakage is only about 20 % of the total leakage.

Torque due to Time Harmonics

Harmonics with slip of less than unity have a positive sense of rotation and develop a useful torque whereas those with slip greater than unity have a negative sense of rotation and develop a braking torque. The equivalent circuit for these time harmonics is that of reverse current, producing a negative torque. Consequently the motor consumes mechanical and electrical energy. These torques are calculated in exactly the same manner as for the fundamental oscillation. The torque of an induction motor is

$$M \sim \frac{I_2' \,.\, E_2' \,.\, \cos\varphi_2}{n_S} = \frac{I_2'^2 \,.\, R_2'^2}{n_S \,.\, s} \text{ [mkgf]}$$

or

$$M \sim I_2' \,.\, \hat{\Phi} \,.\, \sin(90 - \varphi_2) \text{ [mkgf]}$$

$I_2' \,.\, E_2' \,.\, \cos\varphi_2$ = Inherent power of machine [W]
n_S = Synchronous speed [rev/min]
s = Slip [p.u.]
φ_2 = Angle between I_2' and E_2' = Secondary phase angle
I_2' = Rotor current referred to primary side [A]
E_2' = Voltage induced in rotor, referred to primary side [V]
$\hat{\Phi}$ = Amplitude of air gap flux [10^6 Mx = 10^{-2} Vs]

With the resistances and reactances calculated earlier in this article it is possible to calculate currents and voltages and therefore also the torque of each harmonic. For example the torque of the 7th harmonic

$$M_7 = \frac{0{\cdot}974}{n_7} \,.\, 3 \,.\, I_{2_7}'^2 \,.\, \frac{R_{2_7}'}{s_7} \text{ [mkgf]}$$

and of the 5th harmonic

$$M_5 = -\frac{0{\cdot}974}{n_5} \,.\, 3 \,.\, I_{2_5}'^2 \,.\, \frac{R_{2_5}'}{s_5} \text{ [mkgf]}$$

In accordance with the statements made above the torque of the 5th harmonic has a negative sense of rotation.

Hunting Torques

Hunting can occur if the two factors I_2' and Φ or E_2', which create the torque, rotate at different synchronous speeds. This is illustrated in the vector diagram (Fig. 6). The torque of one phase is the product of the projection of vectors $E_2'\sqrt{2}$ and $I_2'\sqrt{2}$ to the true axis.

Hunting torques make no contribution towards forming a useful torque because their mean value with respect to time is zero. Each current I_{2_ν}' together with each air gap flux Φ_ν or E_{2_ν}' forms a torque ($\nu = 1, 5, 7, 11, 13, 17$, etc.).

With n voltages forming rotating fields there are
$n \,.\, n = n^2$ torques and hunting torques.

These can be broken down into

1	fundamental oscillation torque
$n - 1$	harmonic torques (useful or braking)
$n^2 - n$	hunting torques

By way of example let us calculate the hunting torque which results from interaction between the voltage induced by the fundamental oscillation E_{2_1}' and the current of the 7th harmonic I_{2_7}'.

The instantaneous value of the hunting torque phase R is

$$m_{7-1} = \frac{0{\cdot}974}{n_1} \,.\, I_{2_7}' \,.\, \sqrt{2}\sin(7\,\omega t - \varphi_2)\, E_{2_1}'\sqrt{2}\sin\omega t \text{ [mkgf]}$$

In the expression m_{7-1} the first index refers to current and the second to voltage. The actual indices are equal to the orders of magnitude. Angle φ_2 takes the phase displacement of both functions where $\omega t = 0$ into account. The hunting torques in the other phases are displaced in terms of time by $\frac{2\pi}{3}$ and $\frac{4\pi}{3}$, and as a total we have

$$m_{7-1} = \frac{0{\cdot}974}{n_1} \,.\, 3 \,.\, I_{2_7}' \,.\, E_{2_1}' \,.\, \cos(6\,\omega t - \varphi_2) \text{ [mkgf]}$$

The resultant hunting torque is a cosine function whereas the hunting torque of the individual phases are functions

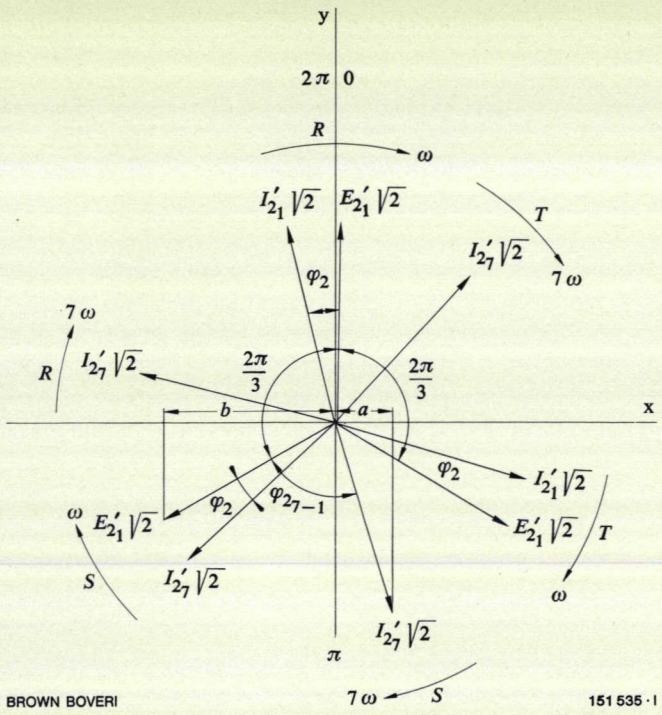

Fig. 6 – Vector diagram of the forces which cause torque and hunting torque in phases R, S and T of an induction motor

E'_{2_1} and I'_{2_1} refer to the fundamental oscillation and I'_{2_7} to the 7th harmonic.

Example: hunting torque in phase $S = a \,.\, b =$

$$= I'_{2_7}\sqrt{2}\sin\left(7\omega t - \frac{2\pi}{3} - \varphi_{2_{7-1}}\right) E'_{2_1}\sqrt{2}\sin\left(\omega t - \frac{2\pi}{3}\right)$$

at time $t = 0$
where
x = Real axis
y = Imaginary axis

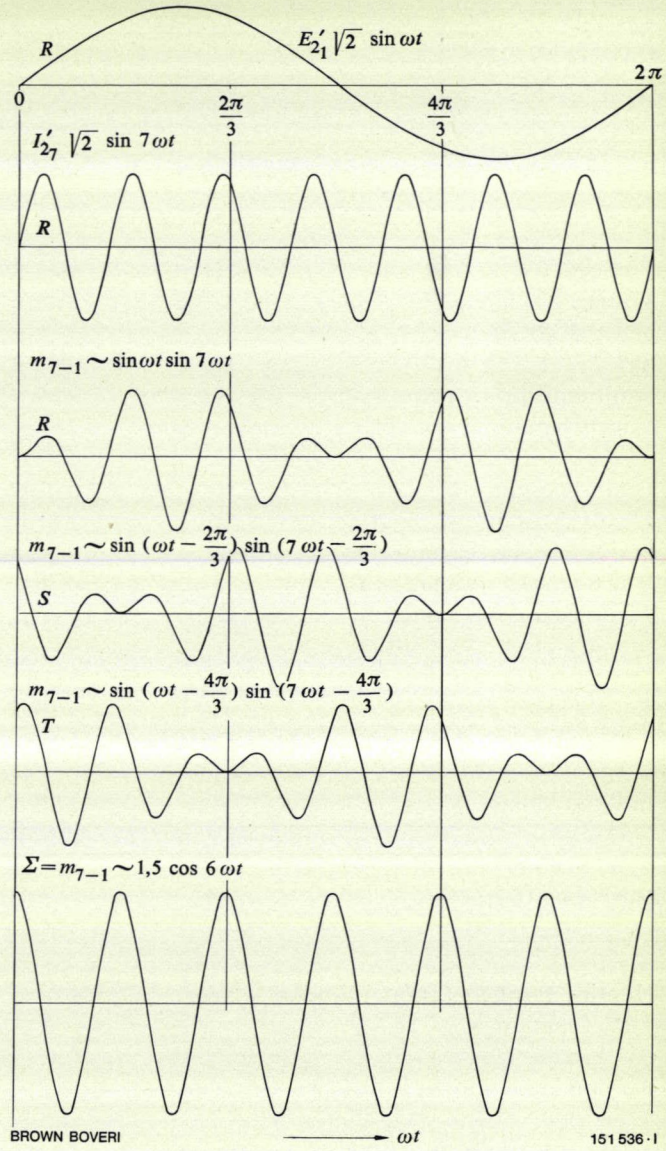

Fig. 7 – Hunting torques in phases R, S and T and their sum total, created in an induction motor by the air-gap flux of the fundamental oscillation Φ_1 or E'_{2_1} and current I'_{2_ν} of a harmonic

Example: 7th harmonic (current and voltage are shown for phase R only).

of $\sin\omega t \,.\, \sin 7\,\omega t$ (Fig. 7). Introducing angle φ_2 the hunting torque can be determined in its correct phase location. Angle φ_2 has no effect on the amplitude of the hunting torque.

This method enables any arbitrary hunting torque to be calculated. It must be considered, however, that certain voltage harmonics cause rotating fields with a negative sense of rotation. For instance, the hunting torque generated by the current of the 5th harmonic I'_{2_5} with the voltage of the fundamental oscillation E'_{2_1} is

$$m_{5-1} = \frac{0{\cdot}974}{n_1} \,.\, 3 \,.\, I'_{2_5} \,.\, E'_{2_1} \,.\, \cos(6\,\omega t + \pi - \varphi_2) \text{ [mkgf]}$$

The two hunting torques m_{7-1} and m_{5-1} are time functions of the same periodicity. Apart from angle φ_2 their phases are displaced by 180° and therefore they partly compensate each other. Angle φ_2 differs for each hunting torque. As has already been stated in [13] the hunting torques must be added geometrically.

The frequency of any arbitrary hunting torque can be derived from the difference in the orders of magnitude and the sense of rotation is given by the positive or negative sign, e.g.

$\omega_{m_{11-13}} = +\,|\,(-11) - (+13)\,| =$ 24 times the frequency of the fundamental oscillation

or

$\omega_{m_{7-11}} = +\,|\,(+\ 7) - (-11)\,| =$ 18 times the frequency of the fundamental oscillation

Sample Calculation

Using a concrete example with numerical values let us now examine the effects of the harmonics.

Operating point (fundamental oscillation): 1495 kW, 1300 V, 440 A, 2400 rev/min, 80 Hz, $s = 0{\cdot}0061$ p.u. The

Table IV: Results of loss calculation. Comparison between fundamental oscillation and harmonics. Reference temperature 75 °C

		Fundamental oscillation	5th harmonic	7th harmonic	11th harmonic	13th harmonic
Frequency f	Hz	80	400	560	880	1040
Voltage per phase U	V	1300	260	185	118	100
Sense of rotation		+	−	+	−	+
Slip s	p.u.	0·0061	1·2	0·858	1·09	0·925
Slip frequency of rotor f_{rot}	Hz	0·49	480	480	960	960
Synchronous speed n_s	rev/min	2400	12 000	16 800	26 400	31 200
Stator resistance R_1	Ω	0·039	0·09	0·14	0·285	0·362
Rotor resistance R'_2	Ω	0·0167	0·113	0·113	0·16	0·16
Motor resistance $R_1 + R'_2$	Ω	0·0557	0·203	0·253	0·445	0·522
Stator leakage reactance X_{σ_1}	Ω	0·59	0·295	4·12	6·5	7·68
Rotor leakage reactance X'_{σ_2}	Ω	0·38	1·16	1·63	2·5	2·97
Total leakage reactance X_σ	Ω	0·972	4·11	5·75	9·0	10·65
Primary or short-circuit current	A	440	63	32	13	9·4
Copper losses in rotor	W	9212	1340	347	81	43
Total copper losses	W	31 834	2420	775	226	139
	(%)	(100)		3560 (11·2)		
Induced voltage E'_2	V	1200	73	52	33	28
	(% of U)	(92·5)	(28)	(28)	(28)	(28)
Fundamental oscillation torque M_1	mkg	611	–	–	–	–
Harmonic torque M_ν	mkg	–	−0·091	+0·0236	−0·00275	+0·00142
				−0·06873		
Hunting torque $m_{\nu-1}$ (amplitude)	mkg	–	92	48	19	13·7
Time function			$\cos(6\omega t + \pi)$	$\cos 6\ \omega t$	$\cos(12\omega t + \pi)$	$\cos 12\ \omega t$
Air-gap flux $\hat{\Phi}_\delta$	10^6 Mx	7·45	0·0905	0·046	0·0185	0·0133
Air-gap induction $\hat{B}_\delta$	Gauss	6450	77·5	40	16	11·4
	(%)	(100)	(1·2)	(0·62)	(0·25)	(0·178)
Stator-yoke induction B_j	Gauss	11 500	312	143	64	46·5
Iron losses P_{Fe}	W	10 067	125	45	20	10
	(%)			200 . 3 = 600 (6)		
Additional losses P_{sp}	W	15 300	3500	1420	483	326
	(%)	(100)		5720 (37·4)		
Total losses P_{tot} (without mech. losses)	W	57 201		9880		
	(%)	(100)		(17)		

operating point selected is at the highest fundamental oscillation frequency and lies in the range of rectangular or six-step voltage (Fig. 1) which contains the 5th, 7th, 11th, 13th, 17th, 19th etc. harmonics.

All results apply to 75 °C winding temperature. They are listed in Table IV and cover the range up to the 13th harmonic.

It is clearly shown that the additional copper losses amount to 3560 W which corresponds to 11·2 % of the copper losses at fundamental oscillation or 12·2 % referred to the rated operating point at 47·5 Hz according to Table II. This amount cannot be ignored. More than half of it (2420 W) is caused by the 5th harmonic. Viewed as a whole, the additional copper losses occur half at the stator and half at the rotor.

The useful and braking torques due to harmonics have no decisive numerical influence. The large slip indicates that the harmonics operate virtually in a short circuit and therefore cannot create any power worth mentioning. The sum total is a very small braking torque of 0·06873 mkg.

In accordance with a statement made earlier, in the case of $n = 5$ voltages creating rotating fields there are $n(n-1) = 20$ hunting torques. The numerical values for the following sample calculations are also given in the Table. Of these, only four are considered in Table IV, i.e. those which are caused by interaction between the harmonic

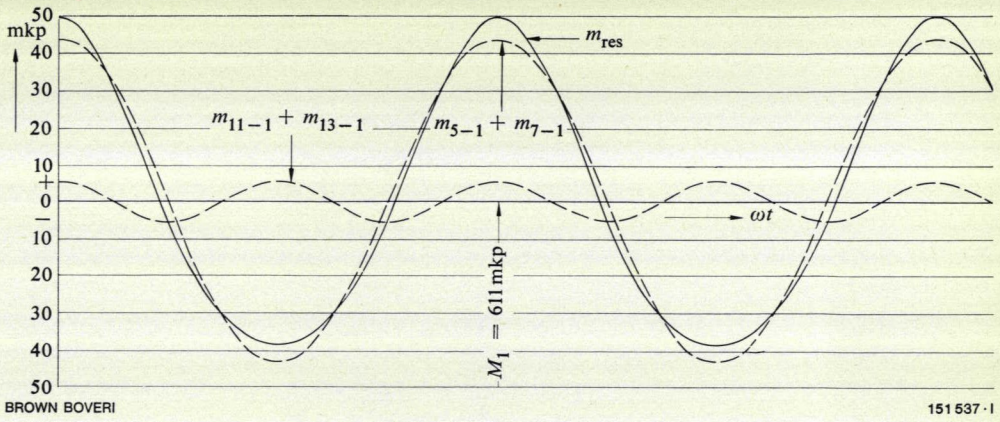

Fig. 8 – Hunting torques of the 5th, 7th, 11th and 13th harmonics at the shaft of an induction motor (sample calculation at 80 Hz fundamental oscillation frequency)

M_1 = Torque due to fundamental oscillation
$m_{5-1} + m_{7-1}$;
$m_{11-1} + m_{13-1}$ = Hunting torques
m_{res} = Resultant hunting torque (480 Hz)

currents $I'_{2\nu}$ and the fundamental oscillation flux Φ_1 or E'_{2_1}. All other hunting torques become infinitesimally small because of the low value of the harmonic flux $\Phi_\nu \sim \frac{E'_{2\nu}}{n_\nu}$ and are of no further interest. Their amplitudes are in the range 0·04 to 4 mkgf, and their frequencies are the 6th, 12th, 18th or 24th multiples of the frequency of the fundamental oscillation.

The four hunting torques $m_{\nu-1}$ listed in Table IV must be added geometrically to find the resultant hunting torque while taking angle φ_2 into account. From the vector diagrams it was found that in every case angle $\varphi_2 = \sphericalangle (E'_{2_1}, I'_{2\nu}) = 76°$. This means that hunting torques of equal periodicity can be added algebraically

$$m_{5-1} + m_{7-1} = 46 \ (\cos 6\,\omega t + \pi) \quad [\text{mkgf}]$$
$$m_{11-1} + m_{13-1} = 5{\cdot}3 \ (\cos 12\,\omega t + \pi) \quad [\text{mkgf}]$$

These two functions are added geometrically to give the resultant hunting torque (Fig. 8) which is superposed on the torque of the fundamental oscillation. The amplitudes of the hunting torques attain a mean value of 7·5 % of the fundamental oscillation. This value can also be described as torque ripple.

Calculated according to the superposition method the additional iron losses are very small. As shown in Table IV the majority (72 %) of the harmonic voltages are absorbed by the primary leakage reactance. The harmonic air-gap flux $\hat{\Phi}_\nu = \hat{\Phi}_1 \cdot \frac{E_\nu}{E_1} \cdot \frac{f_1}{f_\nu}$ reduces correspondingly and therefore so does the additional loading of the magnetic circuit. However, it must be considered here that the flux in the stator yoke deviates considerably from the air-gap flux. Nevertheless, the absolute values are very small. This also applies to the induction in the teeth. The resultant additional iron losses are about 200 W or 2·5 % of the iron losses of the fundamental oscillation. Because of the nonlinearity of the magnetic flux, however, there is some uncertainty in calculating the additional iron losses. To be on the safe side, therefore, three times the value is used in the calculations, i.e. 600 W or 7·5 %.

The additional losses generally referred to as stray load losses have also to be taken into account. They are caused by the rotor and stator slot configurations, the leakage fluxes of stator and rotor overhangs and skew-leakage fluxes. Because of the relatively smaller air gaps, the stray load losses of induction machines are rather more prominent than in other electrical machines. The stray load losses occur at the surface and in the teeth of the stator and rotor iron, in the squirrel cage windings and in the inactive components such as end shields, pressure plates and frame ends. It would be too much to investigate here the origin of these losses and even calculate them. Actual sample calculations are given in [12] and [16] and the literature survey [17] quotes 24 publications.

The fundamental oscillation as well as the harmonics (in the stator voltage supply) cause such stray load losses. The results are listed in Table IV. The losses due to the fundamental oscillation are assumed to be 1 % of the consumed active power of the fundamental oscillation, i.e. an average value derived from a large number of measurements carried out on machines of this size range. The values for the harmonics are calculated from the stray load losses due to the fundamental oscillation using the conversion factor $\left(\frac{I_\nu}{I_1}\right)^2 \cdot \left(\frac{f_\nu}{f_1}\right)^{1.5}$. The powers 2 and 1·5 are empirical values gained from experience and can vary between certain limits from case to case. It is also possible for the stray load losses due to the fundamental oscillation to equal 0·5 % of the consumed power. The stray load losses due to the harmonics would reduce by a corresponding amount. It can be seen that the stray load losses (5720 W) are more than the additional copper losses.

The total additional losses are 9880 W or 17 % of the losses of the fundamental wave (without mechanical losses) or 20 % referred to the defined operating point at 47·5 Hz.

Other authors obtained similar results. It is shown in [12] that the additional losses of a motor are 20 % of the losses in the fundamental oscillation (at the same six-step voltage wave form as used in the case under consideration here). It is shown in [16] that the additional losses due to slot skewing can reach very considerable values.

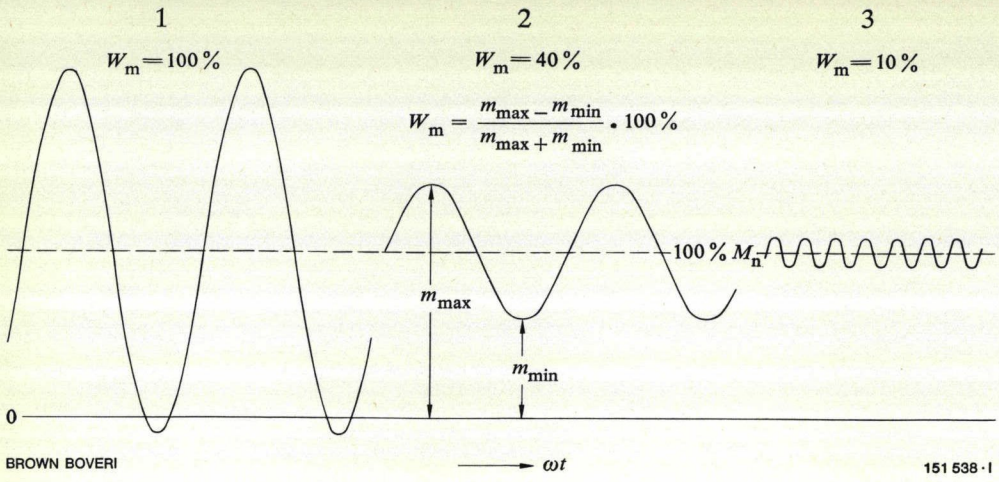

Fig. 9 – Torque curves with respect to time of three different types of traction motor

1 = Single-phase a.c. commutator motor
2 = Pulsating current motor
3 = Induction motor with supply through static frequency changer
M_n = Rated torque
W_m = Torque ripple

How Harmonic Phenomena Affect Motor Design

There are no reasonable means of preventing the flow of harmonic currents. For economic reasons it is out of the question to fit filters. Harmonic currents and their consequences must be accepted as being an inherent fact.

The additional copper losses cause a greater temperature rise in the windings but this can be taken into account in the stator windings by applying new types of insulation materials with higher thermal stability. Other feasible measures include enlarging the cooling surfaces and/or increasing the ventilation.

Particular attention must be paid to the squirrel cage winding. It is a known fact that excessively high losses can cause dangerous mechanical stresses in the bars and rings. Where the slots are skewed the additional losses can be kept low by insulating the bars but this measure is avoided wherever possible.

Hunting torques are not unusual as far as traction motors are concerned. With single-phase commutator motors the torque pulsation is 100 %. It is about 40 % in the pulsating current motor used here for comparison (Fig. 9). We are concerned here with the hunting torque occurring at the periphery of the rotor. Because of the mass of the rotor and the very slight elasticity between the shaft journals and the stacks of laminations, the torque pulsations appearing at the motor shaft are greatly reduced. Whereas the frequency of the hunting torque of pulsating current motors remains constant throughout the speed range, this is not the case with the induction motor. The amplitude of the hunting torque remains virtually constant for a given frequency of fundamental oscillation. At small driving torques the hunting torque passes through zero and causes negative torque for certain periods of time. These jarring vibrations must be taken into account at the design stage.

One means of reducing these harmonic currents is to increase the leakage reactance. As far as the static frequency changer is concerned it is also desirable to keep the harmonic currents as low as possible because these also affect its design output. The more harmonic currents involved, the more semiconductor devices required.

At high leakage inductance X_σ the harmonics reduce at a ratio of $\frac{1}{X_\sigma}$ if the voltage is constant. On the other hand the breakdown torque of the fundamental oscillation also reduces in the same ratio. In the motor under consideration this is 220 % of the rated torque or 147 % of the starting torque. The breakdown torque would therefore be reduced to 118 % of the starting torque. It can be seen that the higher the torque utilization of the motor becomes, the tighter are the limits within which the leakage reactance can be increased. It must also be considered that the breakdown torque remains inversely proportional to the frequency within the field weakening range. The earlier the field weakening range commences, the greater the breakdown torque must be within the range of the linear voltage/frequency characteristic in order to remain adequate at maximum frequency. The breakdown torque is shown in Fig. 1 for 25 % higher leakage reactance and also for the case where field weakening commences from the defined rated operating point at 47·5 Hz.

How Additional Losses and Hunting Torques are Affected by the Slip and Frequency of the Fundamental Oscillation

All values which cause additional copper losses are virtually independent of the slip in the fundamental oscillation. The change in the slip of the harmonics in relation to the slip of the fundamental oscillation is very small in the range under consideration (between synchronism and breakdown torque), i.e.

$$s_\nu = \frac{\nu \pm 1 \pm s_1}{\nu}$$

For the four numerically largest hunting torques $m_{\nu-1}$ there can be at most a slip-dependence of this nature when the induced voltage E'_{2_1} changes slightly as slip increases while the motor is operating at constant voltage. The hunting torque would thus be at a maximum when the motor is running under no load. On the other hand, if the motor is operated at constant flux, voltage E'_{2_1} remains constant and the terminal voltage must be raised slightly relative to the current or slip. The hunting torques would then be smallest with the motor running under no load and as slip increases they would grow linearly with the voltage rise. The copper losses and, as an approximation, the iron losses and stray load losses, vary as the square of the voltage increase. It is impossible to derive a general rule to cover the relationship between frequency, additional losses and hunting torques. The harmonic voltages and their frequency spectra as well as the resistances and reactances vary for each value of the fundamental oscillation.

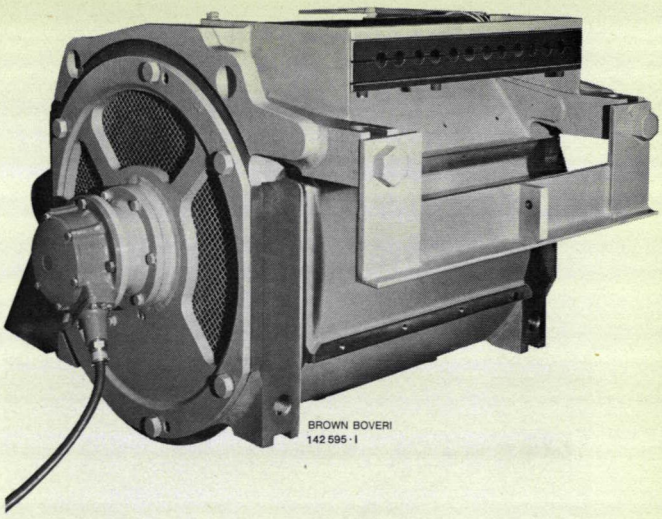

Fig. 10 – Prototype 250 kW induction motor
A tacho-generator is fitted at left for measuring the slip.

General Comparison Between Commutator Motors and Induction Motors

Because of its simple design the induction motor is expected to have several important advantages in traction applications. In comparison, experience has shown that the following service results are to be expected from a commutator motor:

– Brush wear about 0·1 mm per 1000 km. This was measured at the pulsating current motor used in the comparison. Assuming a useful length of 40 mm this means a brush life of 400 000 km. The normal brush wear in single-phase a.c. motors is 0·2 to 0·25 mm/1000 km.
– Commutator life about 30 to 50 years. These values can be attained in service or can be calculated from test measurements. For example, a commutator was skimmed down after 1·2 million kilometres of service. The diameter was found to be 1·5 mm less than in the original condition. With a permissible wear of 20 mm on the diameter, the life of the commutator can be calculated as $\frac{20}{1{\cdot}5} \cdot 1{\cdot}2 = 16$ million kilometres. If the vehicle covers 300 000 km in service annually the commutator can be expected to last about 50 years.
– Winding life about 20 to 30 years. Under favourable conditions windings with insulation corresponding to class B can attain these figures whereas class F insulation, together with impregnation under vacuum, is expected to increase the life still further.

These life expectancies for the individual machine components apply only for favourable operating conditions. It can happen, however, that commutator traction motors suffer damage at a comparatively early stage of their lives. More often than not it is the commutator or rotor winding which suffers most. Although a great deal of progress has been made in the design and manufacture of commutator motors there remains a certain amount of uncertainty and a certain breakdown rate.

It is expected that the induction motor will overcome virtually all these drawbacks and there will also no longer be any brushes to change or commutators or brush mechanisms to inspect.
Although maintenance will be greatly reduced, the induction motor will require a certain amount of attention. The bearings will still require lubrication and the stator winding insulation will still be subjected to the well known ageing processes. The mechanical stresses in the cage windings, due to higher utilization, require special attention. These stresses are caused by centrifugal forces and thermal expansion. In addition to this the bars are pressed against the slot bottom by a force which pulsates at twice the slip frequency. This problem has been given special attention in recent publications [18, 19]. Experience gained with stationary motors must be given due consideration with respect to traction requirements.

Prototype

In order to gain practical experience with induction motors supplied through static frequency changers, Swiss Federal Railways placed an order for a motorcoach with prototype electrical equipment by Brown Boveri. The prototype motor used is shown in Fig. 10. It has a continuous rating of 250 kW at 283 V phase voltage and 50 Hz. The maximum values for this four-pole motor are 360 V and 100 Hz. In the lower frequency range the static frequency changer operates on the undershooting or 'subharmonic' principle whereas in the upper range the six-step or rectangular voltage is applied to the motor windings. Exhaustive laboratory tests were carried out in the 0 to 100 Hz range with both sinusoidal and distorted terminal voltages. The tests showed that the behaviour of the motor satisfied every expectation. Oscillograms of current and voltage, made while the motor was supplied through the static frequency changer, are shown in Fig. 11. The undershooting process is shown on the left with the six-step waveform on the right.

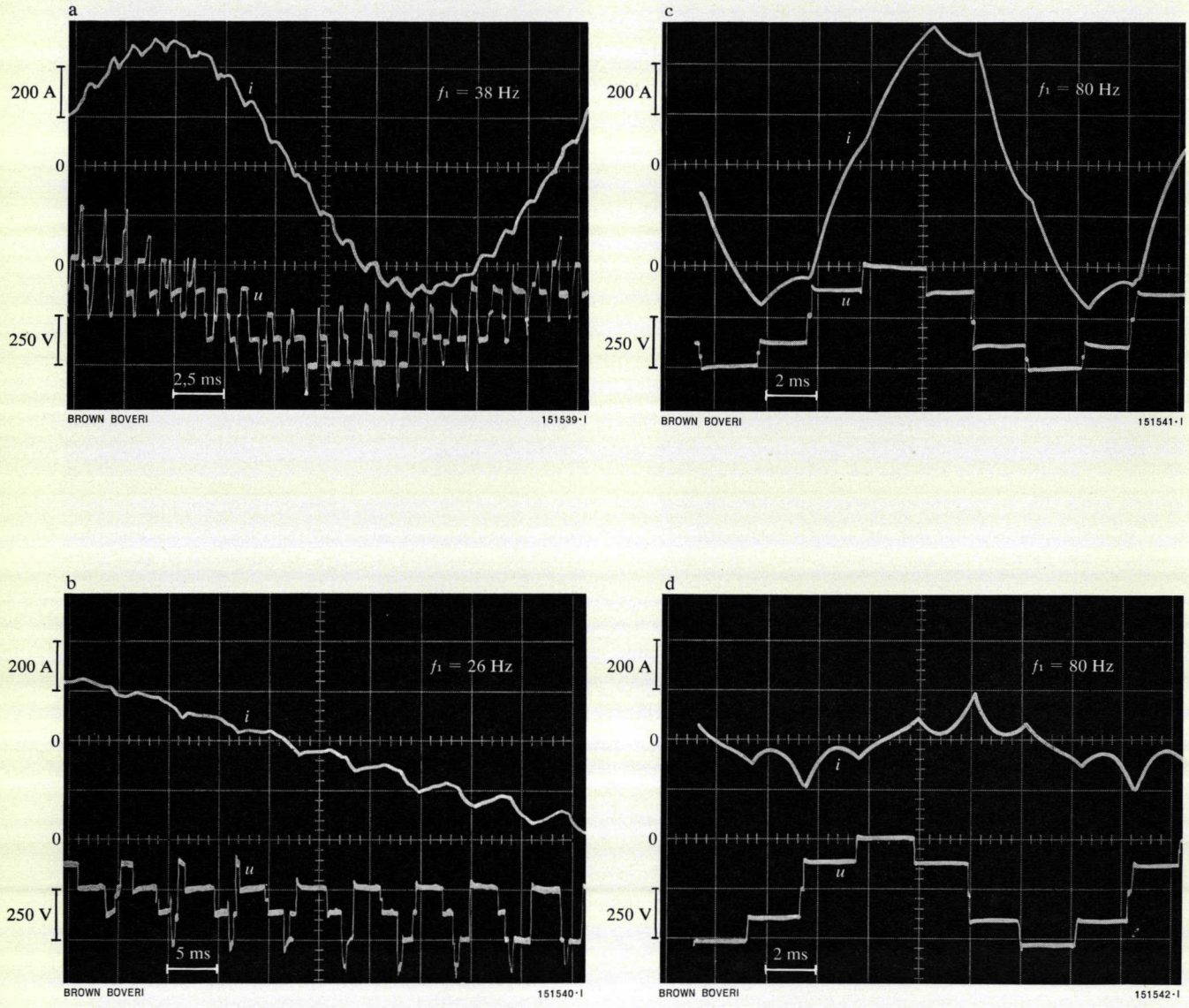

Fig. 11 – Oscillographic recordings of current and voltage of the prototype motor shown in Fig. 10 while supplied through a static frequency changer

Left: Undershooting
Right: Six-step

f_1 = Fundamental oscillation
u = Voltage per phase
i = Current per phase

a: U = 214 V, I = 340 A
b: U = 148 V, I = 245 A
c: U = 360 V, I = 355 A
d: U = 360 V, I = 80 A
} r.m.s. values per phase

a, b, c: Motor current under load (b: transition from positive to negative halfwave)
d: Motor current under no load = short-circuit current of the harmonics + magnetizing current of the fundamental oscillation.
The voltage in the d.c. intermediate circuit is 400 V.

Bibliography

[1] *E. Hugentobler:* Modernization of two typical Swiss mountain railways. Brown Boveri Rev. 1947 *34* (12) 239–248.

[2] *G. Bodmer, P. Leyvraz, E. Anderegg, H. Süssli:* The Oerlikon 50 cycles goods locomotives C_0C_0, serial numbers 14001 to 14020 of the Société Nationale des Chemins de fer Français (SNCF). Bull. Oerlikon 1957 (320) 1–24.

[3] *E. Rodewald:* Die Asynchronmaschine bei Betrieb mit kleiner Frequenz. Elektrotech. Z. 1933 *54* (33) 793–796.

[4] *K. Heumann, K. G. Jordan:* Das Verhalten des Käfigläufermotors bei veränderlicher Speisefrequenz und Stromregelung. AEG-Mitt. 1964 *54* (1/2) 107–116.

[5] *A. Schönung, H. Stemmler:* Static frequency changers with subharmonic control in conjunction with reversible variable-speed a.c. drives. Brown Boveri Rev. 1964 *51* (8/9) 555–577.

[6] *T. Berger:* Betriebsverhalten frequenzgesteuerter Asynchronmaschinen. Elektrie 1964 *18* (4) 120–126 and (5) 154–156.

[7] *H. Hödle, H. Stemmler:* New equipment and control systems for a.c. traction vehicles. Brown Boveri Rev. 1965 *52* (9/10) 706–719.

[8] *E. Kocher, E. Isler, A. Fehr*: The Ae 4/4 II rectifier locomotives of the Berne–Lötschberg–Simplon Railway. Brown Boveri Rev. 1965 *52* (9/10) 661–679.

[9] *E. Wiedemann, H. Nordmann, G. Schuster:* New medium-output high-voltage squirrel-cage motors. Brown Boveri Rev. 1967 *54* (9) 519–523.

[10] *P. Laube:* Das Betriebsverhalten des asynchronen Käfigläufermotors als Fahrmotor für Vollbahnlokomotiven. Elekt. Bahnen 1968 *39* (10) 227–233.

[11] *G. C. Jain:* The effect of voltage wave shape on the performance of a three-phase induction motor. IEEE Trans. Pwr Appar. & Syst. 1964 *83* (6) 561–566.

[12] *E. A. Klingshirn, H. E. Jordan:* Polyphase induction motor performance and losses on nonsinusoidal voltage sources. IEEE Trans. Pwr Appar. & Syst. 1968 *87* (3) 624–631.

[13] *K. Heumann, K. G. Jordan:* Einfluss von Spannungs- und Stromoberschwingungen auf den Betrieb von Asynchronmaschinen. AEG-Mitt. 1964 *54* (1/2) 117–125.

[14] *R. Richter:* Elektrische Maschinen. Vol. 1, Birkhäuser. Basle 1951.

[15] *A. Press:* Resistance and reactance of massed rectangular conductors. Phys. Rev. II, 1916 *VIII* (4) 417–422.

[16] *B. J. Chalmers, B. R. Sarkar:* Induction-motor losses due to nonsinusoidal supply waveforms. Proc. Instn elect. Engrs 1968 *115* (12) 1777–1782.

[17] *K. K. Schwarz:* Survey of basic stray losses in squirrel-cage induction motors. Proc. Instn elect. Engrs 1964 *111* (9) 1564–1574.

[18] *K. Schweizer:* Stabbrüche bei Käfigläufern von Asynchronmotoren. Thesis, TH Stuttgart, 1966.

[19] *R. Blanchardie, J. Chatelain, M. Jufer, M. Pasdeloup:* Comportement en régime transitoire des cages de moteurs asynchrones. Rev. gén. Elect. 1966 *75* (9) 1059–1070.

Automatic Frequency Changing with Short-Wave Broadcast Transmitters

L. Leng

621.396.714.029.55

The factors favouring automatic frequency changing with short-wave transmitters are considered and the processes controlled by the automatic system are described. Particular reference is made to fine tuning and the discriminators used for this. These convert the requisite RF quantities into control voltages for the actuating drives. Finally, the basic electronic equipment and remote transmitter control are considered.

The Reasons for Automatic Control

Short-wave broadcast transmitters are mainly used for transmitting programmes over large distances, usually to other countries. There are two reasons why transmitters of this kind often have to change frequency during the course of a day. The first concerns conditions along the transmission path. This passes via the ionosphere, the state of which is affected by solar radiation. Consequently, different frequencies have to be used at different times of the day. The second reason concerns the programmes themselves. When transmitting over large distances, the time of day at the receiver is different from that at the transmitter. In order to reach as many listeners as possible the transmission times are adapted to suit the habits of the prospective audience. As a result, different areas are covered at different times of the day, so again the frequency has to be altered.

The frequency must be changed as quickly as possible so that little transmission time is lost. With high-power transmitters this means that the devices which have to be regulated need to be power-actuated because low-geared manual operation would take a considerable time. However, it is still a big step from motorized operation to full automatic control. If this is considered necessary today, there have to be good reasons to justify the decision.

Further time savings are made possible by automatic control because all the controlled devices are adjusted at the same time. It is also becoming increasingly difficult to find suitable staff. Manual operation is uneconomical because staff are required only while the frequency is being changed, and are then unoccupied for long periods. Automatic control also eliminates human error, which has to be taken into account particularly when properly qualified people are not available.

Automation is essential if the transmitter is to be remote controlled. Short-wave stations with a number of transmitters also have a great number of aerials, and these occupy a large area. Long RF feeders cause power losses. For this reason, and to have more freedom in arranging the equipment, there is often much to be gained from dividing the transmitters into groups. Each group is then housed in its own transmitter building, which is in turn located at the middle of the relevant aerial group. Operation must be from a central point, however, if the advantages mentioned are not to be cancelled out by the need for more personnel. This control centre is contained in the main transmitter building, or even in the studio.

The aerials and programme links can be remotely selected with this type of installation. Moreover, with remote control it is possible to control the programme by computer. The present article, however, is limited to those problems which affect the transmitters themselves.

Features Required of Transmitters and Control System

The following features required of the transmitters are not so much actually stipulated by the automatic control system as emphasized by it.

– The number of RF must be reduced to a minimum, so as to lower the number of items which need to be regulated. This is done by using tetrodes up to the high-power output stage. This presents no problem with modern tubes. The preamplifiers are aperiodic, either over the whole frequency range or within a number of selectable parts of the range. They therefore need no fine adjustment.

– The high-power RF stages, up to the output stage, must be designed principally in terms of their RF performance, and should not be complicated by requirements arising from the automatic control system. Π- and L-networks are

particularly suitable; they have the theoretical minimum of control elements, i.e. one for tuning and one for load regulation. The purpose of the automatic control system is thus to simulate manual regulation. This is considered in more detail later.

The automatic control system can come up to expectations only if all its component parts are extremely reliable. Also, it must be possible to locate faults quickly and replace the affected part without delay. Facilities must also be provided for manual operation, should a serious fault occur.

Criteria and Stages of Frequency Adjustment

With any transmitter it must be possible to switch to a certain number of frequencies. These are specified in each case, each frequency corresponding to theoretically determined settings of the controlled devices. However, it is not sufficient simply to store these settings. There are two reasons for this.

The temperature of the transmitter has an influence on the RF characteristics of the components. Conditions are different, depending on whether the transmitter has just been turned on, or has had time to warm up.

The aerials in use have an even greater influence. It is not possible in every instance to match the aerial so perfectly that it provides the transmitter with a clearly defined, pure ohmic impedance. Modern aerials are usually of the wide-band type, and errors in matching to the individual frequencies are unavoidable. Also, with directional aerials the beam wanders both horizontally and vertically, which gives rise to matching errors. Weather conditions, especially icing, cause large changes in the impedance.

The output stage of the transmitter is therefore so designed that all matching errors can be corrected up to a standing wave ratio of 2:1. This correction, in the form of a fine adjustment, is performed by the automatic control system.

A distinction must therefore be made between coarse and fine adjustment. Coarse adjustment brings the components to stored settings which are as close as possible to the correct operating condition. This is sufficient for certain less critical adjustments. Important adjustments, however, such as tuning and load regulation, undergo fine adjustment, in which case they are controlled by the main RF characteristics. These characteristics are converted to control voltages by means of discriminators.

To reduce the number of storage elements required for fine adjustment, the frequency bands employed are divided into channels. The coarse setting then corresponds to the middle frequency of the channel in question. The purpose of fine adjustment is thus to correct the difference between this middle frequency and the operating frequency.

The stages in setting a transmitter to a certain frequency, and also changing from one frequency to another, can be summarized as follows.

a. The desired operating frequency is set by means of push-buttons, or one of the stored frequencies is selected. This can be done while the transmitter is in operation (preselection).

b. By pressing buttons the selected frequency is passed to the decade oscillator and also to the storage elements for coarse adjustment, whereupon the anode voltage is automatically reduced by the thyristor control system, i.e. no switches are operated. The positions of the switch drives are determined in the same way. Coarse adjustment then commences. The drives stop as soon as the stored positions are reached sufficiently accurately.

c. For the less critical adjustments and the switch drives the procedure ends with stage b. The drives of the critical components are set to fine adjustment, i.e. they receive a control voltage from the discriminators. At the same time the anode voltages are switched to lower values and then within a certain time increased automatically to the normal value. When this procedure is completed, the operating condition has been reached. This is indicated by the fact that the control voltages are then at their minimum. Modulation can then begin.

d. During operation the motors are stopped by control voltages from the discriminators, and the discriminators are connected to a supervisory circuit. This is because there is no need to correct every variation immediately. Periodic variations occur, for example, when the aerial sways in the wind. It would be pointless to correct these oscillations and would only cause wear in the moving parts. On the other hand, persistent variations, due to temperature for example, must be corrected once they reach a certain value. The supervisory circuit contains an integrating network. When the output voltage of this reaches a certain value, the discriminator is again connected to the appropriate control drive.

This procedure also prevents the control drives from being affected arbitrarily by internal tube discharges, lightning striking the aerial, and so on, as this would completely upset the controlled condition.

Fine adjustment is dealt with in a later section. For this one must also consider the discriminators used. The latest type of 250 kW transmitter has been chosen as a specific example.

The RF Section of the 250 kW Short-Wave Transmitter

The carrier power of this transmitter can be utilized with up to 100 % modulation in the case of sinusoidal modulation, and 95 % with trapezoidal modulation. The frequency range is 3·9 to 26·1 MHz. The output stage is anode-modulated, and the screen grid is also modulated.

The basic version has an asymmetrical output for 50 Ω. If symmetrical connection to the aerials is specified, a balun can be added which, basically aperiodically, transforms the 50 Ω asymmetrical to 300 Ω symmetrical.

The stages of the RF section can be seen in the block diagram of Fig. 1. The circuits from the output of the final-stage tubes to the transmitter output are shown in Fig. 2. This part poses special problems as regards fine adjustment. This does not apply to the harmonic filter F_1, however, which is less critical and is therefore only coarsely adjusted.

Fig. 2 also shows the discriminators required for this part of the transmitter, the drive motors with their servo-amplifiers, and the position store for coarse adjustment. The switch for changing between coarse and fine adjustment is also shown.

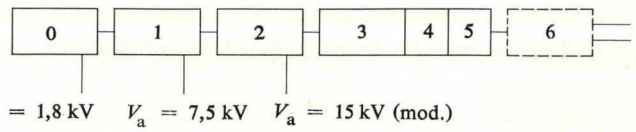

Fig. 1 – Block diagram of the RF section of a 250 kW short-wave transmitter with a frequency range of 3·9 to 26·1 MHz

0 = Decade oscillator
1 = Transistorized preamplifier
2 = Driver stage with tetrode CQL 5–1
3 = Output stage with tetrode CQS 200
4 = Tunable harmonic filter
5 = Supplementary, fixed filter 45 to 230 MHz
6 = Balun (alternatively, 50 Ω asymm./300 Ω symm.)
V_a = Anode voltage

Discriminators

Fine adjustment is governed by certain RF quantities. As mentioned earlier, these are converted into suitable control voltages by means of discriminators. Two types are used, a phase discriminator for tuning and a load discriminator for matching the load conditions.

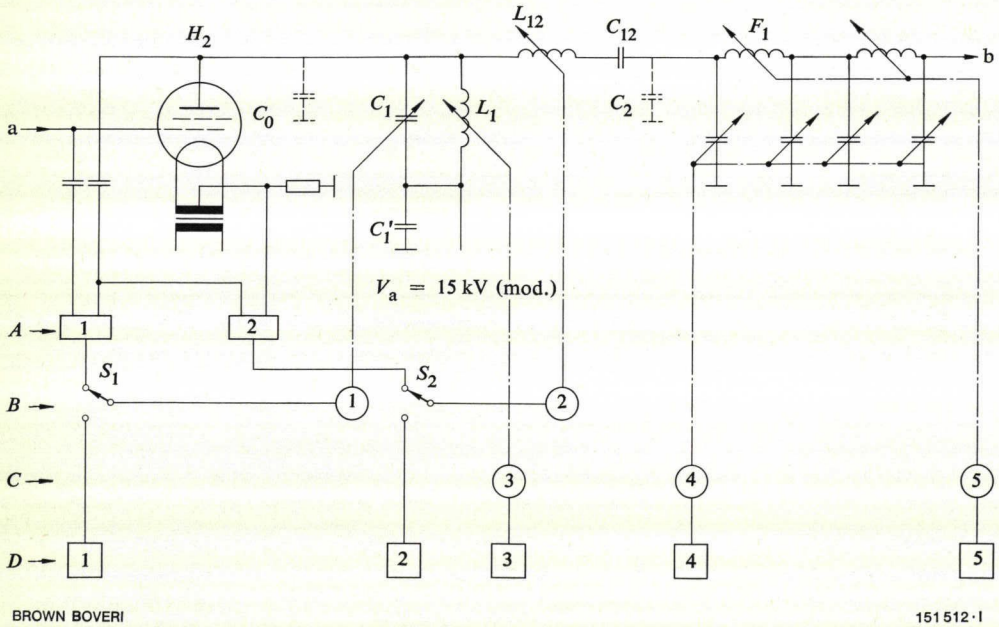

Fig. 2 – Anode circuit of RF output stage H_2 and tunable harmonic filter F_1 of a 250 kW short-wave transmitter

$A1$ = Phase discriminator
$A2$ = Load discriminator
$B1$–2 = Drives for coarse and fine adjustment
$C3$–5 = Drives for coarse adjustment only
$D1$–5 = Position stores
C_0 = Internal tube capacitance and stray capacitance
C_1 = Variable resonant-circuit capacitance
C_1' = Blocking capacitor
C_{12} = Blocking capacitance
L_1 = Resonant-circuit inductance
L_{12} = Variable induction
S_1, S_2 = Selector switches
V_a = Anode voltage
a = Input
b = Output

The Phase Discriminator

The phase discriminator measures the phase between the RF anode voltage and the RF grid voltage. When tuning is correct, this phase angle is 180° and is indicated by the fact that the control voltage supplied by the discriminator is zero.

The basic circuit of the phase discriminator can be seen in Fig. 3. Point A is connected to the RF anode voltage V_{a1} across a small capacitance C. If the input impedance of the discriminator is R, and account is taken of the influence of voltage V_0 between G and earth, we have

$$\overline{V}_A = j\omega C_1 R \overline{V}_{a1} + \overline{V}_0 \qquad (1a)$$

At the same time, using an inverting transformer, there appears at point B a voltage of

$$\overline{V}_B = -j\omega C_1 R \overline{V}_{a1} + \overline{V}_0 \qquad (1b)$$

The components dependent on V_{a1} are thus displaced in phase by 90°. On the other hand, voltage V_0 of grid voltage V_{g1} is taken via a phase-less voltage division with a factor of τ, as

$$V_0 = \tau V_{g1} \qquad (1c)$$

In the untuned condition, V_{a1} has a phase position of $180° + \mu$ with respect to V_{g1} (set value 180°). The absolute values of V_A and V_B are

$$V_{A,\,B} = \sqrt{(\omega C_1 R V_{a1})^2 + (\tau V_{g1})^2 \pm 2\omega C_1 R V_{a1} (\tau V_{g1}) \sin\mu} \qquad (1d)$$

The back-to-back diodes of the discriminators produce a direct voltage in the arrangement of resistors and smoothing capacitors. This voltage is proportional to the difference between V_B and V_A, and is used as a control voltage

$$V_\varphi = k_\varphi (V_B - V_A) \qquad (2)$$

The control voltage is dependent on frequency through the term ωC_1. Without introducing mathematical complications, we can consider two limiting cases which are significant as regards frequency.

Case 1

$$\omega C_1 R V_{a1} = \tau V_{g1}$$

With Eq. (2) and (1d) we obtain the control voltage

$$V_{\varphi(1)} = 2\sqrt{2} \cdot \sin\frac{\mu}{2} k_\varphi (\tau V_{g1}) \qquad (3a)$$

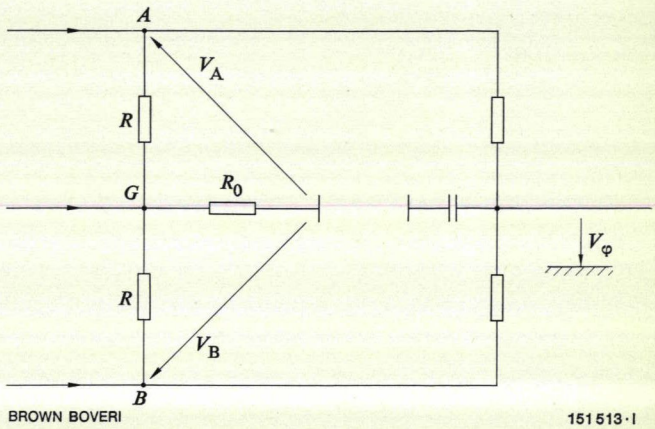

Fig. 3 – Basic circuit of phase discriminator

Symbols, see text.

Case 2

$$\omega C_1 R V_{a1} \gg \tau V_{g1}$$

In this instance the control voltage is described by the equation

$$V_{\varphi(2)} = 2 \sin\mu\, k_\varphi (\tau V_{g1}) \qquad (3b)$$

Equation (3b) yields a close approximation from values upwards of

$$\omega C_1 R V_{a1} = 3\,\tau V_{g1}$$

By assuming that this factor of 3 is attained at the lowest frequency the dependence on frequency is virtually eliminated.

The Load Discriminator

One must choose between two possibilities.

With the first of these the RF anode voltage V_{a1} is compared with a voltage V_p which is proportional to the root of the power output. The anode voltage can be expressed in terms of power P and the resistive parallel component at the anode R_p:

$$V_{a1} = \sqrt{P \cdot R_p}$$

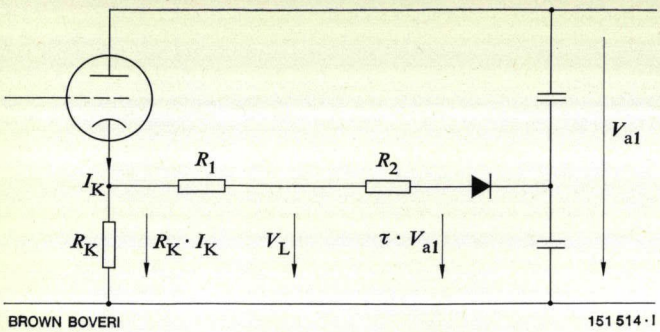

Fig. 4 – Basic circuit of load discriminator

Symbols, see text.

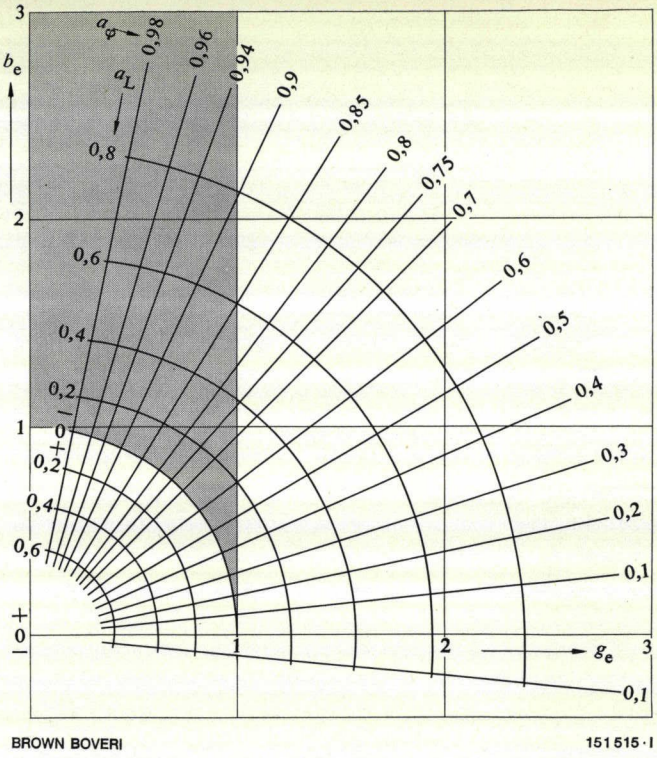

Fig. 5 – Characteristics of the discriminators in the plane $g_e + jb_e$ (standardized input admittances of output stage)

Control voltages:

$V_\varphi = k_\varphi \cdot V_{a0} \cdot a_\varphi$ $\qquad a_\varphi = \sin\varphi = b_e/y_e$

$V_L = K_L \cdot V_{a0} \cdot a_L$ $\qquad a_L = \dfrac{V_{a1}}{V_{a0}}(y_e - 1)$

Voltage V_p is obtained from the reflectometer. The proportionality factor is chosen so that V_p is equal to $\sqrt{P_0 R_{pn}}$. Here, R_{pn} denotes the value of R_p at which the tube operates normally. The control voltage is thus proportional to the relationship:

$$\sqrt{P \cdot R_p} - \sqrt{P \cdot R_{pn}} = \sqrt{P \cdot R_{pn}} \left(\sqrt{\frac{R_p}{R_{pn}}} - 1 \right) \qquad (4a)$$

Therefore, apart from the root of the power, it is dependent on the difference between R_p and the normal value, and drops to zero when $R_p = R_{pn}$. The advantage is that the reactive load has no influence in the event of mistuning. A drawback, however, is that the reflectometer, which has to be kept in reserve for measuring purposes, is additionally loaded by the discriminator.

The second solution does not involve the reflectometer and consists only of rugged components. It is shown in Fig. 4. The voltage produced by the cathode current I_K at shunt R_K is compared with a divided and rectified RF anode voltage $t V_{a1}$. The control voltage is thus

$$V_L = \frac{1}{R_1 + R_2}(R_2 R_K I_K - t V_{a1})$$

The resistances, or the factor t, must be chosen so that the control voltage vanishes when $I_K = I_{Kn}$ and $V_{a1} = V_{a1n}$. Then,

$$V_L = \frac{R_2 R_K}{R_1 + R_2}\left(I_K - I_{Kn}\frac{V_{a1}}{V_{a1n}}\right) = K'_L V_{a1}\left(\frac{I_K}{V_{a1}} - \frac{I_{Kn}}{V_{a1n}}\right)$$

and

$$I_K = I_{a0} + I_{g0} = a_{01} I_{a1} + I_{g0}.$$

The index 0 here denotes the d.c. components of the currents. The RF anode current I_{a1} is linked with I_{a1} by the form factor a_{01}, which is dependent on the angle of current flow.

We make a further substitution, i.e. $I_{a1}/V_{a1} = Y_e$, which is the apparent admittance of the anode. Its normal value is purely resistive, and is denoted G_{en}. Thus we can write the above equation in the form:

$$V_L = K_L V_{a1}\left(a_{01} Y_e - a_{01n} G_{en} + \frac{I_{g0}}{V_{a1}} - \frac{I_{g0n}}{V_{a1n}}\right)$$

The zero of V_L for normal adjustment is exact. The influence of the variables a_{01} and I_{g0}/V_{a1} when deviations from the normal setting occur is of no great significance because a_{01} does not vary greatly and the components of V_{g0} are small. The last equation above can be reduced to the form

$$V_L = K_L V_{a1}(y_e - 1) \qquad (5)$$

Here y_e is the output impedance of the anode, normalized to its nominal value G_{en}.

Here the apparent value of the anode loading occurs, and therefore the reactive loading plays a part.

Remarks on the Discriminator

The equations for the discriminators can be written in other forms.
One uses Eq. (3b) for the phase discriminator. No serious error is incurred if the grid voltage V_{g1} of the output stage is put proportional to the d.c. anode voltage because the driver stage is supplied from the same rectifier as the output stage, half the voltage being used. On the other hand, the anode circuit of the output stage has little effect on its grid voltage. Also, one can make a second approximation by writing the phase shift φ of the anode admittance Y_e instead of the displacement μ between V_{g1} and V_{a1}. Analysis with the aid of the tube characteristics shows that under all the conditions experienced during the control process the difference between these two angles is only a very few degrees. We write:

$$V_\varphi = k_\varphi \,.\, V_{a0} \,.\, a_\varphi; \quad a_\varphi = \sin\varphi = b_e/Y_e \tag{6}$$

where

b_e = Standardized reactive component
Y_e = Standardized apparent admittance at the anode.

For the load indicator we use Eq. (5) in the form:

$$V_L = K_L \,.\, V_{a0} \,.\, a_L; \quad a_L = \frac{V_{a1}}{V_{a0}}(y_e - 1) \tag{7}$$

The ratio V_{a1}/V_{a0} for the various loadings on the CQS200 output-stage tube was determined by analysing the characteristics, with account taken of the automatic variation of the grid bias voltage. The loci thus obtained for a_φ (in Eq. 6) and a_L (in Eq. 7) in the g_e/b_e plane are shown in Fig. 5. From these one can read off the control voltages for any load. Allowance must still be made for the amplitude of the d.c. anode voltage V_{a0} as a factor.

Fine Adjustment of the Output Stage

The fine adjustment process is described below, taking anode-side regulation of the RF output stage as an example. The lowest frequency of 3·9 MHz was chosen as the control procedure then takes the longest time.
Three special cases of 'control curves' can be seen in Fig. 6. The term control curves here denotes the loci in the g_e/b_e plane where one of the two variable RF components varies while the other remains constant. In Fig. 2 these variable components are shown as C_1 for tuning and L_{12} for matching. On the other hand, the tuning inductances L_1 and the components of filter F_1 within one channel do not change. When deriving the control curves the anode circuit is considered as a Π-network composed of the following components (reactive admittances):

transverse input element B_{11}:
C_0 = Internal tube capacitance and leakage capacitance
C_1 = Variable resonant-circuit capacitance
L_1 = Resonant-circuit inductance
C_1' = Blocking capacitor

longitudinal element B_{12}:
L_{12} = Variable induction
C_{12} = Blocking capacitor

transverse output element B_{22}:
which corresponds to the leakage capacitance C_2 of L_{12}. C_2 varies with L_{12}, but within the control range for one channel can be approximated to a constant.

In the following the admittances are denoted by the lower-case letters g and b. These are relative values, referred to the nominal value of the anode admittance. For the control curves we have the relationships given below.

Control Curves for Variation of b_{11} (Tuning)

These are straight lines parallel to the b_e axis which cut the g_e axis at $g_{e(11)}$ (Fig. 6a, b and c):

$$g_{e(11)} = g_a \frac{b_{12}^2}{g_a^2 + (b_a + b_{22} + b_{12})} \tag{8}$$

The parameters b_{12} are expressed by the ratio

$$w = \frac{\text{set no. of turns of } L_{12}}{\text{total no. of turns}}$$

Control Curves for Variation of b_{12} (Matching)

These are circles which touch the b_e axis. The midpoint abscissa (which is also the radius) is calculated as:

$$g_m = \frac{g_a}{2}\left[1 + \left(\frac{b_a + b_{22}}{g_a}\right)^2\right] \tag{9a}$$

For midpoint ordinate b_m we have

$$b_m = b_{11} \tag{9b}$$

The parameters b_{11} are expressed by the ratio

$$n = \frac{\text{set no. of revolutions of } C_{11}}{\text{total no. of revolutions}}$$

(C_{11} is effected by means of spindle-actuated vacuum capacitors).
As can be seen from Eq. (8) and (9), the control curves are dependent on the output load $g_a + jb_a$. The examples in Fig. 6a, b and c apply to instances of mismatching, all of which correspond to a SWR of 2:1. Three cases were considered, representing the most difficult adjustment problems.
The nominal values are:

anode impedance 320 Ω
output impedance 50 Ω

while the standardized values are

$y_e = 1 + j0$ and $y_a = 6{\cdot}4 + j0$

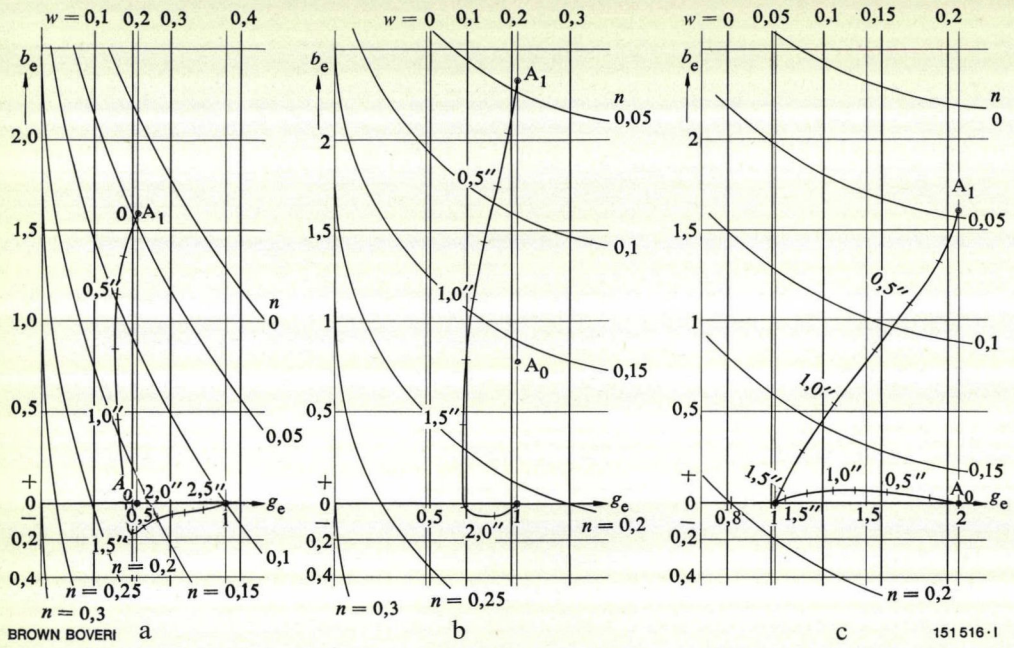

Fig. 6 – Control curves for constant n and w, and control paths with starting points A_1 and A_0 (for 3·9 MHz)

Symbols, see text.

When fine adjustment begins, the components are brought by coarse adjustment to the values corresponding to the nominal output, i.e. the middle frequency of the channel. If the actual operating frequency is the same as this middle frequency, the anode admittances for the cases of mismatching chosen in Fig. 6a, b and c are characterized by the points A_0. These are the starting points for the path of the control process in the g_e/b_e plane.

If the operating frequency does not coincide with the mid-frequency of the channel, however, the starting point is shifted. The discrepancy with b_{12} is slight and is disregarded. That of b_{11}, however, must be taken into account because of the high Q of the tuning circuit, in which A moves on a line parallel to the b_e-axis from A_0 to A_1. This is shown in Fig. 6. The extent of the shift corresponds to the selected channel width of 500 kHz. This means a maximum deviation of 250 kHz from the middle frequency, or 6·3 % when operating at 3·9 MHz. A shift in the opposite direction is quite possible but is not considered because it is easier to regulate.

The cases considered in Fig. 6a and b were chosen because the starting point of the control process A_1 lies in, or at the edge of, the darker area shown in the control voltage diagram, Fig. 5. In this zone $g_e < 1$, but $y_e > 1$. If the load regulation system alone were made to act, the value would not come closer to the nominal value, but draw away from it.

Thus, one could first operate only the phase regulation system, and then start load control when $Q = 0$ has been reached. However, since the curves for constant n cut the g_e-axis at a smaller or larger angle, the result is a phase deviation.

The procedure which is technically the simplest, is suitable for all practical cases, and is also the quickest consists in allowing both movements to run from the moment fine adjustment starts, but the relative speeds are chosen so that the velocity vector in the diagram of Fig. 6 in the direction b_e always has a sufficiently large component directed towards $b_e = 0$. The anode voltage is turned on at the same time and steadily increased. When examining the control sequence account must be taken of the speed characteristic of the actuator motors. These are fitted with servo amplifiers. Up to the full speed, this is proportional to the control voltage. Since low-inertia drives are used, one can, as a first approximation, disregard inertia effects as the speed changes. With Eq. (6) and (7) we obtain the relationships

$$\frac{dn}{dt} = k_n \,.\, a_\varphi \,.\, V_{ao}; \quad \frac{dw}{dt} = k_w \,.\, a_I V_{ao} \tag{10a}$$

which are valid up to the full speed.

The behaviour of V_{ao} with time can be written as

$$V_{ao} = V_{aos} + \frac{V_{aon} - V_{aos}}{T} t \tag{10b}$$

where

V_{aos} = Starting voltage
V_{aon} = Normal operating voltage
T = Total time from V_{aos} to V_{aon}
t = Time

The anode rectifier is provided with a certain starting voltage to prevent overloading of the screen grid. By integration, Eq. (10a) and (10b) can be used to determine the entire control sequence. Since n, on the one hand, and a_φ and φ_L, on the other, are related to g_e and b_e in a complex manner, step-by-step integration is necessary, in which case the full speed must be considered as a maximum speed.

The constants chosen were:

$k_n = 0{\cdot}03$ $\quad k_w = 0{\cdot}05$ $\quad T = 3$ s
$V_{aos} = 4$ kV $\quad V_{aon} = 15$ kV

$\left(\frac{du}{dt}\right)_v = 0{\cdot}1$ ($\triangleq$ 10 s total sequence time)

Control paths in the g_e/b_e-plane calculated in this way are shown in Fig. 6. It can be seen that by a suitable choice of constants k_n and k_w the control paths can be made to converge towards the nominal value.

Times are also marked along the control paths in Fig. 6. One can then not only determine the time taken by the process, but also calculate the corresponding anode voltage with the aid of Eq. (10b). With these data and the tube characteristics it was possible to establish the pattern of the anode current and the anode power dissipation. It was found that these two quantities never become excessive, i.e. that the automatic control sequence runs faultlessly.

It has been assumed here that the RF grid voltage of the output-stage tube is not affected by control processes on the anode side. This is an approximation, but since the grid voltage in fact varies only slightly, it can be considered reliable.

Finally, it can be said that the control process is sufficiently advanced within three seconds to allow modulation to be started. A further interval is required to attain the ideal control condition, when the tube reaches optimum efficiency. This is a relatively long time because the control voltages become progressively smaller. The drives are therefore allowed to continue acting on the discriminators for a few seconds after modulation begins, and the changeover to the normal operating condition is then made after this period has elapsed.

Function of the Automatic and Remote Control System

The automatic system is built largely of electronic components and integrated circuits. The sequence of events can be followed by referring to the control panel shown in Fig. 7.

Frequency Preselection

A seven-digit frequency, in steps of 10 Hz, is fed in code form into a prestore by pressing buttons in panel a_1 of Fig. 7. A check on the selected frequency is provided by the illuminated panel b_1. If an error is made, the contents of the store can be cancelled by pressing button X on panel a_1.

Every day, and for long periods, broadcast transmitters change repeatedly between certain specified frequencies. Feeding these frequencies into the store every time would therefore be tedious, and could also give rise to errors. The buttons in panel a_4 are therefore provided for any ten fixed frequencies. Each button has a corresponding store. These stores are filled by first feeding one of the fixed frequencies into the prestore. The address in the fixed store is then selected by pressing one of the buttons F1 to F10 on panel a_4. When a_3 is pressed, the contents of the prestore go to the address of the fixed store, whereupon any frequency already stored is automatically cancelled. The fixed frequency is then shown on panel b_1, which can also be used at any time to check the contents of the fixed stores.

This whole procedure can be carried out independently of the transmitter, i.e. while it is working on a particular frequency, or when it is not being used.

Changing the Transmission Frequency

The transmission frequency is determined by a decade oscillator (0 in Fig. 1) which, by means of its own electronics, converts the coded stored frequencies into corresponding high-frequency oscillations.

Let us assume that the transmitter is running at frequency f_a which at a certain time must be changed to f_b, and that f_b is one of the fixed frequencies. The appropriate button on a_4 is pressed, and then button a_5. The anode voltage then drops to zero and the contents of the fixed store pass into a 'transmission store', whereupon the frequency is indicated on panel b_2. The oscillator electronics and the channel selector are connected to the transmission store. The oscillator is thus switched to the new frequency. The channel selector starts the coarse adjustment process. When this is finished, i.e. after the middle frequency of the relevant channel has been reached, the anode voltage starts to increase, fine adjustment takes place, and finally operation commences as described earlier.

Any desired frequency fed into the prestore can be passed to the transmitter. In this case one has to press button a_2 together with button a_5.

Turning On the Transmitter

The auxiliaries, cooling system and the various power sources have to be turned on in a set sequence. Suitable interlocks are provided to eliminate errors.

Three modes of control, manual c_1, local c_2 and remote c_3 can be selected with switch S.

Manual control is used for commissioning and maintenance purposes. Panel a_6 contains buttons for switching on and off individually. These buttons must be pressed according to the set sequence. One can, however, give a command of higher priority, whereupon the sequence runs automatically up to this point. When a command is given, the buttons flash. A steady light serves as an indication that the stage in question has been completed. For initial adjustments with manual control each of the positioning drives can be made to run at any desired speed and in either direction.

For local control one has to press only button I of panel a_7, and the whole turn-on procedure then takes place automatically. The purposes of the other buttons in panel a_7 are as follows:

button I′	for switching to reduced power (this facility is available only on request)
button I″	for making the equipment ready (turning on auxiliaries, cooling and heating)
button 0	switch off

Panel d contains fault-indicator lamps with and without retention capability. Those with retention serve to give a persistent indication that an overcurrent relay, for example, has tripped temporarily. A visual indication is accompanied by an acoustic signal. Button e_2 stops the acoustic signal, and e_1 cancels the light. Button e_3 is for testing the lamps. The remaining button e_4 is for emergencies and completely shuts down the transmitter.

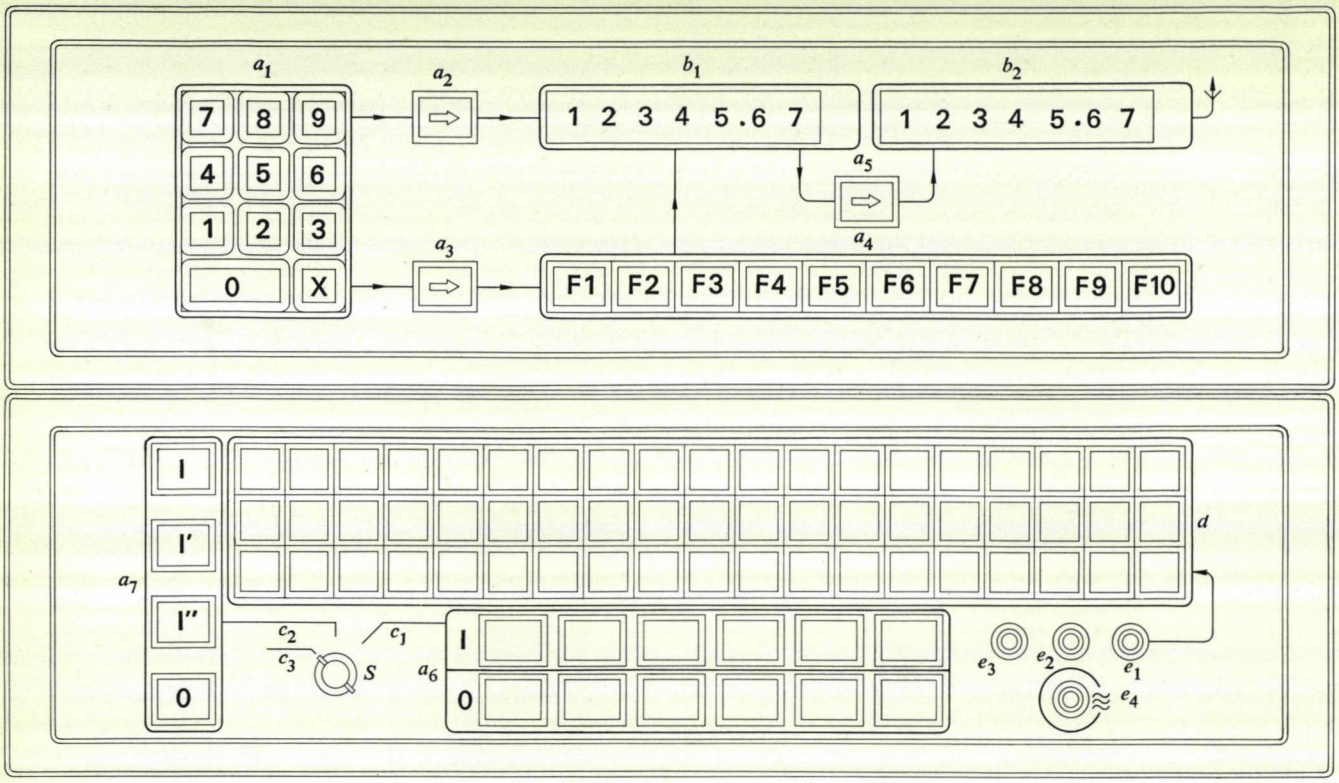

Fig. 7 – Control panel

a_1 = Push buttons for setting frequency
a_2 = 'Prestore' button
a_3 = 'Fixed frequency store' button
a_4 = 'Fixed frequency address' buttons
a_5 = 'Transmitter' button
a_6 = Buttons for manual transmitter turn-on
a_7 = Buttons for automatic transmitter turn-on
b_1 = Frequency indication for preselection
b_2 = Frequency indication for transmission
c_1–c_3 = Switch positions (see text)
d = Fault indicator panel
e_1 = Fault indication cancel button
e_2 = Acoustic fault-signal cancel button
e_3 = Lamp test button
e_4 = Emergency button
S = Mode selector switch
X = Error correction button (panel a_1)

When the control switch is set to 'remote', the transmitter can be operated from some other point. The various processes are exactly the same as with local control. All the buttons required for local control are duplicated at the remote position. So that only one transmission channel each is required for keying the frequencies and indicating the frequencies set, the required frequency settings are coded at the control point, and decoded again at the transmitter.

Continuous supervision of the most important values is desirable with automatic control, but particularly in the case of remote control. This is done by a piece of auxiliary equipment which is able to scan a cycle of up to 40 values. A printer then provides a written log.

The First Generators in Switzerland Driven Direct by Bulb Turbines

A. G. Lalive d'Epinay

621.313.322–82:621.224.14

The data of these bulb-turbine generators are listed and aspects of the design are discussed. The cooling system and method of installation are then described.

Rated Data

Apparent power	9500 kVA
Speed	170 rev/min
Test speed	336 rev/min
Min. moment of inertia	350 tm²
Frequency	50 Hz
Voltage	4250 V ± 5 % ⅄
Current	1290 A ± 5 %
Power factor cos φ	0·79 for Flumenthal 0·86 for Neu-Bannwil

Construction

In all the previous bulb-turbine power stations in Switzerland the power from low-speed turbines is transmitted to the high-speed generators through gearing (the stations at Bürglen TG, Rüchlig in Wildegg and Aue in Baden). Several plants with direct-driven generators have been built in other countries, notably in France. The first machines of this kind in Switzerland comprise six identical generators, three for the Flumenthal station of the Aare-Tessin AG für Elektrizität, and three for Neu-Bannwil station of the Bernische Kraftwerke AG, both situated on the river Aare between Soleure and Olten. The design and construction of these generators are considered in this article.

A bulb turbine and its generator form a compact unit, especially when the two are coupled directly. For this reason, close collaboration with the turbine manufacturer, Escher Wyss, was essential right from the planning stage, and both the structural concept and the electrical design resulted for the most part from this cooperation.

The stator forms an integral part of the bulb, being fixed by flanges between the turbine housing and a hemispherical nose fairing (Fig. 1). The seal between fairing and generator is designed to accommodate thermal expansion in the axial direction. Torque is transferred via the flange at the turbine end to the turbine housing, and from here via the stay vanes to the foundation. To ensure a satis-

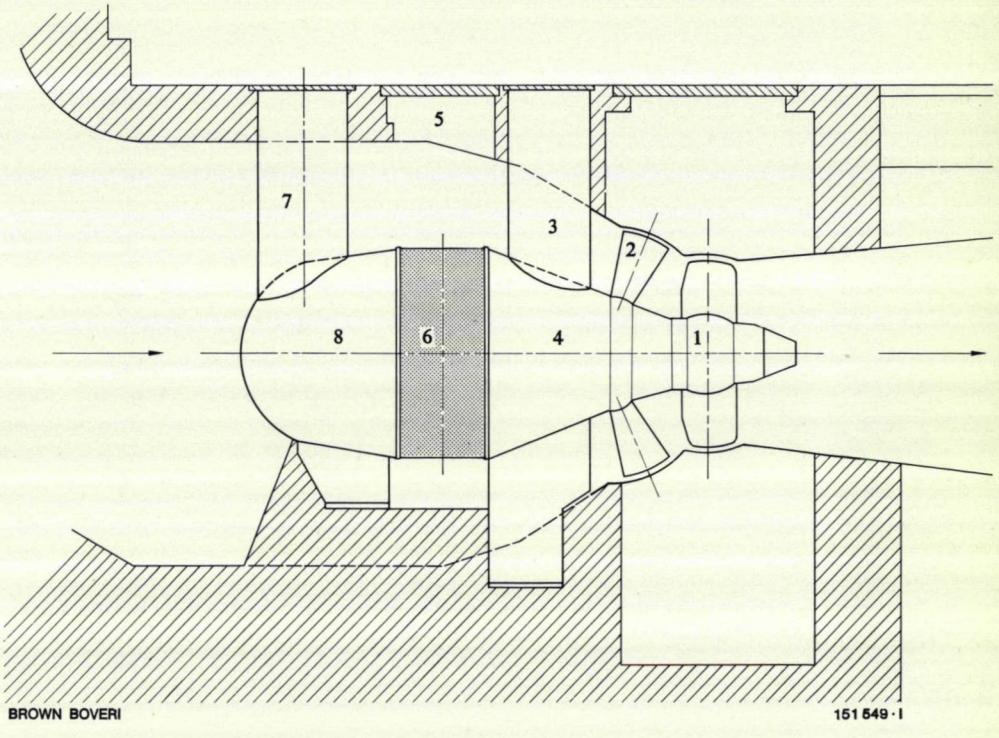

Fig. 1 – Arrangement of turbine and generator in a bulb-turbine power station

1 = Turbine runner
2 = Guide vanes
3 = Turbine access shaft
4 = Turbine casing
5 = Installation shaft for generator
6 = Generator
7 = Access shaft to nosepiece and generator
8 = Nosepiece

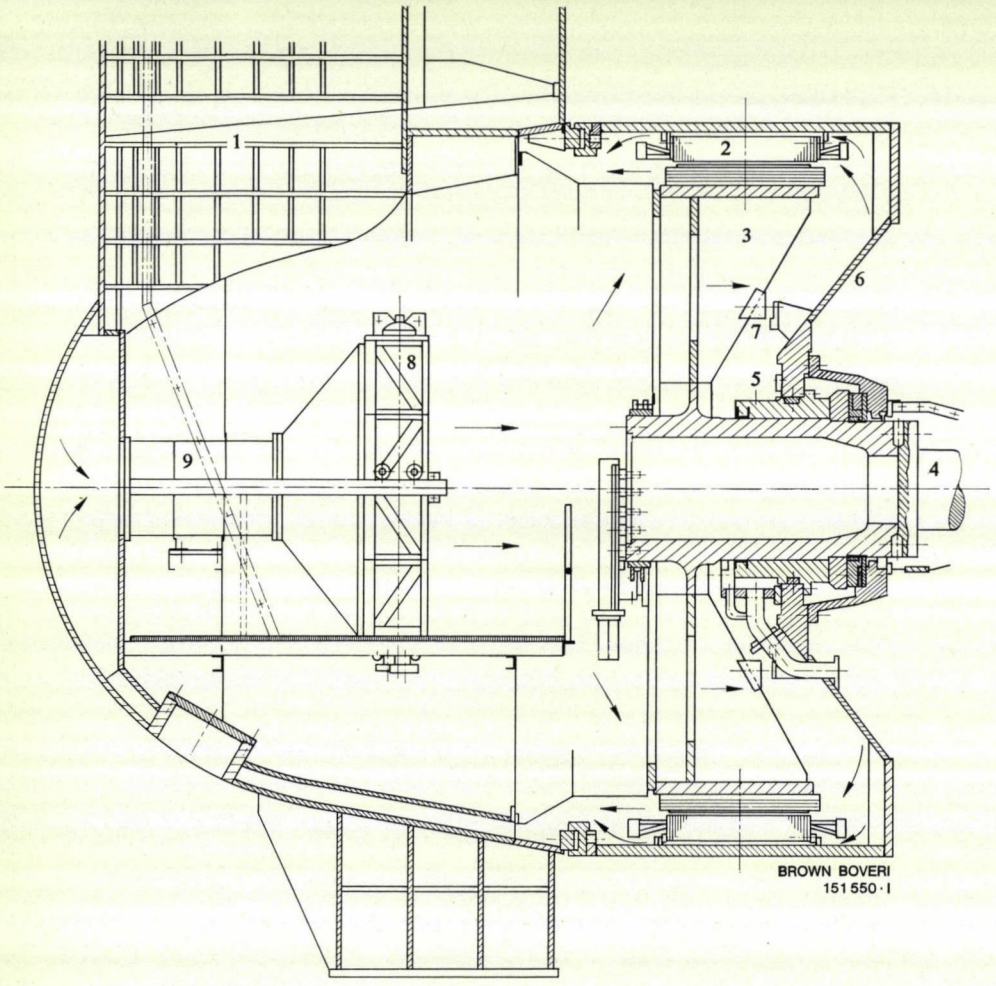

Fig. 2 – Section through generator and nosepiece

1 = Access shaft to nosepiece and generator
2 = Stator
3 = Rotor
4 = Turbine shaft
5 = Bearing
6 = Cone
7 = Plates for fixing rotor during installation
8 = Air/water cooler
9 = Fan
Arrows denote air flow direction.

factory flow pattern, the outside diameter of the generator casing should not be more than 1·1 to 1·2 times the diameter of the turbine runner. With a conventional type of frame this would lead to a very small pole pitch and a correspondingly long core. A solution therefore had to be found which produced the largest possible stator bore. Since, as will be shown later, the air gaps in bulb-turbine generators have to be very small, the construction must be very rigid. The casing consists of a rolled steel shell stiffened on the upstream side by the connecting flange, but particularly by a welded cone on the turbine side. This cone also carries the combined thrust and end bearing of the turbine shaft. The laminations, composed of sections of dynamo sheet, are clamped together with press rings and insulated axial bolts. They are fixed to the frame by means of wedge supports bolted to the shell, thus providing the latter with additional stiffening.

The air gap is 5 mm and the maximum tolerance 10 %. So that this is not exceeded, a tie rod located on the generator shell above the beam carrying the brush rocker allows the stator to be pulled circular after it is in position.

The construction of the rotor was also to some extent governed by the design of the turbine. The desire that the turbine and generator should be delivered completely separately presented no difficulties as all the parts of the turbine are contained on the same side of the generator. Oil access to the shaft, the servomotor and the combined thrust and end bearing are all located between the generator rotor and the turbine runner. To accommodate this bearing, as mentioned earlier, the flange on the turbine side had to be extended and formed into a cone. Because of the overhung construction of the rotor it was possible to lengthen the rotor hub to form the bearing. The rotor is a welded construction, the rim being connected to the hub by a ribbed disc. On one side of the rim is the brake ring. The laminated poles are bolted to the rim and have a damping grid. To enlarge the cooling surface area, the pole winding is made from copper section. Because the runaway speed is very high (more than three times the rated speed) the winding is strengthened in the radial direction. The sliprings are on the hub. Brush rocker and brake cylinder are attached to an easily removable transverse beam bolted to the up-stream frame flange. The nosepiece internals, apart from the integral welded parts, were also supplied by the generator manufacturer.

A section through the generator and nosepiece is shown in Fig. 2. Even with this special construction, the pole pitch of bulb-turbine generators is comparatively small and the core length relatively large. Moreover, because the cooling air has to flow axially, owing to the design, the air heats up more than with conventional radial cooling. The excitation power which can be generated is therefore limited, and usually the required length of the machine is determined by the pole core and winding. In any case, the air gap must be as small as possible. This has various consequences. The additional losses occurring at the pole shoes both at no-load and when under load are dependent

Fig. 3 – View into the nosepiece

One cooler has been removed. A fan and the bottom of the access shaft can be seen.

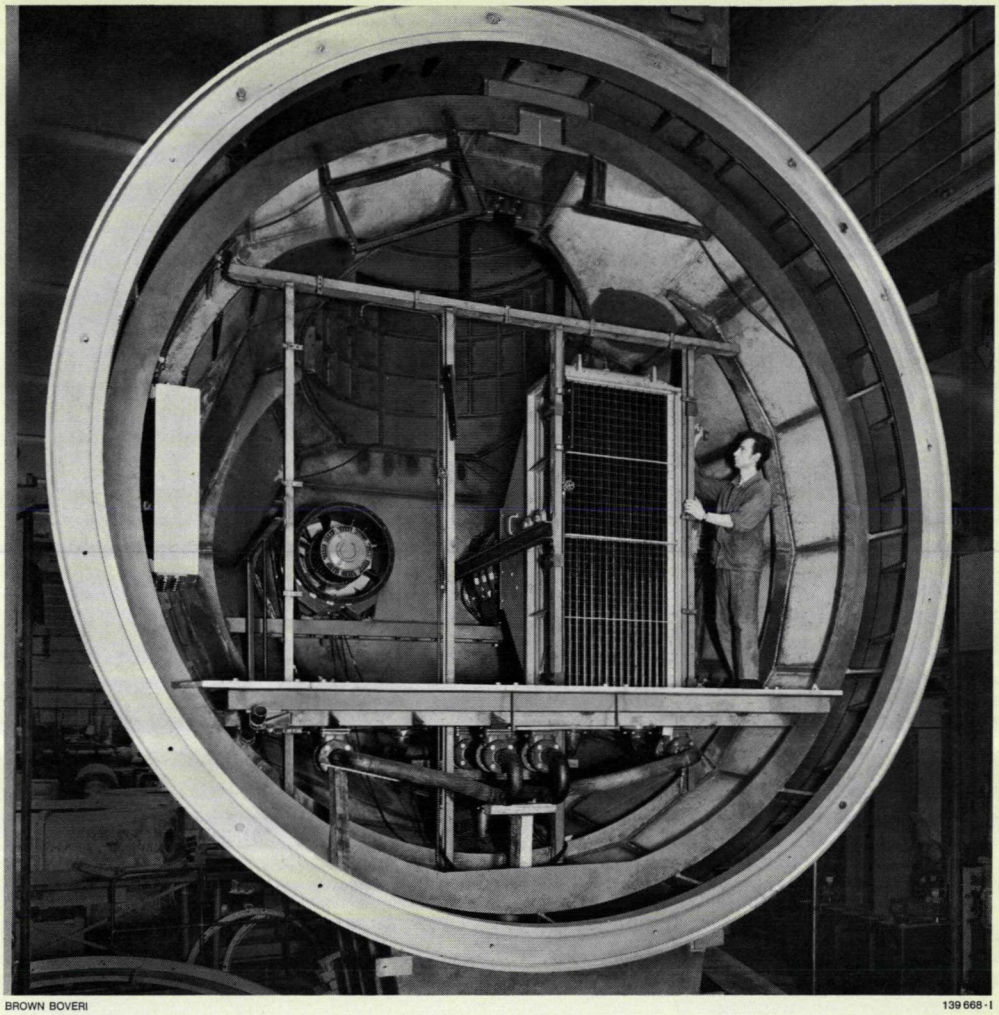

BROWN BOVERI 139 668-I

not only on the material of the pole shoe, but also to a large extent on the ratio of slot opening to air gap. Since the voltage could be chosen freely it was possible to employ a Roebel bar winding with open slots. This type can be fitted and removed particularly easily and requires the minimum number of connections, despite the large number of poles. Laminated poles were thus required to ensure that these slots do not give rise to excessive additional losses.

Furthermore, because the air gap is small the synchronous reactance is relatively large, which imposes certain restrictions on the capacitive load.

Accurate adjustment of the air gap is achieved with the aid of shims inserted between the pole cores and the rotor rim.

Cooling

As the generator is completely immersed it would seem logical to transfer the heat produced by losses to the water. This can take place directly to some extent in the case of the stator, in that heat from the laminations is removed straight through the machine casing. The close contact required between the laminations and the casing is achieved during operation through thermal expansion of the laminations. The remaining losses have to be removed, using air as the transfer medium. As the peripheral velocity of the generator is low, the air is circulated by separate fans. One possible solution would be to guide the air along the inside of the nose fairing, where it would give up its heat to the water. However, one would also have to enlarge the surface area swept by the air by fitting cooling fins or studs. What is more, the general temperature level of the air often has to be raised in order to improve dissipation of the heat.

There are various reasons why both the customers and the generator manufacturer thought it preferable to remove the heat by means of air/water coolers located in the nosepiece. It was feared, for example, that the pollution and high lime content of the river in question could in time result in considerable deposits of sludge or scale on the outside of the bulb. If the heat from the stator were removed direct, the winding temperature would become unacceptably high. For safety reasons, therefore, losses in the form of heat occurring on the outside of the laminations are also first transferred to the air. This is made possible by locating spacers between the laminations and the casing to form ducts through which the air can flow. The area of the heat-emitting surface is greatly increased by providing slots in the back of the laminations. However, it was decided not to provide any additional means of guiding the air in the nose section to improve heat transfer to the water, as this would have necessitated a large increase in fan pressure. Normal air/water coolers are mounted after the fans (Fig. 3). The fact that these heat exchangers require a separate cooling-water supply

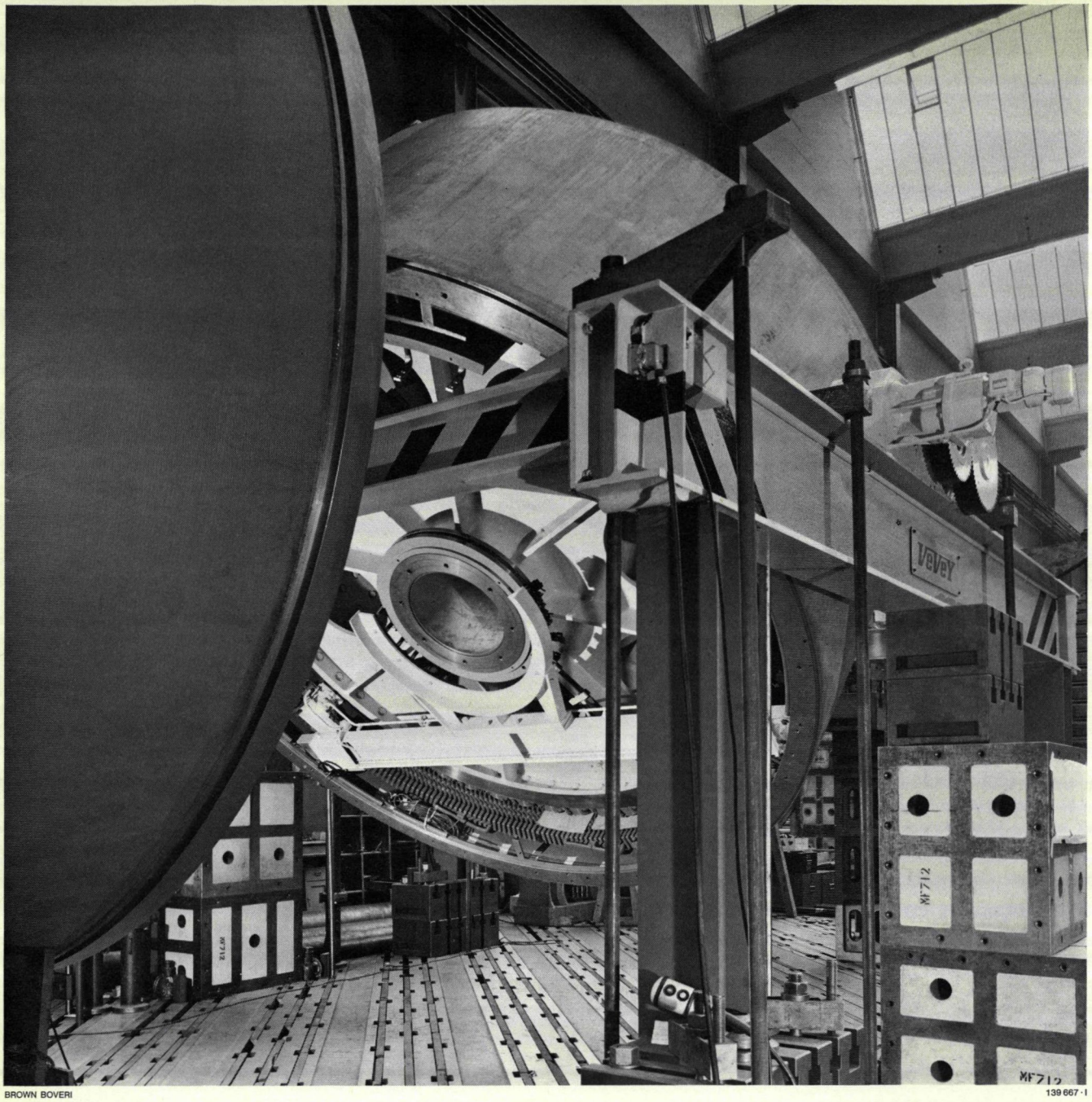

Fig. 4 – Generator in the turning rig

Stator, rotor and bearing are pre-assembled and installed as one unit.

is more than balanced by the advantages of greater safety and much lower windage losses. The fan blades are adjustable so that the air flow rate can be adapted accurately to the temperature rises encountered, i.e. flow rate is reduced until the temperature rise is close to the guaranteed maximum value. Windage losses are thus reduced to a minimum and efficiency is improved.

Comparative measurements carried out in the works and in the station have shown that, even with a comparatively small average temperature difference of 18 deg C between the river water and cooling air, more than 100 kW, i.e. over a third of the losses, are removed direct. The temperature of the air sweeping the inside of the nosepiece alone was lowered by 6 deg C. With a river temperature of 16·5 °C, the overall temperature rise in the power station was more than 10 deg less. This indicates that removal of all the heat to the river water outside would be quite possible while the casing was not fouled. The reasons for not adopting this method, however, have already been stated.

Installation

The procedure used for installing bulb-turbine generators is governed by the design concept chosen. The method used for the two stations in question is very straightforward, but requires cranes of relatively high capacity and the ability to turn the generator.

The turbine housing and nose fairing were lowered into the duct and concreted in so as to leave a gap for the generator. This was then placed in the gap and bolted up on both sides. The generator can thus be removed again at any time. The necessary play is taken up by a sealing ring, developed by the turbine supplier, which can also allow for axial thermal expansion during operation. This has the advantage that the generator can be fully assembled either on site or in the manufacturer's works.

The stator was laid on its side with the cone underneath. Support tabs welded to the fins of the rotor engage in locating shoulders on the cone. The rotor was rigidly bolted to the stator with the aid of intermediate plates. The generator was tilted so that the rotor hung in the stator. As the additional crane hooks required for this operation were not available at Neu-Bannwil, the customer acquired a special tilting rig. A generator being turned in this rig can be seen in Fig. 4.

Once the turbine had been tipped upright the supplier of the turbine could fit the bearing from the cone side. By making the extended rotor hub serve as the bearing point the bearing and hub are entirely inside the generator flange and the junction of hub and turbine shaft is in the same plane as the flange.

Finally fixing the generator was therefore quite straightforward. After the generator had been lowered into the tunnel, the casing had been bolted up and the rotor was coupled to the turbine shaft, the fixing between stator and rotor was removed. It was then a matter of fitting a few air deflector plates and connecting the generator leads.

The poles of the generator can be withdrawn individually into the nose section, using a special retracting device. It is therefore very easy to change the winding bars. The poles and bars, and also the coolers and blowers fitted in the nose section, can be taken out through the access shaft in the nosepiece.

Conclusion

Tests were carried out in the Birr works on the first generator, complete with nose section, bearing and shaft. The tests went smoothly and the three generators for the Flumenthal station have been in service since autumn 1969. Those for Neu-Bannwil will follow during the course of this year.

Electrical Machines for the Santiago Power Station on the Rio Sil, Spain

W. Dreher

621.311.21 (46)
621.313.322–82:621.224.14

A brief review of the generator/motors for the Santiago hydroelectric power station is followed by a description of the design features of the axial turbine generator sets.

In the course of harnessing the water power of the Rio Sil and its tributaries, the Saltos del Sil S.A. power company have systematically built a series of hydroelectric power stations in western Spain (Fig. 1). A dam has been built across the Rio Jares, a tributary of the Rio Sil, near Santa Eulalia. Two 32 000 kVA vertical pump turbine sets have been installed at the Santiago power station near La Rua on the Rio Sil to utilize the head between the Rio Jares and Rio Sil, or alternatively to pump water into the reservoir formed by the dam across the Rio Jares. There are also two 9000 kVA horizontal axial turbines in the same station, driven by the run of the Rio Sil. These four machines were produced by our associate company BBC-Oerlikon in Sabadell, Spain, but were designed in Switzerland.

Generator/Motors

The data of the two vertical pump turbine sets (Fig. 2) are

output	32 000 kVA
voltage	15 000 V
speed	500 rev/min (both directions)
frequency	50 Hz

The rotors (Fig. 3) have solid poles and interpole connectors and are designed for direct run-up although frequency starting can also be used in conjunction with the axial turbines. In either case the pump turbines are blown through with compressed air, and lubricating oil is pumped into the thrust bearing to relieve the load.

The stator is insulated throughout with mica/glass-fibre tapes preimpregnated with epoxy resin. In order to comply with the requirements for direct starting, strong laminated hardwood support rings and glass-fibre tapes were used in the overhangs.

The machines are designed for both senses of rotation and are self-ventilated. The two fans for cooling the rotor by air/water heat exchangers are designed to operate in both senses of rotation.

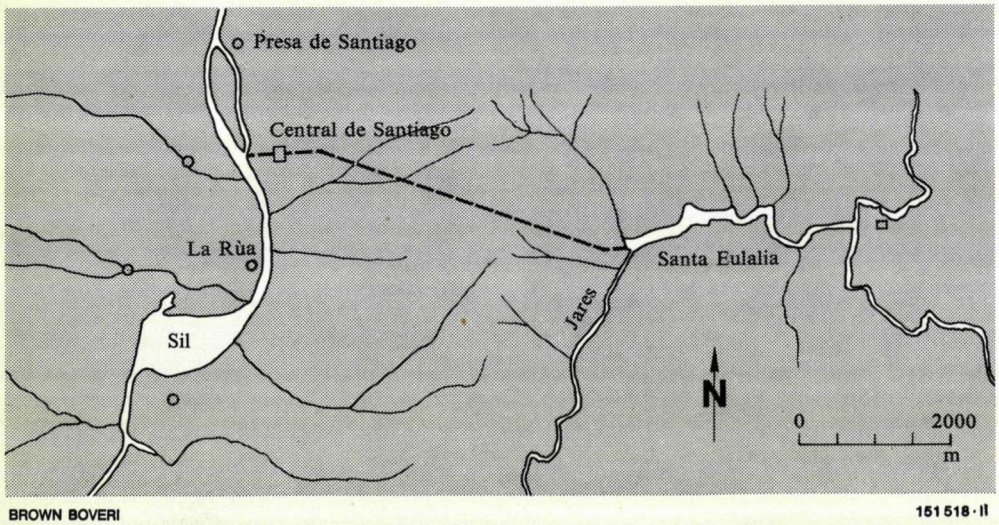

Fig. 1 – Map of the area

(Reproduced by courtesy of Saltos del Sil S.A.)

Fig. 2 – Section through a 32 000 kVA generator/motor for a pump-turbine set in the Santiago power station

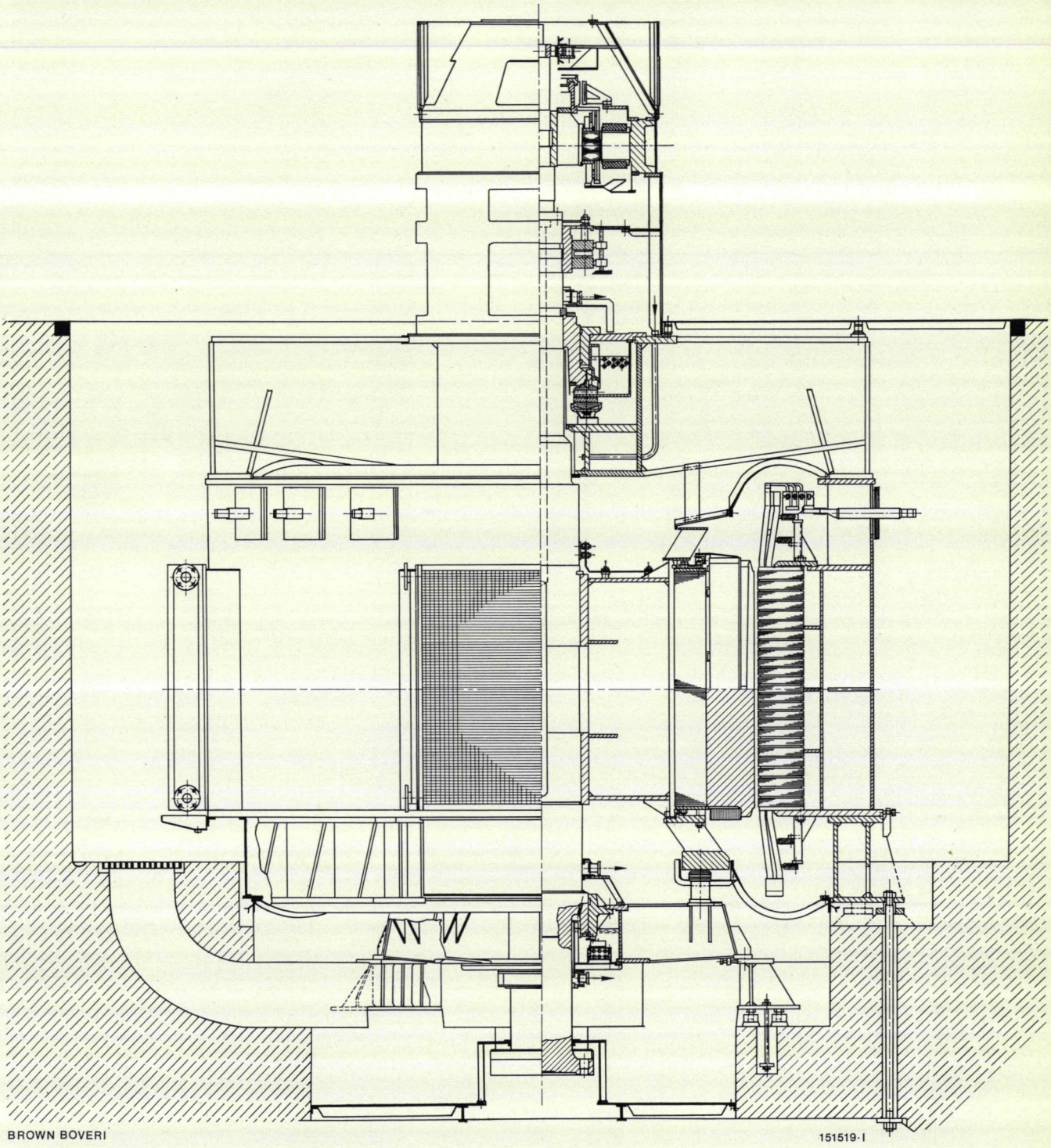

Fig. 3 – Rotor for a 32 000 kVA, 500 rev/min generator/motor

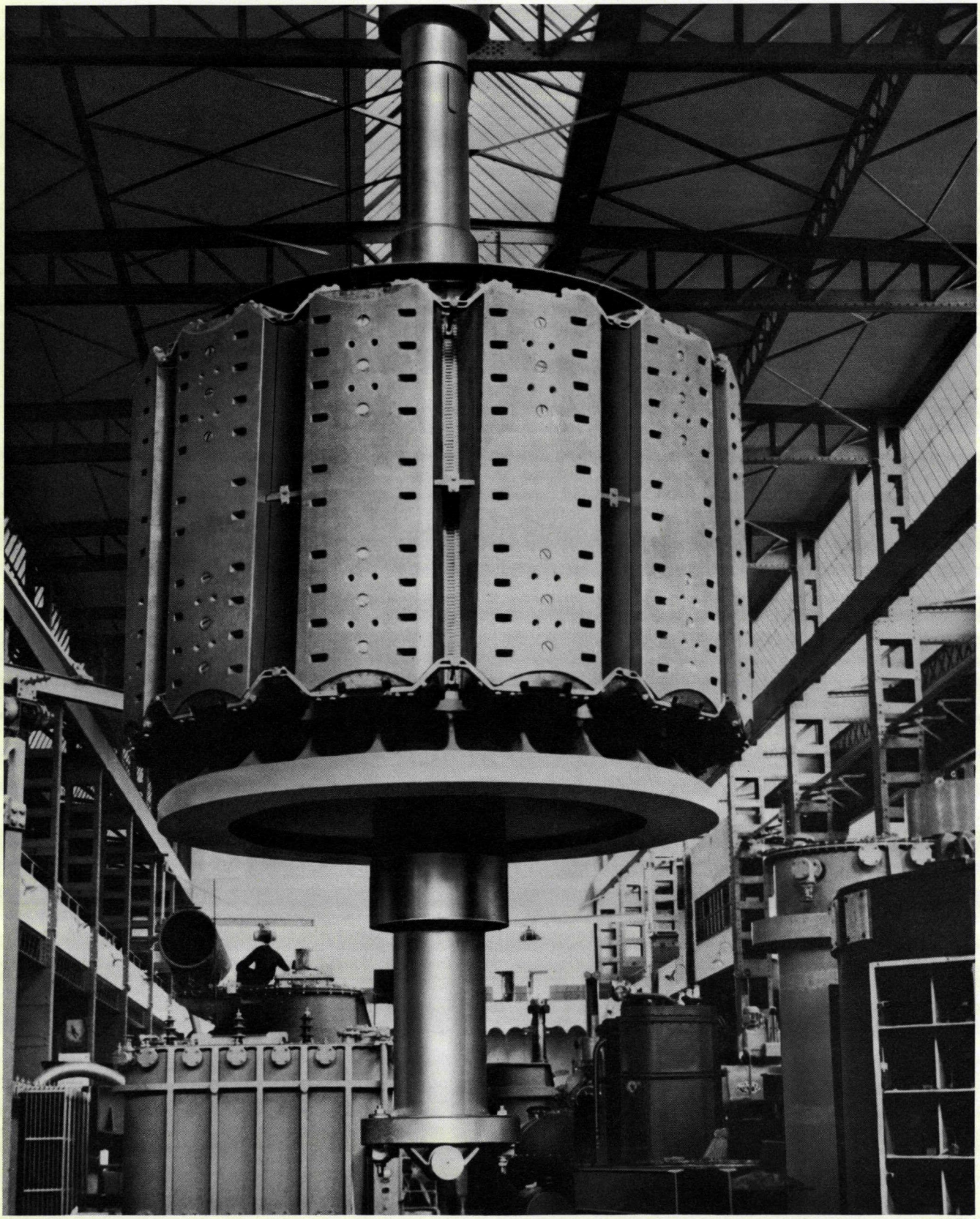

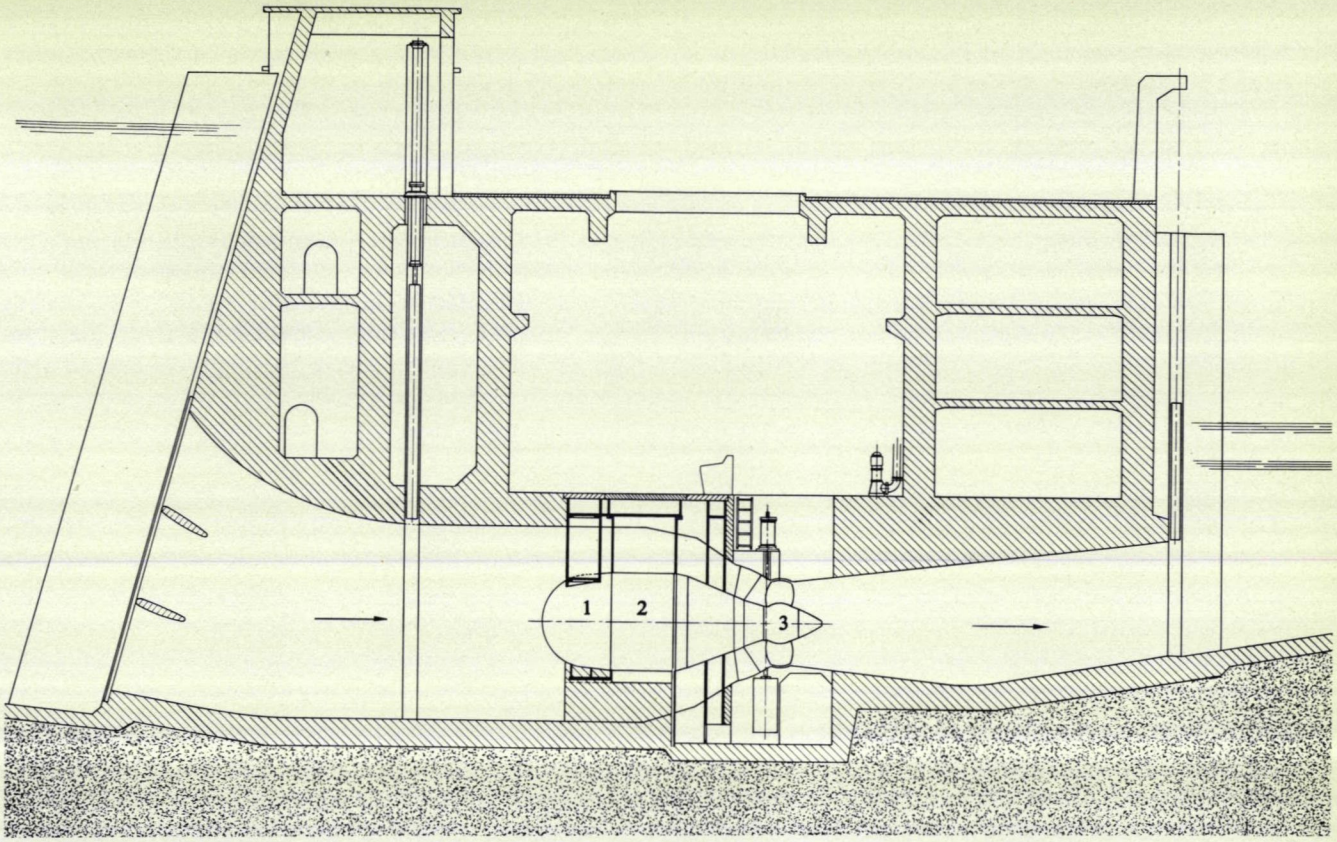

Fig. 4 – Section through a 9000 kVA axial turbine

1 = Nose cone
2 = Generator
3 = Turbine
(Reproduced by courtesy of Escher Wyss Limited)

Axial Turbine Sets

The design data of the two horizontal axial turbine generator sets are

output	9000 kVA
voltage	3000 V
power factor	0·8
speed	158 rev/min
frequency	50 Hz

The river water flows over a capsule formed by nose fairing, stator and turbine. The foundations support only the nose fairing and turbine casing. These carry the cylindrical stator frame between them. Thermal expansion is taken up by a sliding flange between stator frame and nose fairing whereas the torque acting at the stator is transmitted to the foundations through dead-fit bolts and a rigid flange between it and the turbine casing. Separate shafts provide independent access to generator and turbine from the machine room. Both turbine runner and generator rotor are mounted overhung on the two-bearing shaft. The combined thrust and guide bearing is mounted on the generator end-shield.

Cooling

There are several interesting aspects with regard to the cooling of the axial turbines in the Santiago power station (Fig. 5). Of the three possible systems—forced draught with cooling in the machine room, recirculating with air/water heat exchangers, or direct cooling through the shell by the flow of river water—the last-mentioned was chosen. The quality of the river water (low organic pollution and low lime content) means that very little incrustation is to be expected at the surface of the shell. The favourable ratio between surface area and total losses meant that direct cooling could be used without increasing the area of shell. On the other hand, in order to improve heat transfer it was necessary to either accelerate the air circulation in comparison to conventional generators or to compress the cooling air. Taking the high windage losses at high air velocity into account, the second method was chosen and the air is compressed to 2 kgf/cm² at rated load.

The generator losses are 280 kW. Of these, about 100 kW of stator losses flow into the river water through the laminations and frame. The remaining 180 kW comprise rotor, windage and some of the stator losses and these are

carried by the cooling air and passed on to the river water through the heat exchanger in the nose cone. The air is circulated by a separately driven axial fan in the nose and this is assisted by the pressure component of the rotor. About 85 % of the pressure is provided by the fan and the other 15 % by the rotor. The air is drawn axially through the rotor spider, through the cooling ducts in the nose fairing and through the axial fan back to the generator. The flow rate necessary at the nose cone heat exchanger is created by a relatively narrow annular channel at the periphery of the shell. Air ducts at the transition from stator frame to nose cone ensure even air distribution around the shell.

Stator and rotor are designed to temperature class B (ϑ_{max} = 120 and 130 °C, respectively) and the maximum river water temperature is 25 °C. To make optimum use of the nose fairing as a heat exchanger the mean temperature drop between warm air and cooling water was established as 35 deg C. Assuming a cooling water temperature of 25 °C, the air inlet temperature is 51 °C which is rather higher than usual for air cooled generators. On the other hand, taking into account the fact that some of the heat is transferred direct from the stator frame to the cooling water, and also that for reasons of efficiency the rotor poles are only lightly loaded, this high cooling air temperature is perfectly acceptable.

Fig. 5 – Section through a 9000 kVA, 158 rev/min axial turbine and generator

1 = Nose cone
2 = Stator
3 = Rotor
4 = Combined thrust and guide bearing
5 = Sliding ring seal
6 = Generator shaft
7 = Turbine shaft
8 = Bearing support
9 = Water drain
10 = Sliprings
11 = Carrier
12 = Fan
13 = Cooling ducts
14 = Access shaft

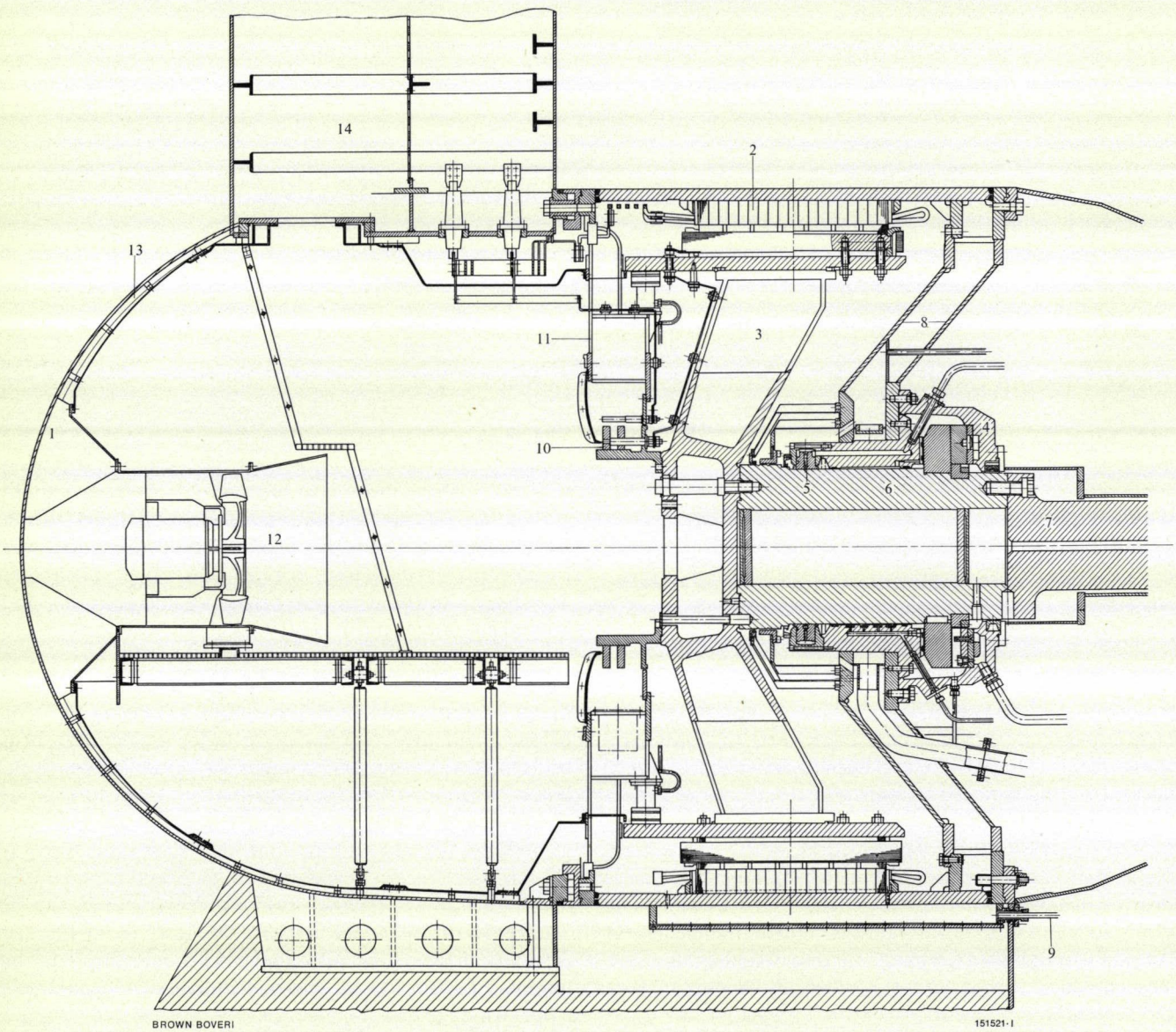

Nose cone

In order to determine experimentally the actual flow conditions in the nose-cone heat exchanger a full scale segment of $^1/_{24}$th of the nose fairing was built and tested in the laboratory in Switzerland (Fig. 6). Water was caused to flow through a water jacket at the surface and the generator cooling air circuit was reproduced by a throttled duct and fan between the nose and the fairing inlet.

The tests were carried out at atmospheric pressure and the results were converted to correspond with actual service conditions at high pressure. The laboratory results were found to agree with the calculated values for heat transfer and pressure drop.

Heat is transferred from the cooling air to the nose fairing through welded steel ribs. For reasons of production engineering the narrower duct cross section towards the centre of the nose cone had to be a composite of simple shapes. This caused certain impact losses in the air flow which could not be entirely avoided.

The covers of the air ducts can be removed to provide access. The inner shrouding is all of glass-fibre reinforced polyester and is in small sections for easy removal for maintenance purposes. As shown in Fig. 5 the nose contains the fan mountings and a steel grid platform. The access shaft which also carries the power output, excitation and control leads and the piping is closed at the junction with the shell by a pressure-tight door.

Stator

As shown in Fig. 7 the stator iron comprises stacks of laminated segments which fit direct onto the stator frame without any air gaps. Direct contact between the dynamo sheet and the steel frame is important as regards the temperature of the stator copper because this would increase by 40 deg C per millimetre air gap at this point. Special measures had to be taken to ensure proper seating over a long period. To a certain extent the iron is prevented from expanding due to the increase in temperature during service, by the cold stator frame. Radial forces are thus caused which the laminated sheet is unable to cope with. The individual sheets slide relative to each other and after cooling there is an air gap between the iron and the frame. With ageing this could lead to permanent looseness. To prevent this, the compressive strength of the iron was increased by sticking the sheets together by a patented process.

The sheets were covered in the normal fashion with insulating varnish and subsequently sprayed with a heat-curing epoxy resin and dried. The lamination segments were then fitted into the stator frame in the normal manner. It was not until this process had been completed that the whole unit was heated under pressure and the resin cured. Unavoidable residual gaps between laminations and frame were filled by injecting cold-curing elastic silicon resin.

Fig. 6 – Laboratory model of a cooling duct

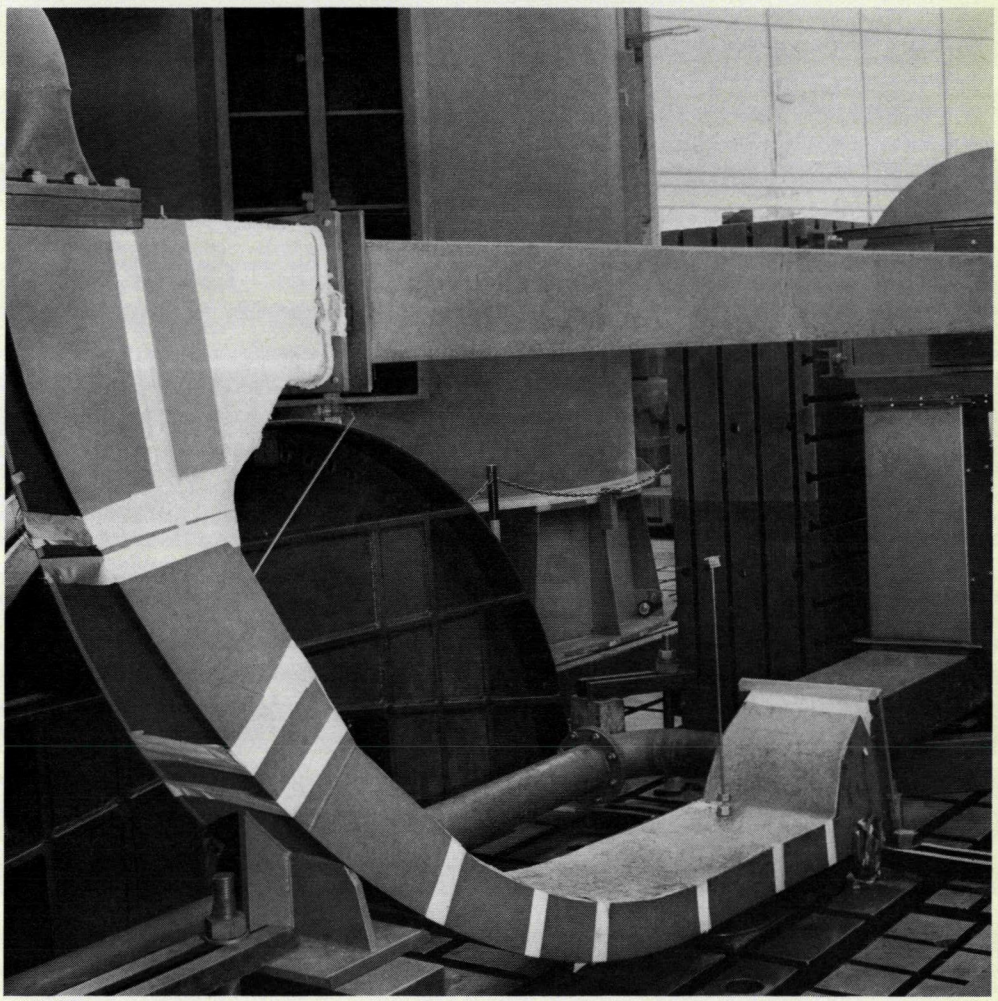

BROWN BOVERI 147 321-I

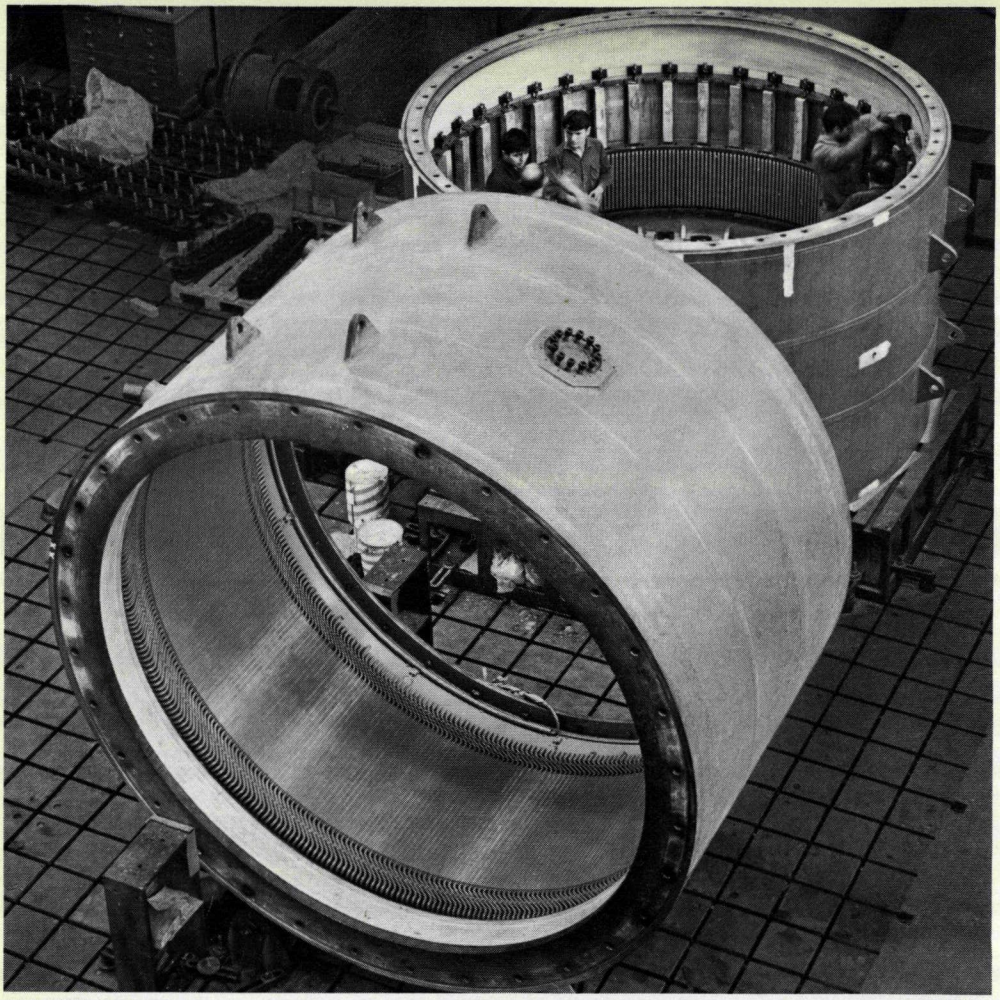

BROWN BOVERI 147318-I

Fig. 7 – Windings being fitted to the 9000 kVA generator stators

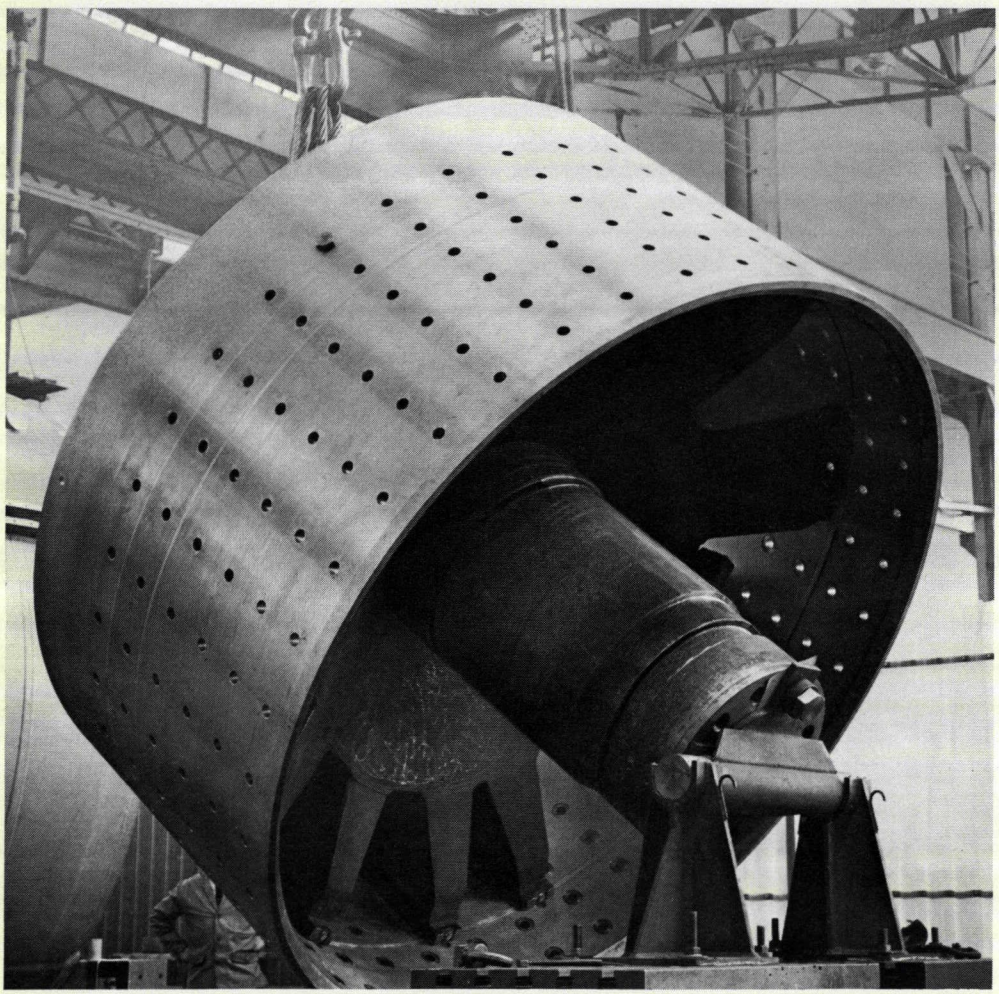

BROWN BOVERI 147319-I

Fig. 8 – Rotor for a 9000 kVA, 158 rev/min axial turbine and generator

The stator winding comprises diamond coils with continuously wound mica/glass tape preimpregnated with epoxy resin, and the slot portion was cured in pressure moulds whereas the overhang portions were not cured until after installation. The conductors were insulated with a thermostable varnish and glass-fibre tape.

Rotor

The rotor spider is mounted overhung on the shaft and comprises a cast steel hub with steel arms welded to it (Fig. 8). The outer rim is also a welded construction which is shrunk on to prevent further stresses due to centrifugal forces from being transmitted to the hub. If the maximum permissible speed is exceeded it can lift off slightly but guides prevent any displacement.
The pole units are laminated and fitted with a closed damping winding. In spite of the relatively high run-away speed of 490 rev/min (3·1 time the rated speed) it is quite sufficient to bolt the poles to the rim. The coils are wound with bare copper, have glass fibre/asbestos insulation and are fixed to the poles by spacing wedges.

Sliprings and Brushes

The static exciter set is located in the machine room. Sliprings are therefore necessary for transmitting the field current to the rotor. They are mounted overhung on the front of the rotor hub. With the closed-loop cooling air circuit the generator must not be allowed to become contaminated by carbon dust from the brushes. For this reason air is taken from the main circuit for cooling the sliprings and brushes and is filtered before return. This air flows radially through the slipring shroud and through the hollow arms of the brake carrier. The separate blower fan enables the two cooling air circuits to operate in parallel without an additional fan.
The sliprings are not accessible for inspection while operating with the cooling air under pressure and therefore they must be monitored from outside. All brush holders are therefore fitted with limit switches which immediately indicate worn-out brushes.

Sliding Ring Seal

The generator designer was faced with the problem that the turbine end has bearings and control equipment which must be accessible at all times, even when operating under compressed air. It was therefore necessary to provide a seal between generator and turbine.
Although it was a simple matter to seal all stationary parts with rubber it was necessary to develop a special sliding ring seal for the shaft at the bearing hub. This comprises a two-piece steel ring with white metal surfaces and a welded annular guide. The sliding ring is loose in the guide with slight radial play between it and the shaft. The actual seal is provided by lubricating oil under pressure which enters through drillings in the ring. At this point some of the oil flows to the low-pressure and some to the high-pressure side. The oil pressure is only slightly higher than the air pressure on the generator side so that only a small quantity of oil flows out on this side to provide lubrication and cooling. The necessary play between the ring and the shaft means that much more oil flows out on the low-pressure side. Although the oil flowing out on the generator side can easily be collected by means of labyrinths, the low-pressure side requires considerable drainage. For this reason the seal was combined with the generator bearing and its lubrication system. The oil leaving the low-pressure side flows back with the bearing oil to the cooler but that leaving the generator side requires collector tanks with float valves before the oil is returned to the lubrication system. To avoid any loss of oil and prevent oil vapour, which would affect the generator, additional shrouds were fitted over the labyrinth seals. These are purged with compressed air and vented to atmosphere. The running characteristics of the sealing ring were checked thoroughly on a laboratory model before installation.

Generator Shield

This seals off the generator from the turbine and also carries the hub for the combined guide and thrust bearing and the sliding seal as well as the support for the stator frame. The air pressure in the generator section imposes an axial load on the shield of 175 t. Added to this is a hydraulic thrust of 117 t from the turbine in the same direction. A double-shell welded construction in the shape of a cone was employed to provide a rigid frame to cope with the total load of 292 t. One cone was welded air-tight and the other oil-tight in the regions where tanks are fitted between the two bulkheads.

Air Pressure for the Generators

A common air pressure supply system was installed to serve both generators. It comprises an air pressure tank fed by two oil-vapour-free compressors. Both compressors are used for raising the initial pressure but in normal service only one set is used and the other is standby. Each branch has its own filters and dehumidifiers and the pressure of the air supplied to the generators is controlled. A pressure-relief valve in the access shaft door prevents the pressure exceeding the prescribed limit.

Fire Prevention

Automatically controlled CO_2 fire extinguishing equipment is installed. Carbon dioxide is released under high pressure into the generator chamber and the air is forced out through the relief valve into the access shaft. The gas is then drawn off through built-in ducts by an extractor fan.

Humidity Control

Using river water to cool the generator after service could lead to condensation which would reduce the effectiveness of the insulation of the electrical equipment including the windings. Condensation could also form on the cold shell during service and be carried to the insulation by the cooling air. The incoming air is therefore dried with silica gel before entry to keep the moisture content of the air in the generator chamber to a minimum. Heating elements are also installed for drying out the chamber before commencing operation. Any condensation occurring in spite of these measures or any water seeping through the casing is easily removed through a drain tube. The water thus collected flows into a tank with float valve control and thence into the drainage system of the machine room.
Although all these measures are taken to keep the insulation dry the carbon brushes require a certain minimum humidity in order to function properly. Investigations have shown that there is still sufficient moisture in the cooling air to maintain a film of lubricant on the sliprings at the minimum expected river water temperature of 6 °C and an ambient relative humidity of 100 %.

Brakes

Brakes are necessary to prevent the set from being turned by water leaking through the race. The air operated brakes are located at the nose-cone end of the generator rotor hub. At this point a slightly oily atmosphere is required for lubricating the piston seals and so the air is taken from the ordinary supply through a pressure tank. Control is either manual or by magnetic valve and all brakes have position indicators.

Temperature Monitoring

To comply with the condition that the installation must be equipped for remote control operation in the future, suitable attention was paid to temperature monitoring. Apart from the usual resistance thermometers and thermostats in the stator windings, stator iron, bearings and cooling air stream a flow monitor was fitted in the air circuit.

Installation

Generators for axial turbine sets are generally assembled before being lowered into the turbine pit. Stator, rotor and bearing components are assembled with the axis vertical and held together by locating bolts. The unit is then raised, turned through 90° and lowered into position between nose fairing and turbine casing. It is then bolted to the turbine casing, nose cone flange and turbine shaft and finally the locating bolts are removed.
The generators described in the above have been in service for about two years to the complete satisfaction of the customer.

A Method for Checking the Turn Insulation of Form-Wound Coil Windings for High-Voltage Rotating Machines

D. Kränkel and R. Schuler

621.313.045.001.4

A method is described for checking the insulating strength between the turns of form-wound coils for high-voltage rotating machines. Experience acquired over the years has shown that systematic testing of each coil with this method during manufacture of the machine helps to improve reliability, and can therefore be recommended for general use.

Introduction

For reasons of design, the stator windings of a.c. machines up to medium outputs are usually composed of form-wound coils. Several such coils are then connected outside the laminations to form a winding or phase. The coils themselves consist of several turns in series, and these have to be insulated from each other and from the earthed iron of the stator (Fig. 1). Under normal conditions the potential difference between adjacent turns is only some 50 to 150 V, depending on the type of machine. The voltage difference between the turns and the stator iron, on the other hand, can be as much as the phase voltage of the machine, depending on the position of the coil in the winding. With the methods of insulation and manufacturer available today, dealing with these voltages presents no real problem.

When designing the insulation, and the turn insulation especially, one must also take account of the fact that in service the windings are subjected to short-lived voltage surges, the amplitude of which can be much greater than that of the service voltage. The stress on the insulation, particularly between the turns of the entrance coils, increases with the rate of rise and the amplitude of the incoming wave.

We have for many years given a guarantee that our high-voltage motors are surge-proof [1]. It was therefore essential to take this special kind of stress into account. As a result, it was decided to carry out not only the usual voltage tests to check the main insulation, but also to perform a special test to verify the dielectric strength of the insulation between the turns. Over the years, systematic testing of the coils has also proved its worth in that the insulation, particularly in the case of form-wound coils, is subjected to severe mechanical stresses while being shaped and fitted. In certain instances this can affect the turn insulation to such an extent that its dielectric strength is no longer adequate.

Several years ago we began to check the turn insulation of coil windings systematically during manufacture. The test method used is described in this article, and the experience acquired is summarized.

The Test Method

There are many known test circuits for checking the turn insulation of coils [2, 3, 4]. While basically similar, many of them differ only in the way in which an inter-turn short circuit is indicated. The principle of the circuit which we use can be seen in Fig. 2. Capacitor C_1 is continually charged with a power-frequency voltage obtained from high-voltage transformer T_2. In each cycle it discharges once or twice across a triggered spark gap 1 to the coil under test L_1. In so doing it causes a damped high-frequency voltage oscillation at the terminals of coil L_1.

With our test rig, the spark gap is triggered by means of a superposed voltage pulse which can be selected to occur at either the positive or negative maximum of the a.c.

Fig. 1 – A form-wound coil

left: basic shape
right: section at A–A through the coil

1 = Conductor (turn)
2 = Insulation between series-connected conductors (turns)
3 = Insulation against slot iron
U_W = Potential difference between adjacent turns
U_E = Potential difference between turns and earth

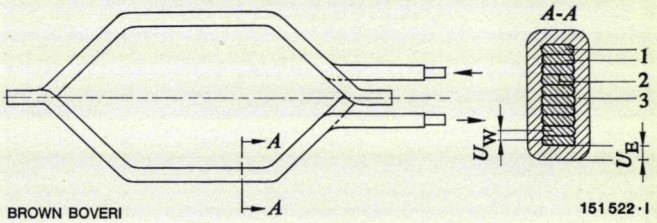

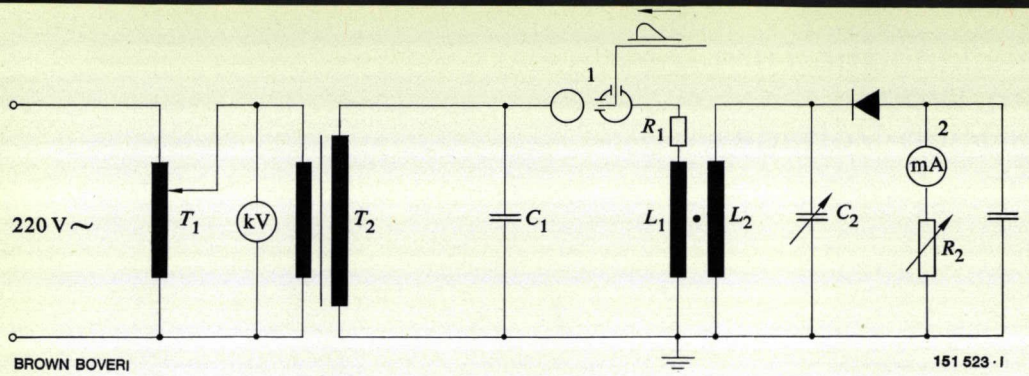

Fig. 2 – Circuit of coil test rig

T_1 = Low-voltage transformer
T_2 = High-voltage transformer
C_1 = High-voltage capacitor
L_1 = Test specimen (coil)
L_2 = Magnetically coupled sampling coil
C_2 = Resonance-tuning capacitor
R_1 = Resistance of test specimen
R_2 = Series resistor for 2
1 = Triggered spark gap
2 = Instrument to indicate inter-turn short circuits

a

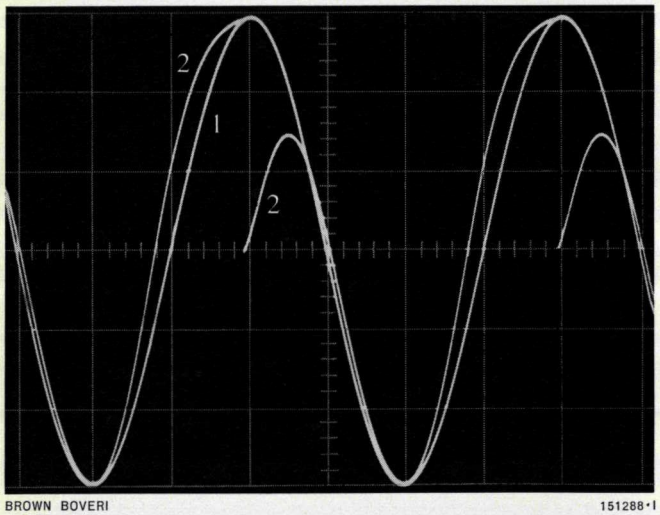

Fig. 3 – Voltage curves

a: 50 Hz voltage, U = 20 kV
1 = Calibration curve
2 = Curve with ignition point

b: decaying voltage oscillation at L_1
U = 20 kV
f = 89 kHz
α = 0·90 mA, deflection on instrument 2 (Fig. 2)

c: decaying voltage oscillation at L_1 with short circuit between two windings
U = 20 kV
f = 109 kHz
α = 0·20 mA

b

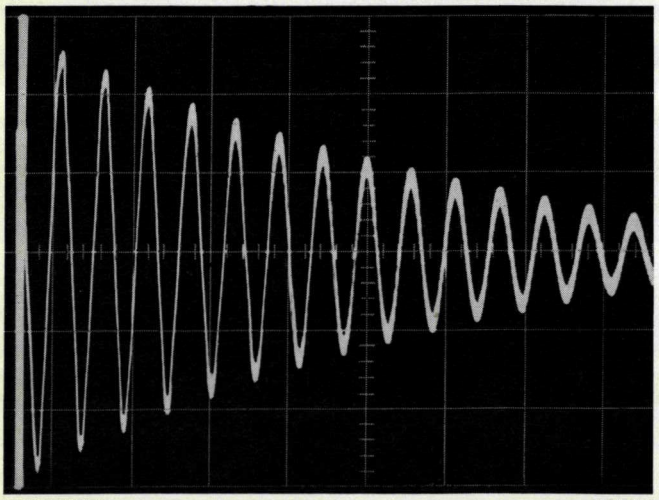

c

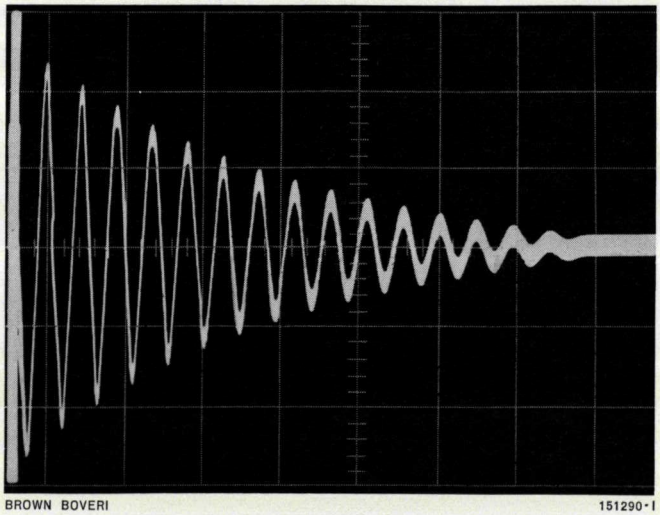

voltage (Fig. 3a). Using this technique one can ensure very accurate triggering of the spark gap with test voltages up to 45 kV peak value. In an earlier version we used a rotary spark gap, but this proved to be unsuitable at the higher test voltages.

When the gap sparks over, a high-frequency damped oscillation occurs in circuit C_1 L_1 R_1 (Fig. 2). The amplitude of the first swing almost reaches the charging voltage of capacitor C_1. This is so, provided R_1 is comparatively small, which is almost always the case with the usual test specimens (Fig. 3b). With the capacitance employed of $C_1 = 30\,000$ pF, the natural frequency of the transient oscillation is between 80 and 100 kHz, depending on the construction of the coil in question.

Resonant circuit L_2 C_2 is coupled with the test coil L_1. The voltage oscillation induced in this circuit produces a current in a parallel auxiliary circuit. The current is rectified and indicated by instrument 2 (Fig. 2). By adjusting the resonance and choosing a suitable value for R_2 the instrument is set to maximum deflection. As soon as an inter-turn short circuit occurs in the test coil the inductance of L_1 changes, and with it the natural frequency of the primary circuit L_1 C_1. The amount by which the instrument is deflected, α, is then greatly reduced (Fig. 3c).

Test Procedure

In addition to the usual power-frequency test, the special turn test is usually performed on each coil of a high-voltage winding during the course of manufacture, before and after it is fitted in the stator. Recent experience has shown, however, that one test after the coil has been fitted is generally sufficient. For this, the coil L_1 (Fig. 2), is connected to the test rig (Fig. 4), and the sampling coil L_2 is introduced into the stator bore in such a way that it can be turned (Fig. 5). Once the indicator circuit has been tuned with C_1, and R_2 set correctly with the selector switch, the desired test voltage is applied to the coil, usually for 10 s. Thus each coil receives more than 500 voltage surges during the test.

The currents obtained with coils of the same kind differ only slightly (Fig. 6). The small discrepancies in the readings can be attributed primarily to the fact that the geometric position of the sampling coil relative to the test coil is not always exactly the same. These slight discrepancies are negligible as regards detecting an inter-turn short circuit. The variation is far greater if a short circuit is present, and the instrument shows a much lower value (Fig. 6, coil 10).

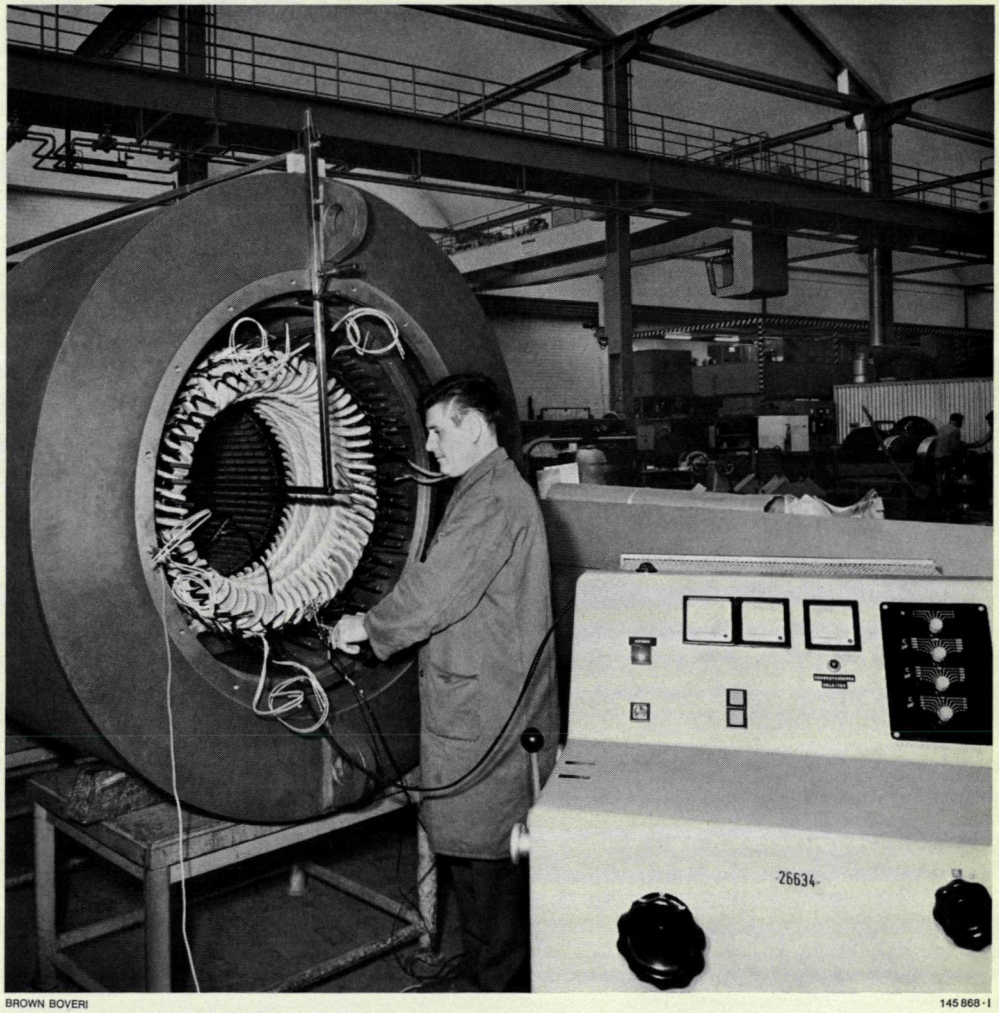

Fig. 4 – Checking the turn insulation of coils in a high-voltage motor

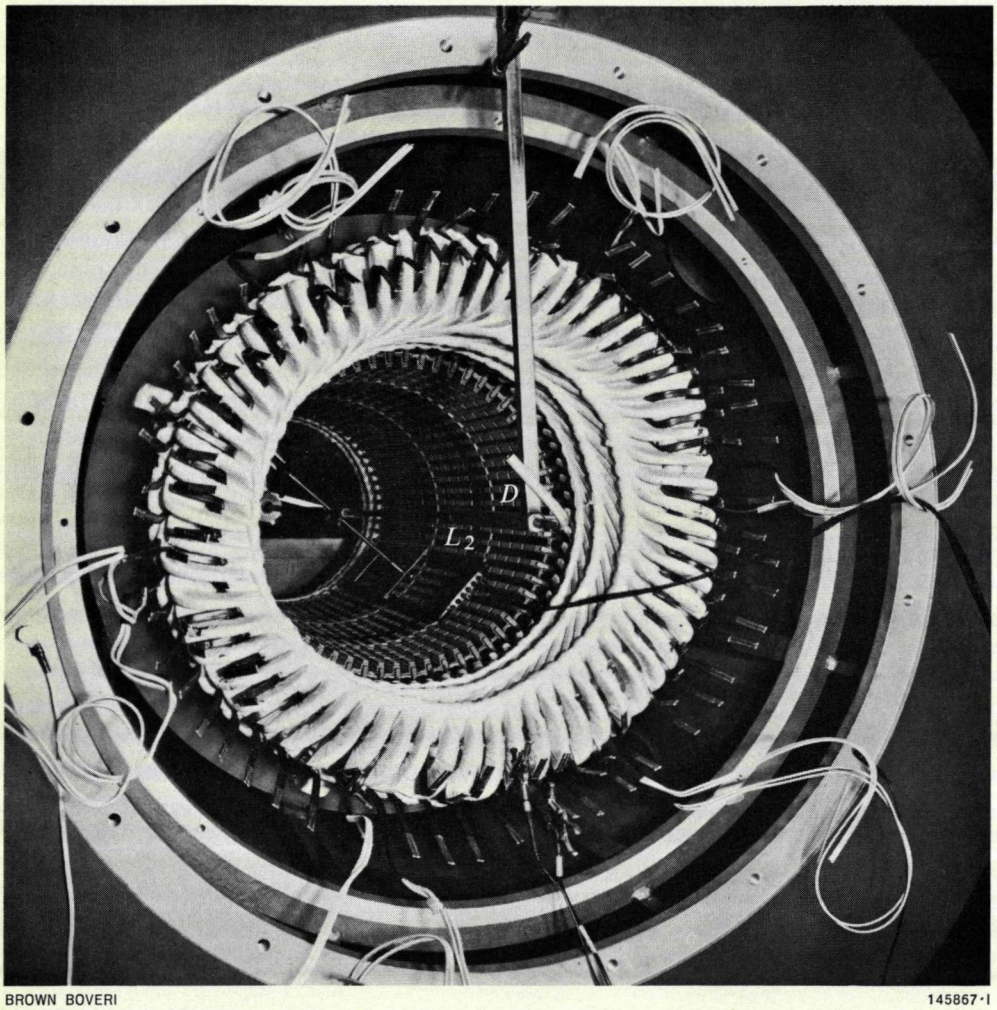

BROWN BOVERI 145867-I

Fig. 5 – Stator ready for testing

L_2 = Sampling coil
D = Turning device

The Test Voltage

Several years ago, when considering the question of insulation coordination, we decided to set the insulation level of high voltage rotating machines in terms of the impulse voltage at $\hat{U}_{St} = 4\ U_n + 5$ kV, where U_n is the rated phase-to-phase voltage of the machine and $\hat{U}_{St}$ is the peak value of a standard 1·2/50 μs impulse.

Detailed investigations have shown that the overvoltage waves resulting from switching and surge phenomena are distributed very unevenly along a winding, the stresses on the line end coils being particularly high. It has also been established that under normal conditions in the network the rise times of the overvoltage waves are usually appreciably greater than 1 μs. Consequently, the voltage drop across the first coil is always smaller than 50 % of the amplitude of the incoming wave. These findings, considered together with the type of insulation and number of turns in each coil, provide a basis for sizing the turn insulation and selecting the test voltages to be used during manufacture.

As an example, Fig. 7 shows the voltages used to test the coils after they have been fitted. Curve 1 relates to coil windings which are fully insulated before fitting in the machine. Curve 2 is taken when the main and turn insulation is not actually impregnated until after the coils are in place in the machine (the fully impregnated winding system [6]). The special test is particularly important with this type of insulation, as subsequent defects in the windings must be avoided at all costs since they are generally difficult to repair. If the voltages are compared with curves 3 and 4, which represent the maximum stresses on the coils occurring during subsequent operation under specified conditions, it is evident that the coils have a wide safety margin compared with the normal service requirements (Fig. 7).

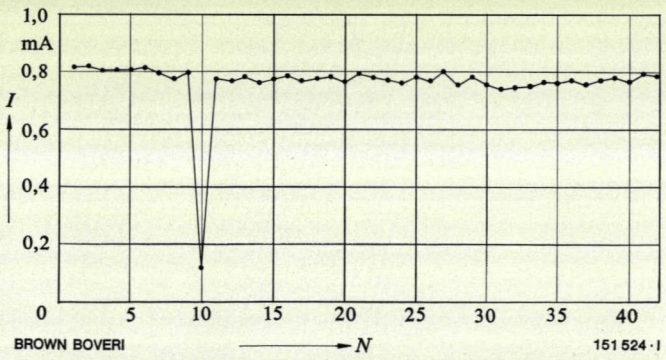

Fig. 6 – Results of checking the turn insulation of 42 coils fitted in a stator

Coil 10 contained an inter-turn short circuit.
N = Number of coils
I = Current at instrument

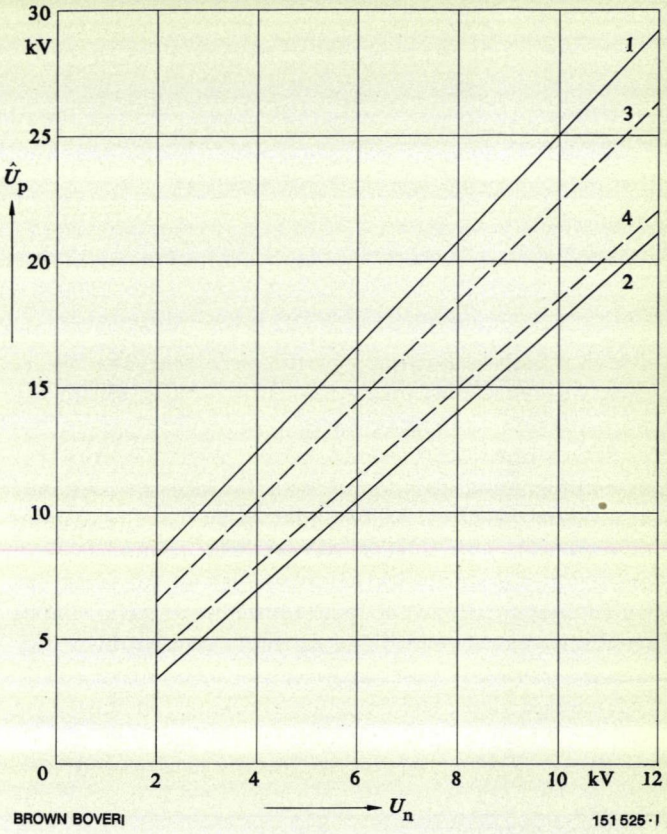

Fig. 7 – Coil test voltages $\hat{U}_p$ in relation to machine voltage ratings U_n

1 = Test voltages for fully insulated fitted coils
2 = Test voltages for coils fitted before final impregnation
3 = $\hat{U}_p = 0{\cdot}5\ (4\ U_n + 5\ \text{kV})$
4 = $\hat{U}_p = 0{\cdot}5\ .\ 1{\cdot}25\ (2\ U_n + 1\ \text{kV})$ [5]

Experience

Several hundred high-voltage machines for between 2 and 16 kV have so far been tested in the manner described here. Some of the coils were insulated with micafolium, but the synthetic-resin systems Micadur-Compact and Micadur-Silast [6] were employed for the great majority. The turn insulation consisted of either enamel and glass fibre or glass-backed mica-paper tape.

When the test was first introduced the number of weak spots found in the turn insulation was relatively high. The reasons for this can be summarized as follows:

– mechanical damage to the turn insulation while shaping the coil or while fitting it in the stator slots (especially in the end winding)
– in the case of enamelled conductors with glass silk, local irregularities in the insulation thickness which had not been detected despite strict checking on receipt
– foreign bodies included between adjacent turns.

By applying the turn voltage test systematically it has been possible to eliminate these shortcomings and also adopt radical measures for improving the quality generally. As a result, the failure rate with this test is now very low. This special check on the turn insulation has thus increased the reliability of our high-voltage machines.

To ensure that the high dielectric strength is maintained for many years, it is important that the main and turn insulation should be able to withstand any other stresses occurring during service. Detailed examination of old machines with coil windings have shown, for example, that practically all faults were due to inter-turn short circuits. The main reason for this was that the electrical field acting between the conductors and the iron core, particularly in voids between the turns and the main insulation, gave rise to corona discharges which led to a marked weakening of the turn insulation. Even insignificant system faults often resulted in inter-turn short circuits which spread until an earth fault occurred and the machine had to be taken out of service. A typical example

of such a fault is illustrated by the piece of coil in Fig. 8. Here, weakened turn insulation led to a short circuit between the first and second turns.

Insulation practically free of voids is available now that the impregnating compound with the classical asphalt/micafolium systems is added under vacuum, while vacuum impregnation with solvent-free synthetic resins has been used from the start with Micadur systems [6]. This has contributed greatly to the fact that high-voltage machines with coil windings are today far more reliable than they were ten or twenty years ago.

The method described here for checking the insulation between the turns of coil windings unavoidably involves a certain amount of extra work, but we nevertheless consider it to be very useful and recommend that it should be employed generally.

Bibliography

[1] *P. Baltensperger, H. Meyer:* Overvoltages resulting from the disconnection of high-voltage motors. Brown Boveri Rev. 1953 *40* (9) 342–350.

[2] *J. L. Rylander:* High frequency voltage test for insulation of rotating electrical apparatus. Trans. Amer. Inst. elect. Engrs 1926 *45* 459–465.

[3] *M. Wellauer:* A new arrangement for testing the insulation of the turns of machine coils. Bull. Oerlikon 1944 (251) 1624–1626.

[4] *G. L. Moses, E. F. Harter:* Winding-fault detection and location by surge-comparison testing. Trans. Amer. Inst. elect. Engrs 1945 *64* 499–503.

[5] AIEE Committee Report: Impulse testing of rotating a-c machines. Trans. Amer. Inst. elect. Engrs 1960 *79* 182–188.

[6] *R. Schuler:* Insulation systems for high-voltage rotating machines. Brown Boveri Rev. 1970 *57* (1) 15–24.

Fig. 8 – Section of a coil with five turns

The main insulation has been partly removed to show the inter-turn short circuit between turns 1 and 2. Traces of corona discharges (light patches) can also be seen on turns 3 to 5.

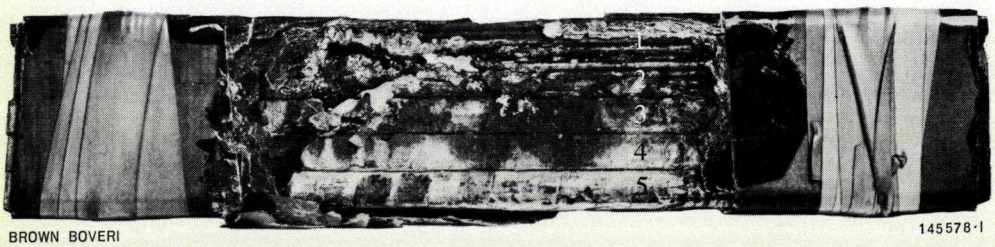

In Brief

621.382.2:546.28

The DSA Range of High-Power Silicon Diodes

H. Gilgen

Over the past ten years, silicon rectifier devices have assumed a dominant role in converter technology. The reasons are well known, and include high blocking capacity, even at high operating temperatures, high specific current density and low forward resistance. The result is a smaller installed volume per kilowatt of rectified power, particularly in the case of high reverse voltages.
From the outset Brown Boveri recognized the advantages of the silicon rectifier device in converter technology. The DS 200 silicon power, for a mean d.c. rating of 200 A, has been in production for more than a decade. The inverse characteristics have been steadily improved over the years, leading to the DSA 200 surge-proof controlled-avalanche silicon diode. With diodes of this kind the maximum permissible power dissipation is of roughly the same order in both forward and reverse directions. They are therefore self-protecting against transient overvoltage peaks. Power diodes with reverse voltages of up to 2300 V have proved extraordinarily reliable in practice, even under extreme conditions.

Table I: Key to type designation of DSA high-power diodes

Diode type DSA 401 – 32 F (C)

Diode — DSA

Silicon — DSA

Surge-proof, with controlled-avalanche characteristic — DSA

Type size with final digit — 401

0 ceramic insulation
hollow cylinder, smooth surface

1 ceramic insulation
hollow cylinder, corrugated outer surface
(longer creepage distance for higher reverse voltages)

Reverse voltage class — 32
(max. repetitive peak reverse voltage)

e.g. 32 denotes 3200 V
23 denotes 2300 V

Construction — F

F flat base with cathode mounting stud
L flat base with flexible cathode lead

Forward voltage drop class — (C)
(for parallel arrays, diodes with the same identifying letters should be used)

Following the trend towards higher diode currents and reverse voltages, Brown Boveri have developed new high-power silicon diodes with mean d.c. ratings up to 500 A for a conducting angle of 180° and maximum repetitive peak reverse voltages of up to 5000 V. The diodes are already in series production. The type designation is explained on the previous page and the main electrical and mechanical features are summarized below.

Type Designation

The earlier type designation has been altered in that the new one includes the repetitive peak reverse voltage (Table I).

Table II: Ratings and characteristics of DSA high-power controlled-avalanche silicon diodes

Device type	I_{FAV} [A]	ϑ_{case} [°C]	U_{RRM} [V]	I_{FSM} [A]	I^2t [A²s]	P_F [W]	$\vartheta_{(VJ)}$ [°C]	R_{thJC} [°C/W]	I_R [mA]	ϑ_S [°C]
DSA 250-11 F			1100							
14 F			1400				−40			
17 F	300[1]	90	1700	5300[1]	140 000[1]	360	to	0·14	≤ 30	180
20 F			2000				+140			
23 F			2300							
DSA 250-11 L			1100							
14 L			1400				−40			
17 L	300[1]	90	1700	5300[1]	140 000[1]	360	to	0·14	≤ 30	180
20 L			2000				+140			
23 L			2300							
DSA 251-26 F			2600							
29 F			2900				−40			
32 F	320[1]	90	3200	6000[1]	180 000[1]	500	to	0·1	≤ 30	180
38 F			3800				+140			
44 F			4400							
50 F			5000							
DSA 400-11 F			1100							
14 F			1400				−40			
17 F	475[1]	90	1700	8900[1]	390 000[1]	630	to	0·08	≤ 30	180
20 F			2000				+140			
23 F			2300							
DSA 401-26 F			2600							
29 F			2900				−40			
32 F	370[1]	90	3200	6900[1]	230 000[1]	560	to	0·09	≤ 30	180
38 F			3800				+140			
44 F			4400							
50 F			5000							

[1] Different forward voltage drop classes available

Key

I_{FAV} = Max. single-phase mean forward current at ϑ_{case}
ϑ_{case} = Case temperature
U_{RRM} = Max. repetitive peak reverse voltage
I_{FSM} = Max. one-cycle (50 Hz) peak surge current (under load)
I^2t = Max. I^2t (less than 10 ms)
P_F = Max. power dissipation
$\vartheta_{(VJ)}$ = Max. operating junction temperature
R_{thJC} = Max. thermal resistance, junction to case
I_R = Max. rated reverse current at U_{RRM}, I_{FAV} and ϑ_{case}
ϑ_S = Storage temperature

Fig. 1 – Brown Boveri high-power silicon diodes DSA 250 L, DSA 250 F, DSA 400 F, DSA 251 F and DSA 401 F, with flexible lead

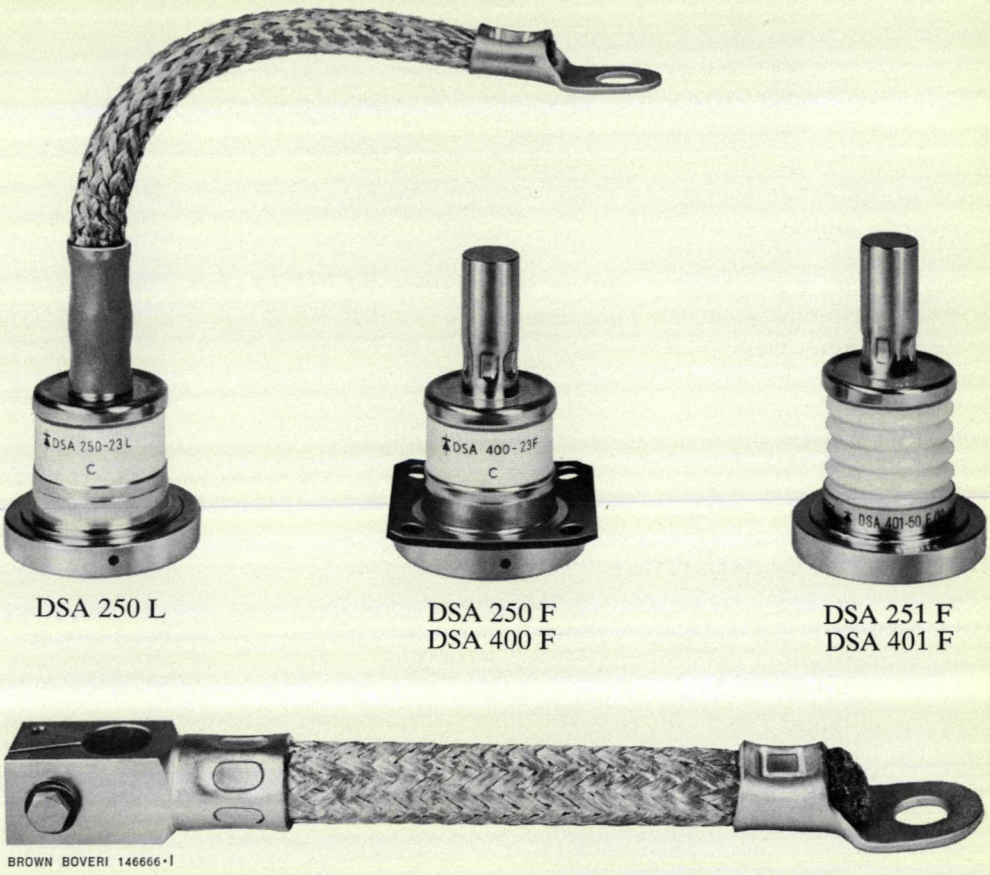

Fig. 2 – Heat sinks types K 25, K 40, K 45 and K 46 for DSA high-power silicon diodes

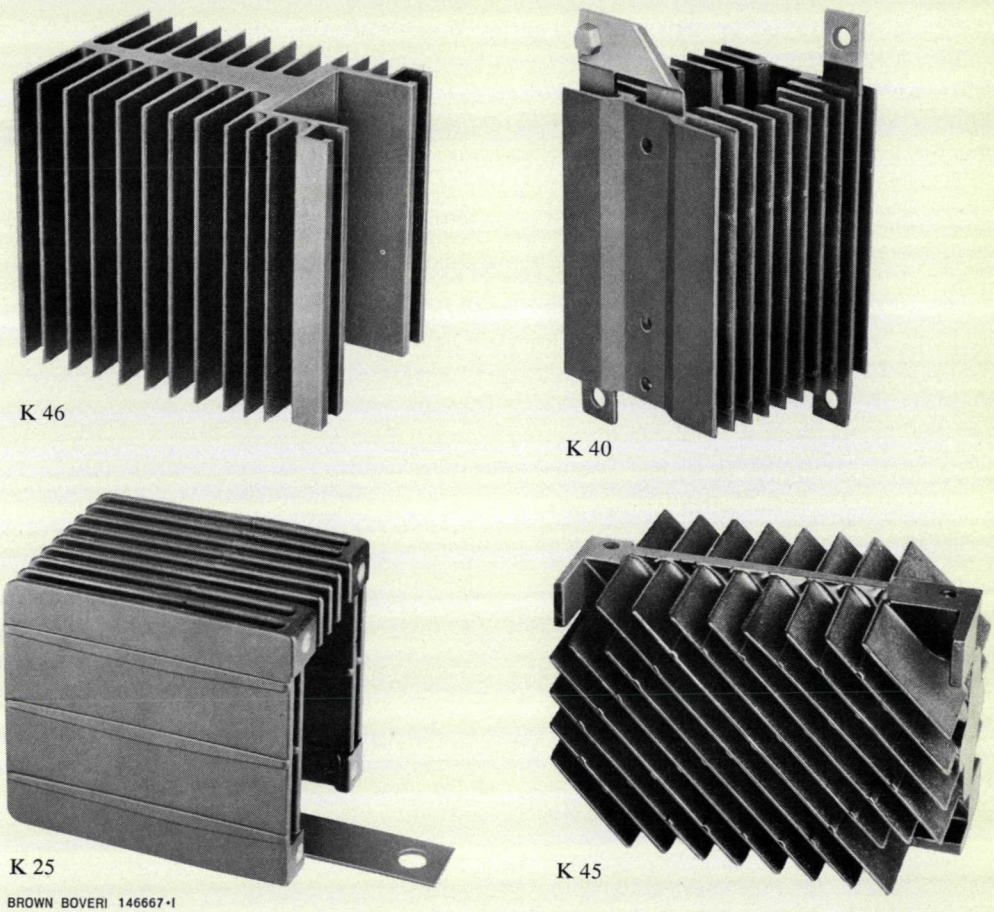

Electrical Features

The main electrical data of the new diodes are listed in Table II. There are five different sizes available, each for five or six different reverse voltage categories. The single-phase mean forward currents given in the Table relate to a mean operating junction temperature of 140 °C. The values given are true operating data, and not absolute maximum ratings, which lie close to the destruction limit.

When diodes are connected in parallel the current is distributed according to the forward resistances. So that these high-power diodes can be used to the best effect, a finely graded system of classifying the forward characteristics has been introduced. It is recommended that diodes connected in parallel should have the same identifying letters.

Mechanical Construction

All the diodes have one feature in common. They all have a flat copper base of uniform dimensions. Each diode is supplied complete with a mounting plate which can be used for all types. This is for fixing the diode to its heat sink. The ceramic insulation of the upper part of the diodes can be in two different forms. The insulation of diodes with reverse voltages up to 2300 V is in the form of a smooth, hollow cylinder, while those for reverse voltages of 2600 V to 5000 V require insulation providing a longer creepage distance. With these, therefore, the outer surface of the ceramic is corrugated. The dimensions of diodes DSA 250/DSA 400 are similar, and those of DSA 251/DSA 401 are identical. Where discrepancies in the dimensions do occur, they are so slight as to be of no significance to the user.

The various types are illustrated in Fig. 1.

Diodes with mounting studs can also be supplied with flexible leads. These have a gold-plated terminal contact at one end, and a cable eye at the other. The leads are obtainable in various lengths to suit different design requirements.

The new range of high-power diodes allows the user to build equipment which is more efficient, smaller, lighter and cheaper. A wide variety of cast aluminium heat sinks is also available. A selection of different shapes for natural and forced air cooling can be seen in Fig. 2. The sink with oblique fins has been specially designed for use in compact units. It is remarkable for its low thermal resistance, small dimensions and ease of assembly.


BROWN
BOVERI